NAVAL POSTGRADUATE SCHOOL

MONTEREY, CALIFORNIA

THESIS

EXTENDING THE UNAMBIGUOUS RANGE OF CW POLYPHASE RADAR SYSTEMS USING NUMBER THEORETIC TRANSFORMS

by

Nattaphum Paepolshiri

September 2011

Thesis Co-Advisors: Phillip E. Pace
David C. Jenn

Approved for public release; distribution is unlimited

THIS PAGE INTENTIONALLY LEFT BLANK

REPORT DOCUMENTATION PAGE			Form Approved OMB no. 0704-0188
Public reporting burden for this collection of information is estimated to average 1 hour per response, including the time for reviewing instruction, searching existing data sources, gathering and maintaining the data needed, and completing and reviewing the collection of information. Send comments regarding this burden estimate or any other aspect of this collection of information, including suggestions for reducing this burden, to Washington headquarters Services, Directorate for Information Operations and Reports, 1215 Jefferson Davis Highway, Suite 1204, Arlington, VA 22202-4302, and to the Office of Management and Budget, Paperwork Reduction Project (0704-0188) Washington DC 20503.			
1. AGENCY USE ONLY ***(Leave blank)***	**2. REPORT DATE** September 2011	**3. REPORT TYPE AND DATES COVERED** Master's Thesis	
4. TITLE AND SUBTITLE Extending the Unambiguous Range of CW Polyphase Radar Systems Using Number Theoretic Transforms		**5. FUNDING NUMBERS**	
6. AUTHOR(S) Nattaphum Paepolshiri			
7. PERFORMING ORGANIZATION NAME(S) AND ADDRESS(ES) Naval Postgraduate School Monterey, CA 93943-5000		**8. PERFORMING ORGANIZATION REPORT NUMBER**	
9. SPONSORING /MONITORING AGENCY NAME(S) AND ADDRESS(ES) N/A		**10. SPONSORING/MONITORING AGENCY REPORT NUMBER**	
11. SUPPLEMENTARY NOTES The views expressed in this thesis are those of the author and do not reflect the official policy or position of the Department of Defense or the U.S. Government. IRB Protocol Number: N/A.			
12a. DISTRIBUTION / AVAILABILITY STATEMENT Approved for public release; distribution is unlimited		**12b. DISTRIBUTION CODE** A	

13. ABSTRACT (maximum 200 words)

Polyphase continuous waveform (CW) radar systems often use the popular Frank code and P4 code due to their linear time-frequency characteristics as well as their low periodic ambiguity sidelobes. The phase relationship of the Frank code corresponds to a sawtooth folding waveform. The phase relationship of the P4 code is symmetrical with a parabolic distribution. The radar system's unambiguous target detection range is limited by the number of subcodes within the code period (code length). Increasing the code length to extend the unambiguous range results in a larger range-Doppler correlation matrix processor in the receiver, a longer compression time and an increase in the receiver's bulk memory requirements. In addition, the entire code period may not be returned from the target due to a limited time-on-target resulting in significant correlation loss. To significantly extend the unambiguous range beyond a single code period, this thesis explores the relationship between the polyphase codes (Frank and P4) and the number theoretic transforms (NTT) where the residues exhibit the same distribution as the polyphase values. The unambiguous range is extended from the number of subcodes within a single code period to the dynamic range of the transform without requiring a large increase in correlation processing. The dynamic range of a NTT is defined as the greatest length of combined phase sequences that contain no ambiguities or repeated paired terms. By transmitting $N \geq 2$ coprime code periods, the unambiguous range can be extended by considering the paired values from each sequence. A new Frank phase code formulation is derived as a function of the *residue number system* (RNS) where each residue corresponds to a phase value within the code period (modulus) sequence. Based on the symmetrical distribution of the P4 code, a new phase code expression is derived using both the *symmetrical number system* (SNS) and the *robust symmetrical number system* (RSNS). Here each phase value within the code period corresponds to a symmetrical residue. MATLAB simulations are used to verify the new expressions for the RNS, SNS and RSNS phase codes. Implementation considerations of the new approach are also addressed.

14. SUBJECT TERMS CW radar, Polyphase sequence, Frank code, P4 code, Unambiguous range, Pulse compression, Residue Number System, Symmetrical Number System, Robust Symmetrical Number System.			**15. NUMBER OF PAGES** 131
			16. PRICE CODE
17. SECURITY CLASSIFICATION OF REPORT Unclassified	**18. SECURITY CLASSIFICATION OF THIS PAGE** Unclassified	**19. SECURITY CLASSIFICATION OF ABSTRACT** Unclassified	**20. LIMITATION OF ABSTRACT** UU

NSN 7540-01-280-5500 Standard Form 298 (Rev. 2-89)
Prescribed by ANSI Std. 239-18

THIS PAGE INTENTIONALLY LEFT BLANK

Approved for public release; distribution is unlimited

EXTENDING THE UNAMBIGUOUS RANGE OF CW POLYPHASE RADAR SYSTEMS USING NUMBER THEORETIC TRANSFORMS

Nattaphum Paepolshiri
Lieutenant, Royal Thai Navy
B.S., Royal Thai Naval Academy, 2005

Submitted in partial fulfillment of the
requirements for the degree of

MASTER OF SCIENCE IN ELECTRONIC WARFARE SYSTEMS ENGINEERING
and
MASTER OF SCIENCE IN ELECTRICAL ENGINEERING

from the

NAVAL POSTGRADUATE SCHOOL
September 2011

Author: Nattaphum Paepolshiri

Approved by: Phillip E. Pace
Thesis Co-Advisor

David C. Jenn
Thesis Co-Advisor

R. Clark Robertson
Chair, Department of Electrical and Computer Engineering

Dan C. Boger
Chair, Department of Information Sciences

THIS PAGE INTENTIONALLY LEFT BLANK

ABSTRACT

Polyphase continuous waveform (CW) radar systems often use the popular Frank code and P4 code due to their linear time-frequency characteristics as well as their low periodic ambiguity sidelobes. The phase relationship of the Frank code corresponds to a sawtooth folding waveform. The phase relationship of the P4 code is symmetrical with a parabolic distribution. The radar system's unambiguous target detection range is limited by the number of subcodes within the code period (code length). Increasing the code length to extend the unambiguous range results in a larger range-Doppler correlation matrix processor in the receiver, a longer compression time and an increase in the receiver's bulk memory requirements. In addition, the entire code period may not be returned from the target due to a limited time-on-target resulting in significant correlation loss. To significantly extend the unambiguous range beyond a single code period, this thesis explores the relationship between the polyphase codes (Frank and P4) and the number theoretic transforms (NTT) where the residues exhibit the same distribution as the polyphase values. The unambiguous range is extended from the number of subcodes within a single code period to the dynamic range of the transform without requiring a large increase in correlation processing. The dynamic range of a NTT is defined as the greatest length of combined phase sequences that contain no ambiguities or repeated paired terms. By transmitting $N \geq 2$ coprime code periods, the unambiguous range can be extended by considering the paired values from each sequence. A new Frank phase code formulation is derived as a function of the *residue number system* (RNS) where each residue corresponds to a phase value within the code period (modulus) sequence. Based on the symmetrical distribution of the P4 code, a new phase code expression is derived using both the *symmetrical number system* (SNS) and the *robust symmetrical number system* (RSNS). Here each phase value within the code period corresponds to a symmetrical residue. MATLAB simulations are used to verify the new expressions for the RNS, SNS and RSNS phase codes. Implementation considerations of the new approach are also addressed.

THIS PAGE INTENTIONALLY LEFT BLANK

TABLE OF CONTENTS

LIST OF FIGURES

LIST OF TABLES

THIS PAGE INTENTIONALLY LEFT BLANK

EXECUTIVE SUMMARY

The Frank phase code and the P4 phase code are often used in continuous wave (CW) polyphase modulation radar systems to detect the target's range due to their linear time-frequency characteristics as well as their low periodic ambiguity sidelobes. Both phase codes limit the unambiguous range R_u to within a single code period $T = N_c t_b$, where N_c is the number of subcodes and t_b is the subcode period. To extend the unambiguous detection range, the radar might simply increase the code period of the polyphase modulation signal. However, the longer code period requires a larger range-Doppler correlation matrix processor, an increase in the compression time, as well as an increase in the bulk memory in the receiver. Moreover, a significant amount of loss is incurred if the total number of code periods returned from the target is less than the number of reference code periods used in the compression process due, for example, to a limited time-on-target. A new set of waveform architectures that can solve these limitations is proposed in this thesis.

Number theoretic transforms (NTT) based on residue number systems are used in many digital signal processing applications to increase the amount of information available from various folding waveforms. With a set of $N \geq 2$ moduli, the paired integer residue terms from the transform sequences must be distinct (no ambiguities) throughout the entire dynamic range. The dynamic range of a NTT is defined as the greatest length of combined sequences of integers that contain no ambiguities or repeated paired terms. Consequently, the NTT residues within the dynamic range can be used to construct a low-power CW polyphase waveform that is useful for detecting targets beyond the single code period unambiguous range.

To significantly extend the unambiguous range beyond a single code period, this thesis explores the relationship between the polyphase codes (Frank and P4) and the NTT where the residues exhibit the same distribution as the polyphase values. The

unambiguous range is extended from the number of subcodes within a single code period to the dynamic range of the transform without requiring a large increase in correlation processing.

A new Frank phase code formulation is derived as a function of the *residue number system* (RNS) where each residue corresponds to a phase value within the code period (modulus) sequence. Based on the symmetrical distribution of the P4 code, a new phase code expression is derived using both the *symmetrical number system* (SNS) and the *robust symmetrical number system* (RSNS). Here each phase value within the code period corresponds to a symmetrical residue. MATLAB simulations are used to verify the new expressions for the RNS, SNS and RSNS phase codes. Implementation considerations of the new approach are also addressed.

The relationship between the Frank phase code and the RNS is developed based on their similar saw-tooth waveform distribution. A new equation using the RNS to derive the Frank phase code is formulated. This new phase code sequence is called the *residue-Frank phase code*. The periodic autocorrelation function (PACF) and the periodic ambiguity function (PAF) show that the new residue-Frank phase code formula gives exactly the same results as using the formula in the Frank phase code. Next, a set of $N = 3$ RNS coprime moduli [3 4 5] (with dynamic range $M_{RNS} = 60$) is chosen to examine the idea of extending the unambiguous range. A MATLAB program is used to plot the results for detecting two targets that lie in an ambiguous detection range bin if a single modulus is used. To solve the unambiguous range, the combined residues from N sequences are used. The result shows that the paired terms from both targets are different, meaning that both targets have different corresponding ranges. Thus, the residue-Frank phase code sequences can be used to extend the unambiguous detection range from $R_u = cT/2 = ct_b N_c/2$ to $R_{u,RNS} = ct_b M_{RNS}/2$ where c is the speed of light in free space. A block diagram of a polyphase CW radar system that uses the residue-Frank phase code is shown below in Figure 1.

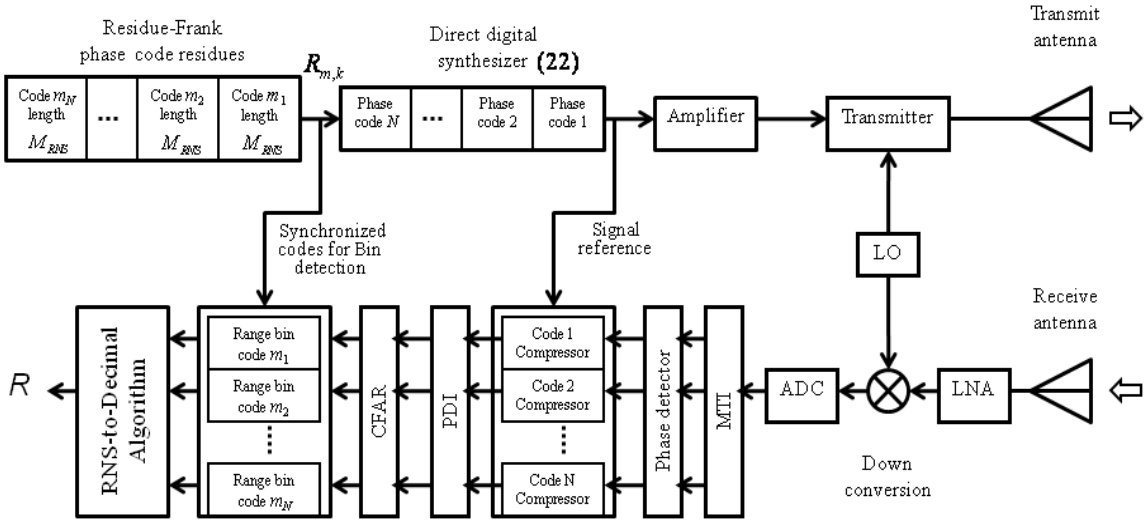

Figure 1. Block diagram of a CW polyphase radar system that uses a residue-Frank phase code.

The relationship between the P4 phase code and the SNS is developed based on their similar parabolic waveform distribution. A new equation using the SNS to derive the P4 phase code is formulated. This new phase code sequence is called the *symmetrical residue-P4 phase code*. The PACF and the PAF show that the symmetrical residue-P4 phase code formula gives the same results as using the formula in the P4 phase code. Then, the symmetrical residue-P4 phase code sequences using a set of $N = 3$ SNS coprime moduli [7 8 9] (with dynamic range $\hat{M}_{SNS} = 37$) are examined for the two targets located in an ambiguous range bin by using MATLAB programming. Similar to the residue-Frank phase code sequences, the result shows that the symmetrical residue-P4 phase code sequences can be used to extend the unambiguous detection range from $R_u = cT/2 = ct_b N_c/2$ to $R_{u,SNS} = ct_b \hat{M}_{SNS}/2$.

Reconstruction of the target's range from the paired RNS and SNS phase terms can contain inaccuracies when the incoming target range straddles two range bins. As a result, the recovered range of the target has a large error. To prevent the target range error, the RSNS is used. The paired terms from all N sequences in the RSNS when considered together change one at a time at each range bin subcode transition (integer Gray code property). This property makes the RSNS particularly attractive for controlling

the target range error. In this thesis, the relationship between the P4 phase code and the RSNS is also developed. A new equation using the RSNS to derive the P4 phase code is formulated. This new phase code sequence is called the *robust symmetrical residue-P4 phase code*. Within each P4 subcode, the phase shifts in the robust symmetrical residue-P4 phase sequences are repeated N times (equal to the number of moduli), resulting in the broader mainlobe for the PACF and the reduction of signal bandwidth as a function of N. The PACF and the PAF show that the robust symmetrical residue-P4 phase code formula gives similar results as using the formula for the P4 phase code. A MATLAB program is used to examine the abilities to extend the unambiguous range and to control the range bin errors by using a set of $N = 3$ RSNS coprime moduli [3 4 5] (with dynamic range $\hat{M}_{RSNS} = 43$). The results verify that the unambiguous range can be extended from $R_u = cT/2 = ct_b N_c/2$ to $R_{u,RSNS} = ct_b' \hat{M}_{RSNS}/2$ where t_b' is the subcode period in the RSNS phase code, and the range bin has an error of only one range bin.

In summary, all three NTT are investigated to show that they can be used to extend the unambiguous range. Also, the target range error from coding can be prevented by using the robust symmetrical residue-P4 phase code sequences. The use of these new derived phase sequences can be applied to CW radar systems in order to have a low probability of intercept characteristic given that the set of moduli and the radar signal parameters are chosen properly. The next step in this research is to investigate the performance of using various sets of coprime moduli, and the hardware implementation and testing of an actual system and is being proposed for future work.

ACKNOWLEDGMENTS

First and foremost, I would like to specially thank my parents and girlfriend, Ying, for their love, encouragement, and understanding. Their continued supports help me overcome any difficulties throughout my life. This thesis, one of the most challenging tasks I have encountered, would not be completed without them.

I would like to thank my advisors, Professor Phillip E. Pace and Professor David C. Jenn for their wise guidance through this process. Their incredible patience and assistance as I struggled through concepts and problems was valued and respected greatly. I have learned so much throughout my time at NPS.

Also, I would like to thank Mr. Matthias Wicht and his wife, Cdr. Peerapong and his family, and Mr. Paul D. Buczynski, who spent time sharing their valuable life experiences with me. Without them, I would be completely overwhelmed by the craziness of school.

Finally, I would like to thank the Royal Thai Navy for providing me an excellent opportunity to get a master's degree from NPS. My dream has been completed for studying at the great institution.

THIS PAGE INTENTIONALLY LEFT BLANK

I. INTRODUCTION

A. CONTINUOUS WAVE RADAR SYSTEMS USING POLYPHASE MODULATION

Continuous wave (CW) radar systems have a superior low probability of intercept (LPI) performance over pulse train radar systems due to their low average power transmitted (e.g., 1 W) and their use of pulse compression techniques. Note we extend the concept of pulse compression to unpulsed CW waveforms since the techniques are similar and the objectives are the same. Power management is also a benefit when a solid state phased array antenna is used. This enables the target return signal-to-noise ratio (SNR) to remain at a constant value within the radar receiver, thus lowering the transmitted power further as the range-to-target decreases. An LPI radar system is defined as a radar system that uses a special emitted waveform intended to detect targets as well as to prevent a non-cooperative intercept receiver from intercepting and detecting its emission [1]. On the other hand, pulsed radar systems require a relatively high peak power (e.g., 10 kW) to be transmitted to obtain the same probability of target detection. Consequently, the non-cooperative intercept range is significantly longer for the pulsed radars.

Since pure CW waveforms cannot resolve the target's range, periodic modulation techniques are used, such as frequency modulated CW (FMCW), frequency-shift keying (FSK), noise modulation, phase-shift keying (PSK), as well as hybrids of these techniques. The first step to designing CW radar systems that use periodic modulations for compression is to decide on the range resolution that is required. This in turn sets the transmitted bandwidth of the waveform for the above techniques (except for FSK where the range resolution is dependent on the duration of each frequency). Due to the advances in high-speed processing and direct digital synthesis modules [2], the use of PSK techniques in CW radar is highly advantageous. CW radars that transmit and receive PSK signals can result in LPI radar systems with small range resolution cells and are ideally suited for many sensor applications for situational awareness, including multiple-input multiple-output (MIMO) configurations.

Binary Barker phase coded sequences (1, –1) are one of the most popular PSK techniques in the design of pulse compression radar signals due to the aperiodic autocorrelation coefficients or time sidelobes being limited to $1/N_c$ (at zero Doppler) relative to a mainlobe level of one, where N_c is the number of subcodes used. The longest code length is $N_c = 13$ (or $N_c = 169$ for a compound code) [3]. These codes are not used in CW radar systems for LPI applications since they are very sensitive to Doppler shifts and can be easily detected by an intercept receiver that uses frequency doubling detection, which consists of multiplying the signal by itself and processing the result through an envelope detector.

Polyphase sequences are also of finite length with N_c subcodes and consist of discrete time complex values with constant amplitude but with a variable phase. Polyphase coding refers to phase modulation of the CW carrier with a polyphase sequence consisting of a number of discrete phase states with each phase corresponding to a subcode. The number of subcodes is taken from an alphabet of size $N_c \geq 2$, which is also the processing gain of the radar excluding any post detection integration. Increasing the number of phase values in the sequence allows the construction of longer sequences, resulting in a greater processing gain or compression ratio in the receiver (or equivalently a larger SNR). The code period is $T = N_c t_b$ where the size of each subcode t_b determines the 3 dB bandwidth of the waveform $B = 1/t_b$ and the range resolution $\Delta R = ct_b/2$. The unambiguous range is limited by the number of subcodes in the sequence as $R_u = N_c \Delta R$.

With a CW polyphase waveform, the matched filter in the receiver is a coherent, range-Doppler matrix correlation processor that performs a cross correlation between the received signal and a reference signal whose envelope is the complex conjugate of N_r code periods of the transmitted polyphase signal. The cross correlation output values are added together to reduce the ambiguity sidelobe levels. When the polyphase signals are returned and have an impressed Doppler shift, the correlation process used in the receiver compression operation is not perfect, resulting in a certain amount of correlation loss due to the phase shifts across the code period T.

Two of the most important PSK codes that are used in CW radar systems include the Frank code [4] and the P4 code [5]. The Frank code is a polyphase code that is derived from a step approximation to a linear FMCW waveform using M frequency steps and M samples per frequency, giving the number of subcodes or processing gain as $N_c = M^2$. The phase steps of the Frank code exhibit a saw-tooth folding waveform distribution. The peak sidelobe level (PSL) of a single compressed Frank code period is $PSL = 20\log_{10}(1/(M\pi))$. The P4 code consists of discrete phases of a linear chirp waveform taken at specific time intervals. It is derived by converting a linear FMCW to baseband using a local oscillator on one end of the frequency sweep and sampling the inphase and quadrature video at the Nyquist rate. The P4 phase steps exhibit a symmetrical parabolic distribution. The PSL of a single P4 compressed code period is $PSL = 20\log_{10}\sqrt{2/(N_c\pi^2)}$.

Although polyphase CW modulations can serve as a transmission waveform for a LPI radar system, there are several limiting factors. Most significantly, the unambiguous detection range of the waveform is limited by the number of subcodes (code length) as $R_u = N_c \Delta R$. By increasing the number of subcodes to extend the unambiguous range, a larger range-Doppler correlation matrix processor in the radar receiver is needed to provide the code compression. To lower the peak sidelobes, N_r copies of the phase code are used to compress the N_p returned code periods from the target. Consequently, the increased code length or processing gain requires a larger code compression time as well as an increase in the bulk memory requirements in the receiver. Further, a significant amount of correlation loss is incurred if the total number of code periods returned from the target N_p is less than the number of code periods N_r used in the correlation processor, as would be the case due to a limited time-on-target.

In this thesis, a novel relationship between the Frank code and the residue number system (RNS) is developed in order to significantly extend the unambiguous range beyond a single code period $T = N_c t_b$ while not having to increase the number of subcodes. In addition, due to the symmetrical distribution of the P4 polyphase code, the

unambiguous range is extended by developing a phase relationship based on symmetrical number systems; both the symmetrical number system (SNS) and the robust symmetrical number system (RSNS) are investigated. The phase relationships are constructed using these number theoretic transforms to extend the unambiguous range of the radar system by associating each phase subcode within the code period T with an integer sequence within a coprime modulus from the set $\{m_1, m_2, ..., m_N\}$. The paired integer terms from each polyphase sequence are unambiguous within the transform's dynamic range. The dynamic range is defined as the greatest length of combined phase sequences that contain no ambiguities or repeated paired terms. The dynamic range for the RNS is denoted M_{RNS} (Frank code). The dynamic range for the SNS is $\hat{M}_{SNS}$ (P4 code). The dynamic range for the RSNS is $\hat{M}_{RSNS}$ (P4 code).

For each case, the length of the dynamic range contains multiple code periods. In the radar receiver, the integer values within each modulus sequence correspond to the phase values from a phase detector [6]. The RNS phase sequence contains multiple Frank codes and extends the unambiguous target detection range from $R_u = cT/2 = ct_b N_c/2$ to $R_{u,RNS} = ct_b(\prod m_i)/2 = ct_b M_{RNS}/2$. The SNS phase sequence contains multiple P4 codes and extends the unambiguous target detection range beyond a single code period to $R_{u,SNS} = ct_b \hat{M}_{SNS}/2$. It is noted that the SNS also has a direct relationship with the discrete Fourier transform (DFT) and has been used to resolve frequency ambiguities in undersampling digital receivers [7]. Similarly, the unambiguous range using the RSNS is extended to $R_{u,RSNS} = ct_b' \hat{M}_{RSNS}/2$ where t_b' is the subcode period in the RSNS phase code.

Reconstruction of the target's range from the paired RNS and SNS phase terms can contain inaccuracies when the incoming target range straddles two range bins or subcodes. For example, if the target is straddling a range bin and a constant false alarm rate (CFAR) processor detects the target in the wrong subcode within a modulus sequence, the recovered range of the target will have a large error. This is shown to be the case for both the RNS and the SNS. Additional signal processing can be used to eliminate

these errors but adds additional complexity to the detection process. A more efficient method to eliminate the target range bin errors uses the RSNS. The RSNS is also a modular scheme; however, the paired terms from all N sequences, when considered together, change one at a time at each range bin subcode transition (integer Gray code property). Although the dynamic range of the RSNS is less than the SNS ($\hat{M}_{RSNS} < \hat{M}_{SNS}$), the RSNS integer Gray code property makes it particularly attractive for controlling the target range error. In summary, all three number theoretic transforms are investigated to determine the feasibility of extending the unambiguous range of the CW polyphase emitter.

B. PRINCIPAL CONTRIBUTIONS

The first step in this thesis was to understand the principles of CW phase modulation radar systems. This included the complex envelope representation of the transmitted signal and the related modulation parameters such as the code period, the subcode period, the number of subcodes within the code period, and the number of cycles of the carrier frequency per subcode. Their relationship to the signal bandwidth, the range bin size, the unambiguous detection range and the processing gain were also studied. Upon reception, the CW signal is compressed, and several code compression techniques were studied and modeled. To understand the receiver performance when a particular CW phase code is used, the periodic autocorrelation function and the periodic ambiguity function were examined. A MATLAB code was written to generate the CW phase coded signals and to call the periodic ambiguity function subroutines.

The next step in the thesis was to study the Frank polyphase code formulation and the phase distribution within a code period. Periodic ambiguity analysis was also performed to quantify the sidelobe levels within the receiver's ambiguity space (range offset – Doppler offset). Next the RNS was studied as a means to generate the Frank code since they both have sawtooth folding waveform representations. By using the RNS to create the Frank polyphase modulation, the unambiguous range of the code can be extended significantly beyond a single code period. A new expression to generate the Frank polyphase code was developed as a function of the coprime RNS moduli chosen.

By using two or more Frank code sequences that are relatively prime, the detected target residue from each sequence is combined within a system of congruences which can be solved in a straightforward manner using the Chinese Remainder Theorem (CRT). The solution is the target's unambiguous range. A MATLAB model was developed to simulate the new Frank polyphase modulation in order to verify the expression and determine the differences in phase values (if any) that might occur. Next a new CW radar signal processing algorithm was developed to transmit and receive the coprime Frank sequences to demonstrate the extension of the unambiguous range. The algorithm also addressed multiple targets within the field of view. Several examples were given to demonstrate the concept. To examine the practical considerations, a simulation of the transmit power versus required compression output SNR was performed in MATLAB for several values of coprime moduli.

Next, the P4 polyphase code was examined the relationships to the SNS and the RSNS. A new formulation of the P4 polyphase code as a function of the SNS and RSNS coprime moduli was developed. Analysis similar to that for the Frank code described above was performed to verify the new P4 expression. Finally, a summary of the different relationships that were developed is given and a comparison was performed.

C. THESIS OUTLINE

In Chapter II, the fundamentals of radar systems that use polyphase modulation are reviewed. In Chapter III, the Frank code and RNS are examined to extend the unambiguous range. In Chapter IV, the relationships between the P4 and the SNS are developed. In Chapter V, the relationships between the P4 and the RSNS are investigated to reduce the possibility of a range bin encoding error. Concluding remarks are offered in Chapter VI.

II. PRINCIPLES OF PHASE MODULATION RADAR

The idea of CW radar using phase modulation is reviewed in this chapter. First, the fundamentals and use of phase modulation in CW radar systems are explained. Next, the concepts of signal analysis and the technique used in the receiver's signal processing are presented. Also, the system equations for a phase modulation in CW radar are given in order to examine the signal's properties. These equations will be used to determine the new phase modulation code's performance in the following chapters.

A. CW PHASE MODULATION CONCEPTS

In Figure 1, the basic CW radar geometry is illustrated. First, the CW radar transmits the phase coded signal $s(t)$ to the target through the transmitting antenna. When the signal propagates to the target at a range R, it reflects back to the CW radar with different characteristics. For example, the signal's amplitude is less and the frequency is shifted in time in accordance with the relative movement between platforms along the line-of-sight ($V\cos\theta$ in Figure 1) or Doppler shift ν. The return signal $x(t)$ is then captured by the receiving antenna. In the radar system's receiver and digital signal processor, the compression processing output is used to detect and extract the target's characteristics.

In phase coded CW radar systems, the phase shifting operation is performed in the radar's transmitter, with the timing information generated from the receiver-exciter. The transmitted complex signal can be written as [1]

$$s(t) = Ae^{j(2\pi f_c t + \phi_k(t))} \tag{1}$$

where A is the signal amplitude, f_c is the carrier frequency, and $\phi_k(t)$ is the time dependent phase modulation code. The inphase I and quadrature Q representations of the complex signal from the transmitter can be represented as

$$I(t) = A\cos(2\pi f_c t + \phi_k(t)) \tag{2}$$

and

$$Q(t) = A\sin(2\pi f_c t + \phi_k(t)). \tag{3}$$

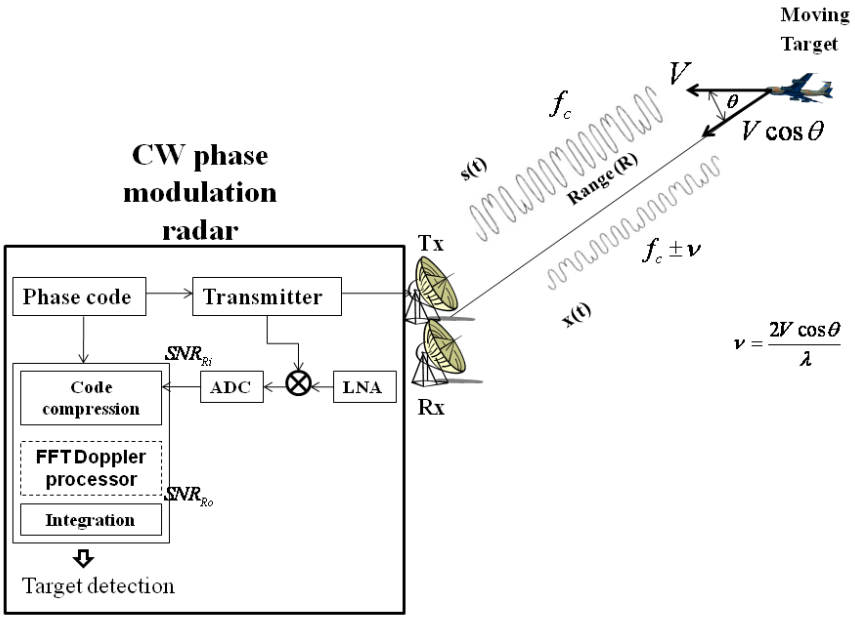

Figure 1. Geometry of CW radar using phase modulation codes to sample a moving target.

For one code period T, the CW signal is shifted in phase every subcode with each code period consisting of N_c subcodes. Each subcode with phase ϕ_k has a duration of t_b which is the subcode period. For a specific code sequence, the code period is

$$T = N_c t_b. \tag{4}$$

The transmitted signal can be expressed as

$$u_T = \sum_{k=1}^{N_c} u_k [t - (k-1)t_b] \tag{5}$$

for $0 \le t \le T$ and zero elsewhere. The complex envelope u_k is

$$u_k = e^{j\phi_k}. \tag{6}$$

If *cpp* is the number of cycles of the carrier frequency per subcode, the bandwidth B of the transmitted signal is

$$B = \frac{f_c}{cpp} = \frac{1}{t_b}. \tag{7}$$

To understand the concepts of phase modulation, a binary Barker phase code is examined [3]. In Figure 2, an example of one code period with $N_c = 7$ is shown. Here, the carrier frequency is $f_c = 1$ kHz, the subcode period $t_b = 1$ ms, and from (7) $cpp = 1$.

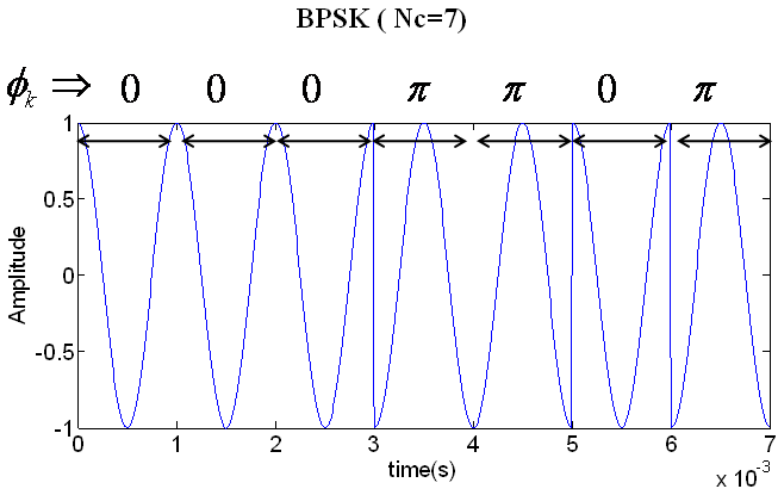

Figure 2. Phase coded signal with the Barker code $N_c = 7$, $A = 1$, $f_c = 1$ kHz, $t_b = 1$ ms.

The received return signal $x(t)$ from the target can be written as

$$x(t) = \eta A e^{j\{2\pi(f_c+\nu)(t-\tau)+\phi_k(t-\tau)\}} \tag{8}$$

where η is the amplitude attenuation coefficient of the received signal due to target scattering and propagation attenuation. The two-way roundtrip delay τ for a monostatic radar system is $\tau = 2R/c$, where c is the speed of light in free space. The Doppler frequency ν due to the target motion is $\nu = 2V\cos(\theta)/\lambda$ where λ is the signal wavelength and V is the target velocity.

B. CODE COMPRESSION OF RECEIVED SIGNAL

Code compression (CC) is a signal processing technique designed mainly to minimize the range resolution cell and increase the SNR of the returned signal. The idea of CC is similar to that in signal correlation in pulse train radar. As shown in Figure 3a, the CW radar repeats the phase sequence every code period T. A similar pulse train

signal would also have a pulse repetition interval PRI = T. Referring to Figure 3b, if the pulse width τ_{pw} of the pulse train signal is equal to the width of the subcode period t_b in the CW phase coded signal, the output's mainlobe from both correlator and compressor would have the same duration ($2\tau_{pw} = 2t_b$). These CC peaks represent the targets if the peaks are higher than the threshold desired in a constant false alarm rate (CFAR) process.

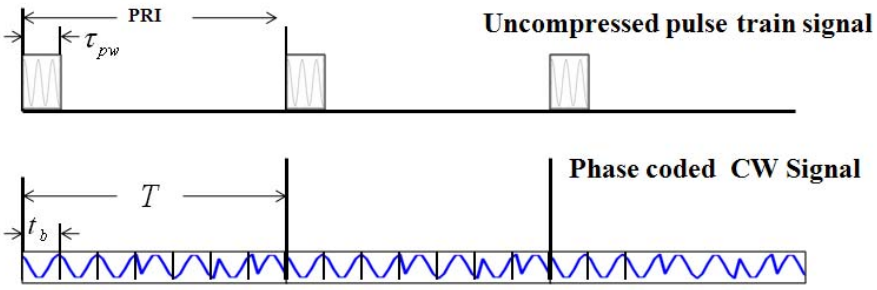

(a)

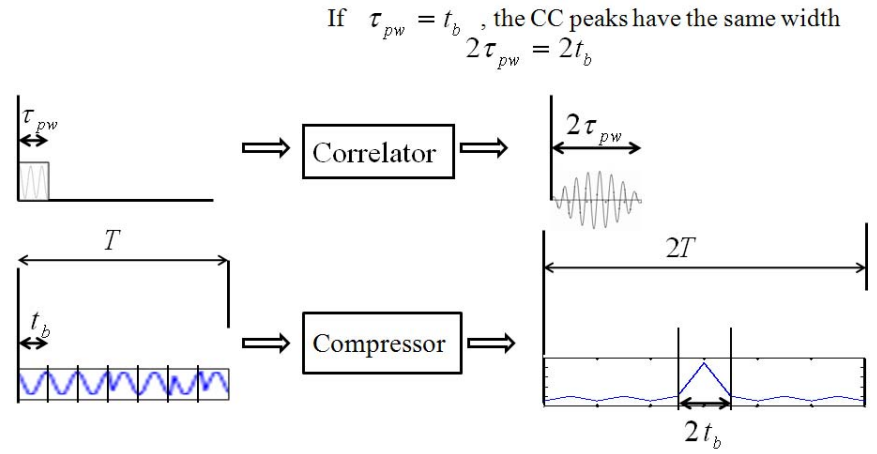

(b)

Figure 3. The relationship between uncompressed pulse train and phase-coded CW signal for (a) Transmitted signal, and (b) The output of the signal processed in the receiver.

The phase-coded signal is transmitted to detect the target at a range R. When reaching the target, the reflected signal returns to the radar. At the radar receiver, the phase coded return signal is correlated with the reference phase code. This is achieved by convolving the incoming signal's phase code with a conjugated and time-reversed version of the transmitted signal's phase code. This operation can be done either in the

digital or analog domain. Many digital signal processing architectures have been proposed for fast correlation using fast Fourier transforms. If no compression loss is present, the correlated output will give a very narrow pulse width at the compression output for the detected target. The correlation output is then sent to a target detection process such as a constant false alarm rate processor. If there is any alteration of the return signal's phase (for example from a Doppler shift or a less than adequate bandwidth in the receiver $B < 1/t_b$), a certain degree of correlation loss occurs.

The received waveform from the target is digitized and correlated using a phase code compressor. The range-Doppler correlation matrix can contain a cascade of N_r sets of N_c reference coefficients to improve the sidelobe structure. In Figure 4, the range-Doppler correlation matrix receiver for zero Doppler offset is illustrated. Here, the received signal consists of N_p code periods, each of which has N_c subcodes. The return signal is first processed by a filter matched to a rectangular subcode of length t_b, followed by a phase detector that sends forward the phase values. The detected output signal is then sent through a tapped delay line where each delay D is t_b. As the signal progresses through the tapped delay line, it is multiplied by the reference signal. At each step, the multiplication for each delay is summed separately for each of the N_r reference code periods. To reduce the sidelobe structure, a weighting function C_i can also be added [8]. To compute the entire range-Doppler ambiguity function, the correlation outputs from each subcode are multiplied by $q^k = e^{j2\pi k\Delta\nu t_b}$ for $\nu = \Delta\nu$ where k ranges from 0 to $N_r N_c - 1$. For $\nu = 2\Delta\nu$, the output of the previous $\nu = \Delta\nu$ operation are again multiplied by $q^k = e^{j2\pi k\Delta\nu t_b}$ and so on for the entire ambiguity space [9].

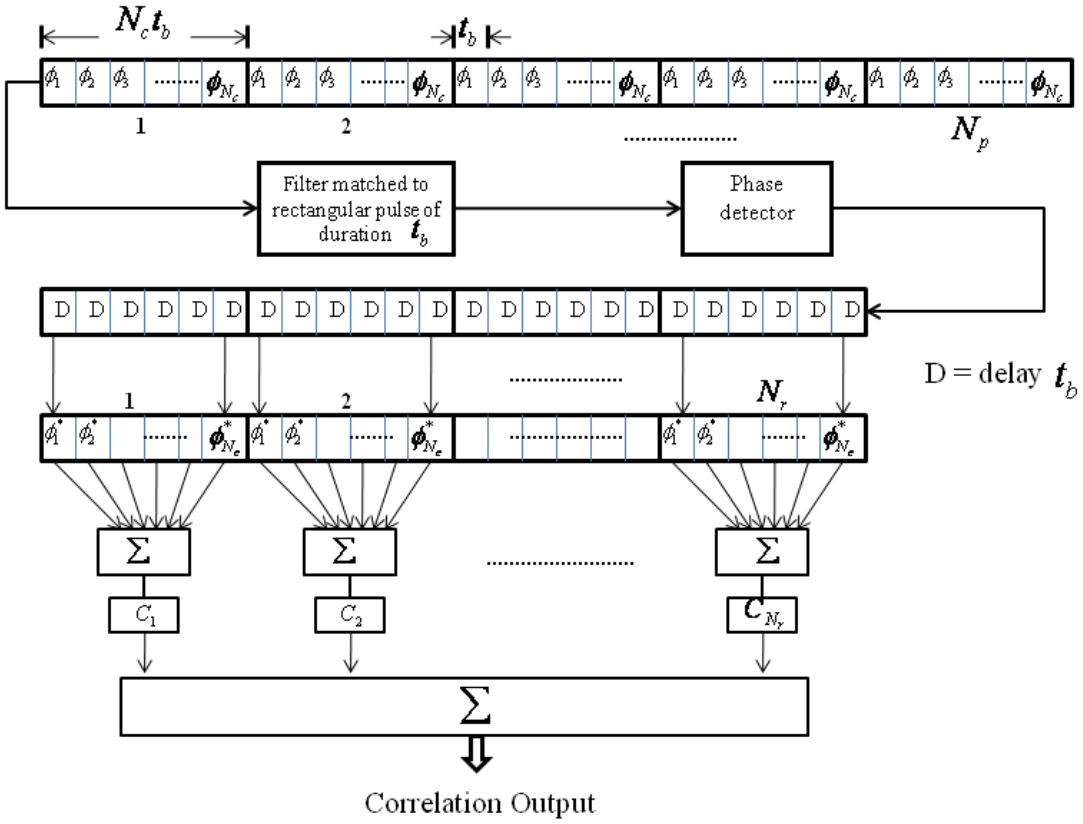

Figure 4. Correlation receiver matched to N_r periods of a transmitted polyphase code for $\nu = 0$ (After [9]).

In Figure 5, an illustration of the code compression for CW binary Barker code with $N_c = 7$ is shown. The radar receives the returned Barker sequence with the number of code periods $N_p = 3$. The number of reference code periods used in the receiver is $N_r = 1$. The receiver starts compressing the first returned code T_1 at $\tau = 0$, giving the correlation output peak at a normalized delay of $\tau / t_b = 0$ representing the detected target. At each step in the compression, the returned signal is shifted one subcode period $\tau = t_b$. When the returned code is shifted by one code period T, the correlation output gives another peak value due to the second code T_2 being compressed at a normalized delay of $\tau / t_b = 7$. The last peak from the third code T_3 compressed is also shown at a normalized delay offset of $\tau / t_b = 14$. That is, the peak value for the detected target

repeats every code period T. Generally, the width of the PACF mainlobe is $2t_b$. To be able to distinguish between two targets close to one another, the pulses have to be separated by at least $\tau = t_b$ period (which is defined as the range resolution cell).

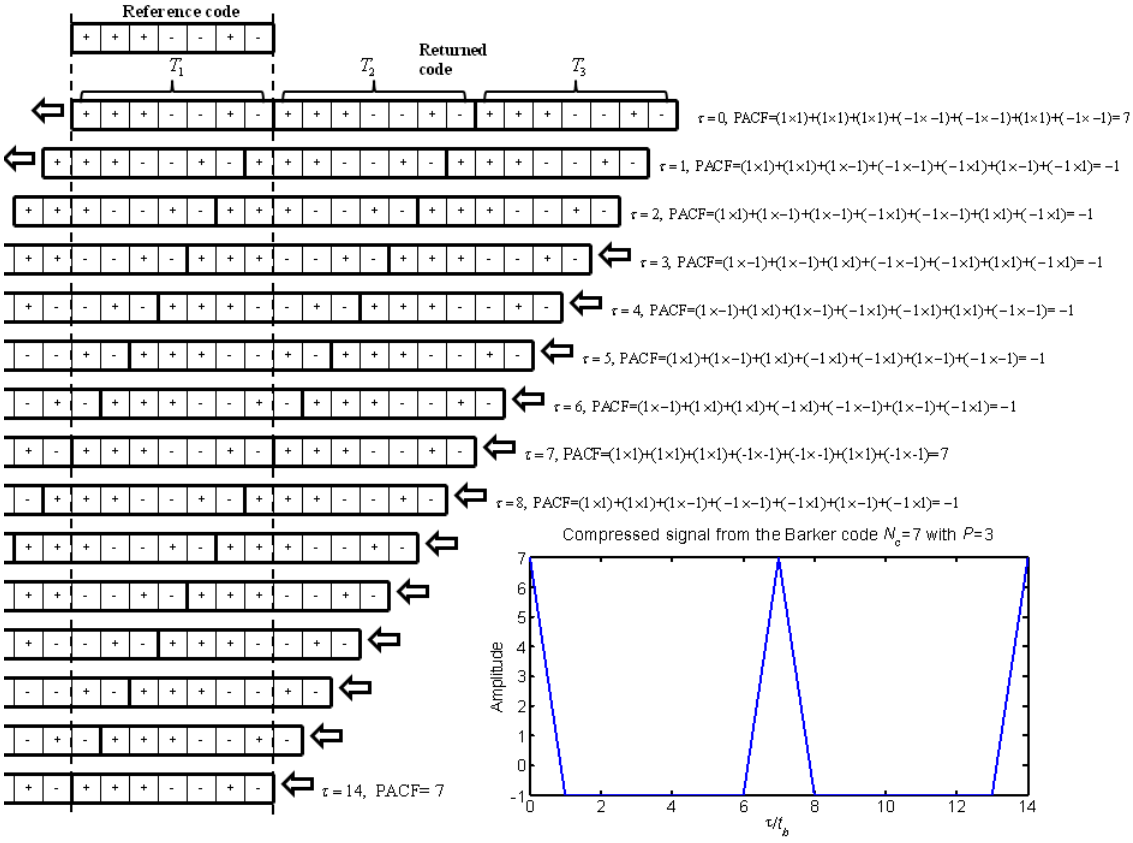

Figure 5. Example of code compression in CW Barker code $N_c = 7$ and $N_p = 3$.

In summary, the unambiguous range of a specific CW phase-coded sequence is

$$R_u = \frac{cT}{2} = \frac{cN_c t_b}{2} \tag{9}$$

and the range resolution for one transmitted polyphase signal is

$$\Delta R = \frac{ct_b}{2}. \tag{10}$$

Another important parameter in pulse compression is the pulse compression ratio (PCR) or time-bandwidth product. This is also referred to as the radar's processing gain

(PG) and is the preferred term in this thesis. In general, the higher the PG, the higher the SNR improvement in the signal processing step. The radar signal processing input SNR is SNR_{Ri} and the radar signal processing output SNR is SNR_{Ro} (see Figure 1). They are related to the processing gain of the signal processor by

$$PG = \frac{SNR_{Ro}}{SNR_{Ri}}. \tag{11}$$

For a polyphase code, the PG is equal to the time-bandwidth product or the number of subcodes as

$$PG = T(1/t_b) = (N_c t_b)/t_b = N_c. \tag{12}$$

In the Barker code $N_c = 7$ example, the processing gain is 7. For a carrier frequency f_c, narrowing the subcode period t_b enables the transmitted signal to be spread over a larger bandwidth. Also, increasing the number of subcodes N_c, the correlation output sidelobes can be decreased significantly while providing a larger PG. This comes at the expense of a larger range-Doppler correlation matrix processor in the receiver. In addition, a longer compression time and an increase in the size of the bulk memory is required.

The signal processing function used for the compression is the autocorrelation function (ACF). For CW radars, the compression is accomplished with a *periodic* autocorrelation function (PACF). Also, the periodic ambiguity function (PAF) is used to show the delay-offset versus frequency-offset in the receiver and shows the resulting sidelobe structure. This is especially useful for monitoring the ambiguity space for secondary targets that might hide in the sidelobe structure. Note that the zero Doppler cut of the PAF is the PACF [1].

C. PERIODIC AUTOCORRELATION FUNCTION

It is important that in order to achieve high range resolution for a polyphase code sequence, the coded signal has to have a noise-like PACF property, close to an impulse function. The ACF is used for signals of finite energy. For a CW polyphase code

sequence with the number of phase codes N_c, subcode duration t_b, and a code period $T = N_c t_b$, a periodic complex envelope $u(t)$ is given by [1]

$$u(t) = u(t + nT) \tag{13}$$

for $n = 0, \pm 1, \pm 2, \pm 3, \ldots$. The values of the PACF as a function of the delay r (which are the multiples of t_b) are given by

$$R(rt_b) = \frac{1}{N_c} \sum_{n=1}^{N_c} u(n) u^*(n + r). \tag{14}$$

Ideally, a perfect periodic autocorrelation function (zero-sidelobe) is desired where $R(rt_b) = 1$ when $r \equiv 0 \pmod{N_c}$, and $R(rt_b) = 0$ when $r \neq 0 \pmod{N_c}$. Since the CW signal is continuous, a perfect periodic autocorrelation function can be achieved.

In Figure 6a, the ACF output for a $N_c = 7$ Barker code is plotted (in dB) with no noise using $f_c = 1$ kHz, $f_s = 7$ kHz, $cpp = 1$ and $N_r = 1$ using the MATLAB m-file (amfbn7.m) [11]. The highest peak mainlobe is at the zero time delay. The width of the mainlobe is equal to the length of the subcode t_b. For the Barker code, it is found that the PSL is equal to $-20\log_{10}(N_c) = -17$ dB. The PACF in Figure 6b shows that the peak is repeated every code period $T = N_c t_b$ at the value of 7. Also note from (14) that the CW binary Barker code is not a perfect code.

(a)

(b)

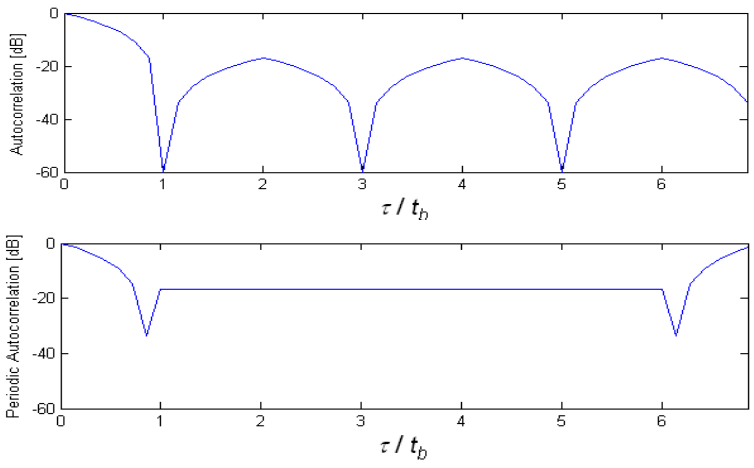

Figure 6. Normalized correlation output of Barker code sequence $N_c = 7$ and $N_r = 1$ for (a) ACF and (b) PACF.

Today, many studies on PSK show that the PSL of the phase-coded sequences can be reduced by choosing a proper phase coding. Moreover, there are CW polyphase codes able to achieve a zero sidelobe (perfect codes).

D. PERIODIC AMBIGUITY FUNCTION

In a realistic environment, the returned signal will be shifted in frequency if the target is moving relative to the radar's antenna beam axis (Doppler effect). The PAF is an important tool to assess the response of a correlation receiver. In pulsed radar analysis, the ambiguity function $\chi(\tau,\nu)$ is a two-dimensional function of time delay offset τ and Doppler frequency offset ν showing the correlation between the returned signal and the receiver matched filter. For the finite duration signal, the ambiguity function (AF) is determined by the properties of the pulse and the matched filter. If $u(t)$ is the complex envelope of both the transmitted signal and received signal, the AF is given by [10]

$$\left|\chi(\tau,\nu)\right| = \left|\int_{-\infty}^{\infty} u(t)u^*(t-\tau)e^{j2\pi\nu t}dt\right| \tag{15}$$

where * denotes the complex conjugate. A target further from the radar than the reference ($\tau = 0$) position will correspond to positive τ. A positive ν implies a target moving toward the radar.

A more concise way of representing the ambiguity function consists of examining the one-dimensional zero-delay and zero-Doppler cuts; that is, $\chi(0,\nu)$ and $\chi(\tau,0)$, respectively. The matched filter output as a function of a time (the signal one would observe in a radar system) is a delay cut, with constant frequency given by the target's Doppler shift $\chi(\tau,\nu)$. Ideally, the ambiguity diagram should show the diagonal ridge centered at the origin and zero elsewhere, no ambiguity.

The PAF, introduced by Levanon and Freedman [11], describes the response of a correlation receiver to a CW signal modulated by a periodic waveform with period T, when the reference signal is constructed from an integral number N_r of periods of the transmitted signal (coherent processor length N_rT). The target illumination time (dwell time) N_pT must be longer than N_rT. As long as the delay τ is shorter than the

difference between the dwell time and the length of the reference signal $0 \le \tau \le (N_p - N_r)T$, the illumination time can be considered infinitely long and the receiver response can be described by the PAF given as [8]

$$\left|\chi_{N_r,T_r}(\tau,\nu)\right| = \left|\frac{1}{N_r T_r}\int_0^{N_r T_r} u(t-\tau)u^*(t)e^{j2\pi\nu t}dt\right|. \tag{16}$$

(a)

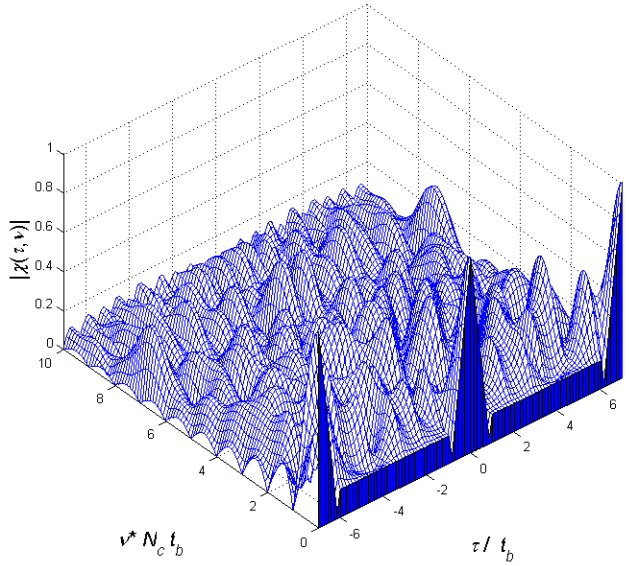

(b)

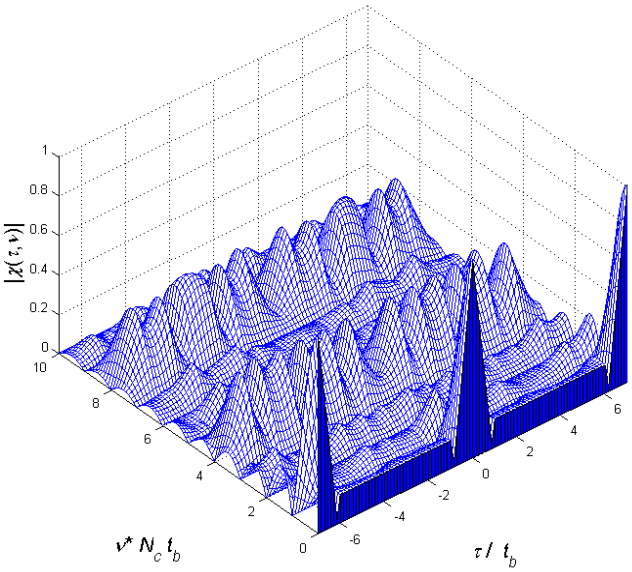

Figure 7. PAF of Barker code $N_c = 7$ with (a) $N_r = 1$ and (b) $N_r = 4$.

In Figure 7a, the PAF of the Barker code $N_c = 7$ with $N_r = 1$ is plotted using MATLAB m-file (amfbn7.m) from [10]. Also, the PAF of the Barker code $N_c = 7$ with $N_r = 4$ is plotted in Figure 7b. By increasing N_r, the Doppler sidelobes have been significantly lowered.

In the next chapter, the PACF and PAF are used to characterize the CW Frank code. The residue number system is introduced and a relationship to the Frank code is developed.

Since there are many variables used throughout this thesis, all of important variables are listed in the Appendix to provide unambiguous meanings.

III. FRANK POLYPHASE MODULATION AND THE RESIDUE NUMBER SYSTEM

In this chapter, the Frank phase code and the residue number system (RNS) are introduced. Their relationship is presented.

A. FRANK PHASE CODE

The Frank code is derived from a step approximation to a linear frequency modulation waveform using M frequency steps and M samples per frequency [4]. If i is the sample number in a given frequency and j is the frequency number, the phase of the ith sample of the jth frequency is given by

$$\phi_k = \phi_{i,j} = \frac{2\pi}{M}(i-1)(j-1) \tag{17}$$

where k is the time index for a single phase change per subcode and it ranges from 1 to M^2, and $i, j = 1, 2, ..., M$.

The phase values and the phase values modulo 2π of the Frank code for $M = 8,\ N_c = 64$ are shown in Figures 8 and 9, respectively. The carrier frequency is $f_c = 1$ kHz, the sampling frequency is $f_s = 7$ kHz, and the number of carrier cycles per subcode is $cpp = 1$. The ACF and the PACF are shown in Figure 10 where N_r is the number of reference code periods in the receiver. The delay axis is normalized by the subcode period t_b. Note from Equation (14) and Figure 10b that the Frank code is a perfect code. The PSL is $PSL = 20\log\left(1/(M\pi)\right)$ or -28 dB. The PAF in Figure 11 shows the delay-offset and Doppler-offset sidelobes. Note that the Doppler tolerance is reflected in the way the sidelobes are arranged about the mainlobe. The study on Doppler tolerance is presented in [5] and [12].

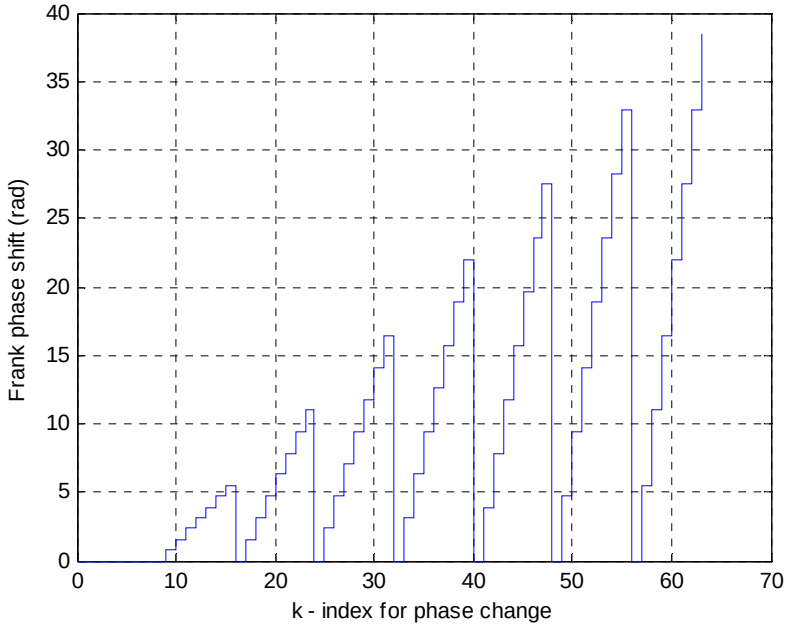

Figure 8. Frank code modulation for $M = 8, N_c = 64$ (From [1]).

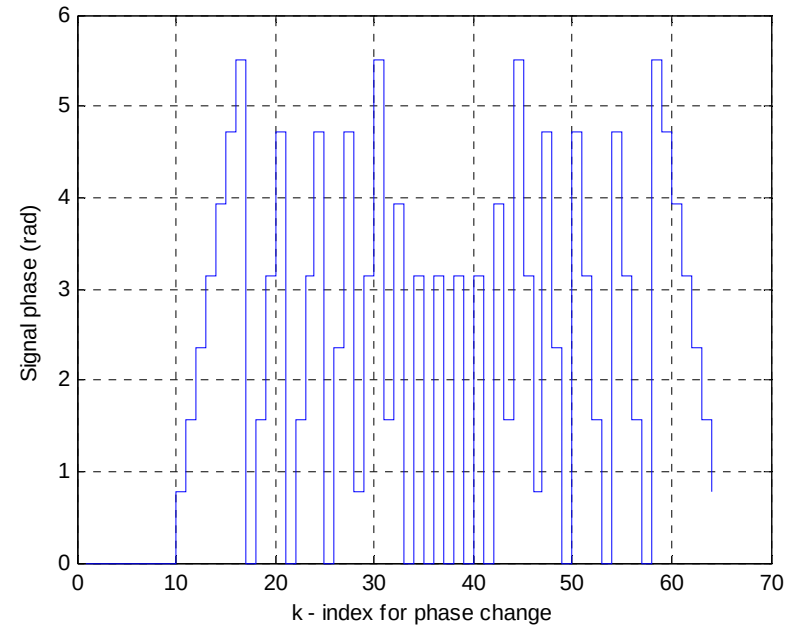

Figure 9. Signal phase (radians) modulo 2π versus k-index for phase change of the Frank code with $M = 8, N_c = 64$ (From [1]).

(a)

(b)

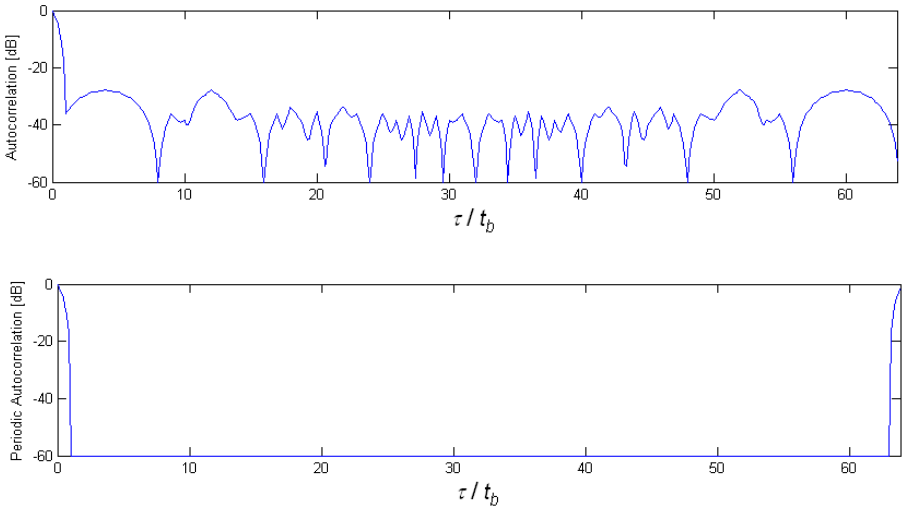

Figure 10. ACF (a) and PACF (b) for the Frank code with $M = 8$, $cpp = 1$, and $N_r = 1$ (From [1]).

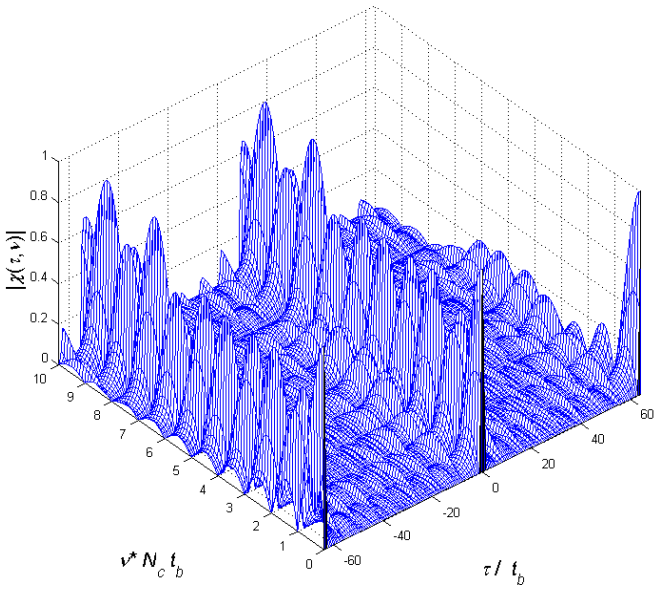

Figure 11. PAF for the Frank code modulation with $M = 8$, $cpp = 1$, and $N_r = 1$ (From [1]).

B. THE RESIDUE NUMBER SYSTEM

The RNS was introduced by Szabo [13]. It has been established as an important tool in parallel processing applications and high speed computations [14]–[16]. The RNS can serve as a source for extending the unambiguous range by decomposing the unambiguous range into a number of parallel sub-ranges (moduli) that have a smaller number of subcodes. Each sub-range for a different coprime modulus requires only a code period in accordance with that modulus. A much larger unambiguous range is achieved after the results of these smaller sub-range operations are recombined. Thus, by developing a relationship between the RNS, the polyphase distributions within the Frank code period, and the target detection processing, the extension of the unambiguous range beyond a single code period is feasible.

The RNS residue distribution is based on a saw-tooth folding waveform, where the discrete residue values rise gradually and fall quickly as the input value rises gradually (i.e., in mod 5 the succession of discrete values for an increasing input is 0, 1, 2, 3, 4, 0, 1, 2, 3, …). A single RNS sequence can be generated as

$$a \equiv R_m (\mathrm{mod}\, m) \tag{18}$$

where $0 \le R_m < m$, m is the modulus, and R_m is the residue of a modulo m. The integer values R_m within each modulus sequence are

$$R_m = [0,1,...,m-1,] \tag{19}$$

and are representative of the saw-tooth folding waveform. The sequence is repeated in both directions forming a periodic sequence with the period

$$P_{RNS} = m. \tag{20}$$

Given a set of RNS coprime moduli, a complete residue number system is formed. A set of integers $y_0, y_1, \ldots, y_{m-1} (\mathrm{mod}\, m)$ form a complete residue system if $y_g \equiv g (\mathrm{mod}\, m)$ for $g = 0,1,\ldots,m-1$. The dynamic range M_{RNS} of the RNS is the number of paired terms from the sequence of values that contain no ambiguities and is

$$M_{RNS} = \prod_{i=1}^{N} m_i \tag{21}$$

where m_i is the ith coprime modulus and $N \geq 2$ is the number of moduli, $1 \leq i \leq N$. In Figure 12, an RNS example for $N = 2$ moduli, $m_1 = 4$ and $m_2 = 5$, is shown. Note the stair step relationship of the residues.

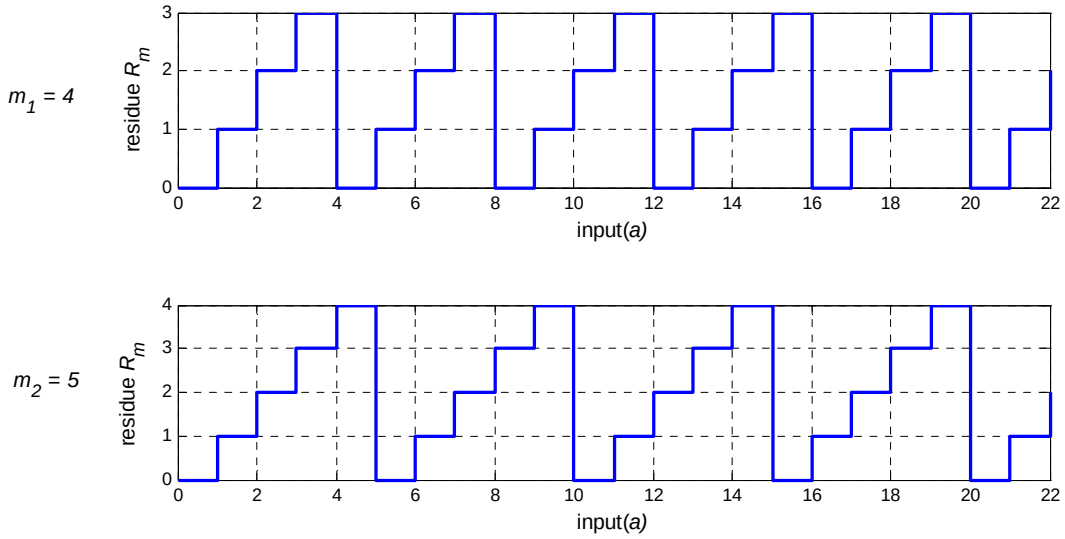

Figure 12. The RNS residue folding waveforms for $m_1 = 4$ and $m_2 = 5$.

From Equation (21), for $m_1 = 4$ and $m_2 = 5$, the dynamic range is $M_{RNS} = 20$. In Table 1, the two sequences are shown along with the input a. Starting at $a = 0$, the total number of distinct paired terms is 20, $0 \leq a \leq 19$. The index value $l = a + 1$ in Table 1 is shown to count the integer number of distinct paired terms within the dynamic range.

Table 1. Finding the RNS dynamic range for $m_1 = 4$ and $m_2 = 5$.

Input(a)	0	1	2	3	4	5	6	7	8	9	10	11	12	13	14	15	16	17	18	19	20	21	22
$m_1 = 4$	0	1	2	3	0	1	2	3	0	1	2	3	0	1	2	3	0	1	2	3	0	1	2
$m_2 = 5$	0	1	2	3	4	0	1	2	3	4	0	1	2	3	4	0	1	2	3	4	0	1	2
l	1	2	3	4	5	6	7	8	9	10	11	12	13	14	15	16	17	18	19	20			

C. RESIDUE-FRANK PHASE CODE

The RNS residues $R_{m,k}$ can be folded into the Frank phase code sequence by associating $R_{m,k}$ with the Frank subcode phases. The phase index k starts from 1 to N_c, where N_c is the number of subcodes within one code period. The residue-Frank phase code sequence from modulo m is given by

$$\phi_{m,k} = \frac{2\pi}{m}\left\lfloor \frac{k-1}{m} \right\rfloor R_{m,k} \tag{22}$$

where $k = 1, 2, 3, ..., m^2$ is the phase index for each phase change, and $\lfloor x \rfloor$ indicates the greatest integer less than or equal to x. In Equation (22), the number of subcodes within one code period is $N_c = m^2$. For example, if we choose $m = 4$, $N_c = 16$, the RNS folding waveform becomes $R_{m=4,k=1,2,...,16} = \{0, 1, 2, 3, 0, 1, 2, 3, 0, 1, 2, 3, 0, 1, 2, 3\}$.

Next, the phase sequences from equations (17) and (22) are compared. For Equation (22), the parameters used to calculate the residue-Frank phase code sequence are $m = 4$, $m^2 = 16$ with $R_{m=4,k=1,2,...,16} = \{0, 1, 2, 3, 0, 1, 2, 3, 0, 1, 2, 3, 0, 1, 2, 3\}$. For the Frank code from Equation (17), the parameters are $M = 4$, $N_c = 16$ with $i, j = 1, 2, 3, 4$. In Table 2, the phase code sequences are shown for comparison.

The phase code sequences of both waveforms are identical. The ACF, PACF, and PAF of the CW waveform generated by Equation (22) with $m = 8$, $N_c = 64$ are also identical to those shown in Figures 10 and 11, which were generated by Equation (17) with $M = 8$, $N_c = 64$.

Table 2. Comparison of the residue-Frank phase code sequence ($m = 4$) with the Frank phase code sequence ($M = 4,\ N_c = 16$).

Time index	Residue-Frank phase code (22)			Frank phase code (17)		
(k)	$R_{m=4,k}$	$\left\lfloor \frac{k-1}{m} \right\rfloor$	$\phi_{m=4,k}$ (rad)	i	j	$\phi_k = \phi_{i,j}$ (rad)
1	0	0	$\phi_1=\frac{2\pi}{4}\cdot 0\cdot 0=0$	1	1	$\phi_{1,1}=\frac{2\pi}{4}0\cdot 0=0$
2	1	0	$\phi_2=\frac{2\pi}{4}\cdot 1\cdot 0=0$	2	1	$\phi_{2,1}=\frac{2\pi}{4}1\cdot 0=0$
3	2	0	$\phi_3=\frac{2\pi}{4}\cdot 2\cdot 0=0$	3	1	$\phi_{3,1}=\frac{2\pi}{4}2\cdot 0=0$
4	3	0	$\phi_4=\frac{2\pi}{4}\cdot 3\cdot 0=0$	4	1	$\phi_{4,1}=\frac{2\pi}{4}3\cdot 0=0$
5	0	1	$\phi_5=\frac{2\pi}{4}\cdot 0\cdot 1=0$	1	2	$\phi_{1,2}=\frac{2\pi}{4}0\cdot 1=0$
6	1	1	$\phi_6=\frac{2\pi}{4}\cdot 1\cdot 1=\frac{\pi}{2}$	2	2	$\phi_{2,2}=\frac{2\pi}{4}1\cdot 1=\frac{\pi}{2}$
7	2	1	$\phi_7=\frac{2\pi}{4}\cdot 2\cdot 1=\pi$	3	2	$\phi_{3,2}=\frac{2\pi}{4}2\cdot 1=\pi$
8	3	1	$\phi_8=\frac{2\pi}{4}\cdot 3\cdot 1=\frac{3\pi}{2}$	4	2	$\phi_{4,2}=\frac{2\pi}{4}3\cdot 1=\frac{3\pi}{2}$
9	0	2	$\phi_9=\frac{2\pi}{4}\cdot 0\cdot 2=0$	1	3	$\phi_{1,3}=\frac{2\pi}{4}0\cdot 2=0$
10	1	2	$\phi_{10}=\frac{2\pi}{4}\cdot 1\cdot 2=\pi$	2	3	$\phi_{2,3}=\frac{2\pi}{4}1\cdot 2=\pi$
11	2	2	$\phi_{11}=\frac{2\pi}{4}\cdot 2\cdot 2=2\pi$	3	3	$\phi_{3,3}=\frac{2\pi}{4}2\cdot 2=2\pi$
12	3	2	$\phi_{12}=\frac{2\pi}{4}\cdot 3\cdot 2=3\pi$	4	3	$\phi_{4,3}=\frac{2\pi}{4}3\cdot 2=3\pi$
13	0	3	$\phi_{13}=\frac{2\pi}{4}\cdot 0\cdot 3=0$	1	4	$\phi_{1,4}=\frac{2\pi}{4}0\cdot 3=0$
14	1	3	$\phi_{14}=\frac{2\pi}{4}\cdot 1\cdot 3=\frac{3\pi}{2}$	2	4	$\phi_{2,4}=\frac{2\pi}{4}1\cdot 3=\frac{3\pi}{2}$
15	2	3	$\phi_{15}=\frac{2\pi}{4}\cdot 2\cdot 3=3\pi$	3	4	$\phi_{3,4}=\frac{2\pi}{4}2\cdot 3=3\pi$
16	3	3	$\phi_{16}=\frac{2\pi}{4}\cdot 3\cdot 3=\frac{9\pi}{2}$	4	4	$\phi_{4,4}=\frac{2\pi}{4}3\cdot 3=\frac{9\pi}{2}$

D. RESOLVING RANGE AMBIGUITIES USING N RESIDUE-FRANK PHASE CODE SEQUENCES

1. Block Diagram of the Residue-Frank Radar System

To extend the unambiguous detection range, $N \geq 2$ coprime moduli are used with Equation (22) to generate the residue-Frank phase code sequences necessary to modulate the CW frequency. The block diagram of the radar using the residue-Frank phase code modulation is shown in Figure 13. In the transmitter, the first step is to generate and store the sequence values $R_{m,k}$ for each modulus. Then, a direct digital synthesizer uses each residue sequence $R_{m,k}$ to generate the $N_c = m^2$ subcodes $\phi_{m,k}$ according to Equation (22) for each modulus. Each subcode corresponding to $R_{m,k}$ has a length of t_b. Together the N_c subcodes have a code period of T. To detect the target's unambiguous range, each phase code sequence must have M_{RNS} subcodes. Each sequence is amplified and transmitted in succession.

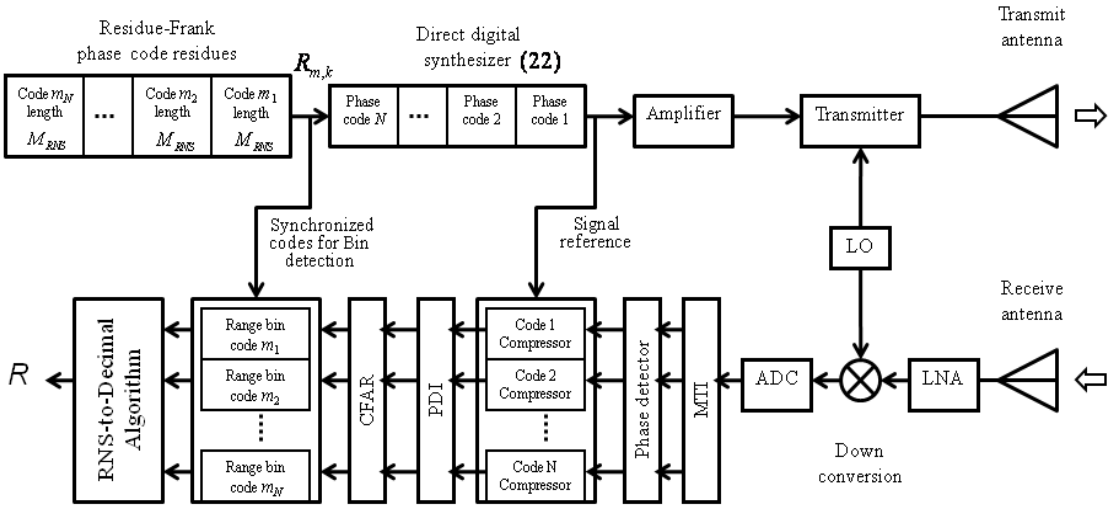

Figure 13. Block diagram for the radar using N residue-Frank phase code sequences.

Upon reception, the signal is amplified and downconverted to an intermediate frequency compatible with an available analog-to-digital (ADC) converter technology. The output of the ADC is processed by a moving target indication (Elliptic) filter to remove the clutter, and then a phase detector is used to determine the phase and

magnitude of each subcode. The output of the phase detector is processed by a phase code compressor which is followed by a noncoherent post-detection integration (PDI) process. The output of the PDI is sent to a constant false alarm rate processor to detect and save the range bin of the target for that modulus sequence. This series of steps is performed for each residue-Frank phase code sequence, and the detected target's range bin R_m is sent to a RNS-to-decimal algorithm to resolve the target's true range after all N residues R_m are obtained.

2. Transmitted and Reference Codes for Compression

In this section, the transmission of the set of N residue-Frank phase code sequences is discussed. The use of each phase code sequence as a reference sequence for code compression is discussed. An example using $N = 3$ moduli with $m_1 = 3,\ m_2 = 4,$ and $m_3 = 5$ is illustrated. The dynamic range from Equation (21) for these RNS moduli is $M_{RNS} = 3 \times 4 \times 5 = 60.$

The transmitted sequence for each modulus requires the number of subcodes equal to the dynamic range M_{RNS}. The transmitted signal is shown in Figure 14. For modulus $m_1 = 3,$ there are three residues within a code period (0, 1, 2). For the residue-Frank phase code period, the sequence has $N_c = m_1^2 = 3^2 = 9.$ To cover a dynamic range of $M_{RNS} = 60$ subcodes, the number of code periods required is

$$\hat{N}_{p,m} = \frac{M_{RNS}}{m^2}. \tag{23}$$

For $m_1 = 3,\ \hat{N}_{p,3} = 60/9 = 6.67$ code periods. The last 3 subcodes ($9 \times 7 - 60 = 3$) are not used since they are ambiguous.

For $m_2 = 4$ and $m_3 = 5,$ the number of subcodes N_c for each code period are $m_2^2 = 4^2 = 16$ and $m_3^2 = 5^2 = 25,$ respectively. Also, the maximum number of transmitted and received code periods are $\hat{N}_{p,4} = 3.75$ (the last 4 subcodes are not used) and

$\hat{N}_{p,5} = 2.4$ (the last 15 subcodes are not used), respectively. In Figure 14, the code period corresponding to each modulus is denoted as $T_{m_i,p}$ where p represents code period number. Note that the number of received code periods processed in the range-Doppler matrix N_r should be less than the number of code periods received N_p. That is $N_r < N_p \le \hat{N}_p$. Otherwise, a certain amount of correlation loss occurs.

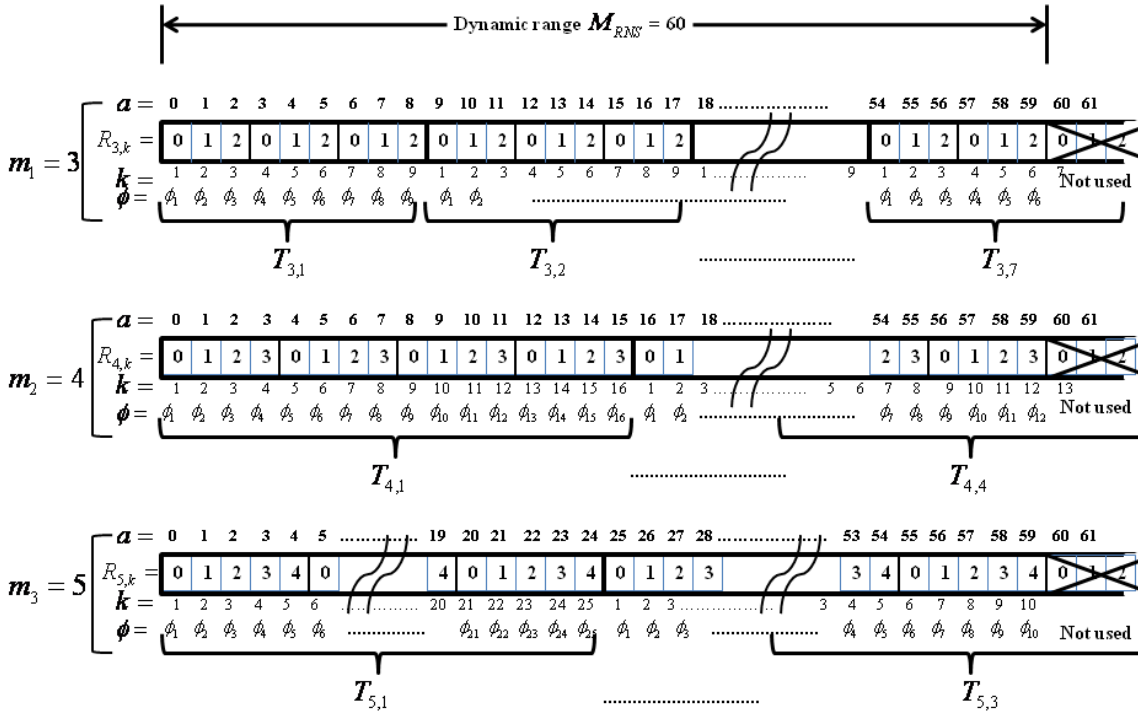

Figure 14. Illustration of transmitted signal using $N = 3$ residue-Frank phase code sequences for $m_1 = 3$, $m_2 = 4$, and $m_3 = 5$.

In Figure 15a, the residues $R_{m,k}$ for $m_1 = 3$, $m_2 = 4$, and $m_3 = 5$ ($M_{RNS} = 60$) are shown with $R_{m,k} = R_{m,k+nm^2}$ where $n \in \{0, \pm 1, \pm 2, ...\}$. The residue-Frank phase sequences $\phi_{m,k}$ from each modulus are shown in Figure 15b. Each phase code sequence has a length $N_c = m^2$, giving $\phi_{m,k} = \phi_{m,k+nm^2}$. If the receiver uses one code period as a reference ($N_r = 1$), the reference code sequence for compression has a phase sequence from index $k = 1$ to m^2.

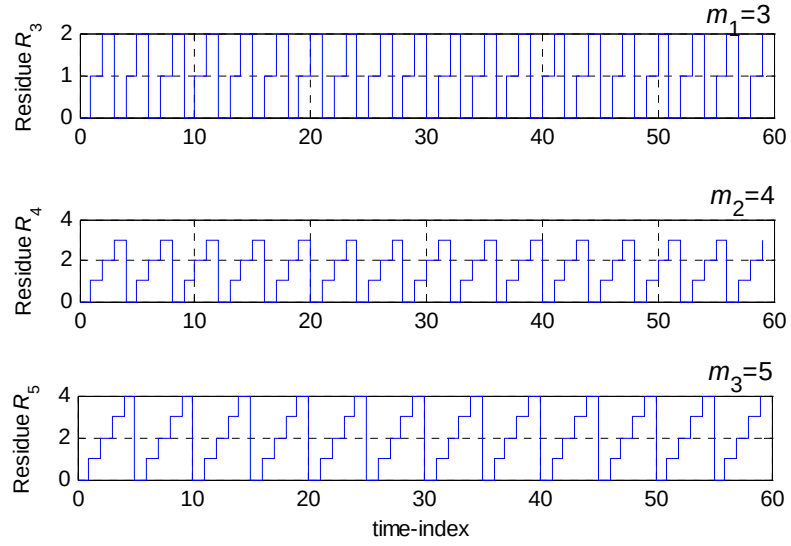

(a)

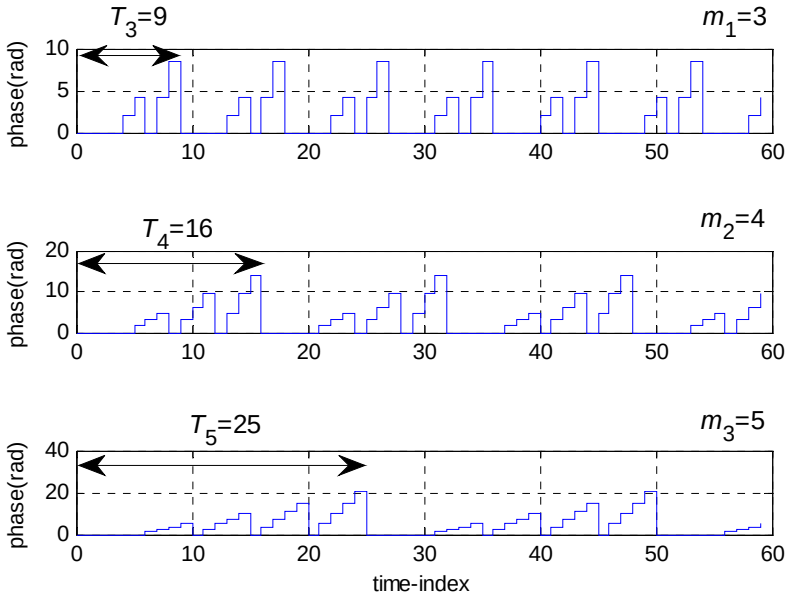

(b)

Figure 15. Plot of the residue-Frank phase code sequence for $m_1 = 3$, $m_2 = 4$, and $m_3 = 5$ ($M_{RNS} = 60$) showing (a) residues, and (b) phase sequences from (22).

In Figure 16, the compression and range bin detection process is illustrated for $m_1 = 3$ and $N_r = 1$. The residue-Frank phase code sequence is returned to the radar receiver with delay τ and then processed by a filter matched to a rectangular pulse of

duration t_b. The phase detector is used to calculate the phase of the signal which is passed to the compressor. The output from the compression is then processed by the threshold detection to see whether the amplitude reaches the desired minimum value. The compressor processes a single compression delay within a sampling period t_s. If the threshold detector detects the pulse, the presence of the target will be saved and associated with residue R_m. Each delay D_l has a duration of t_b (e.g. D_1 is for the time delay between 0 to t_b, D_2 is for the time delay between t_b to $2t_b$ and so on). For $m_2 = 4$ and $m_3 = 5,$ the process is similar, except the phase reference values have to correspond to the transmitted phase code sequence that is being received.

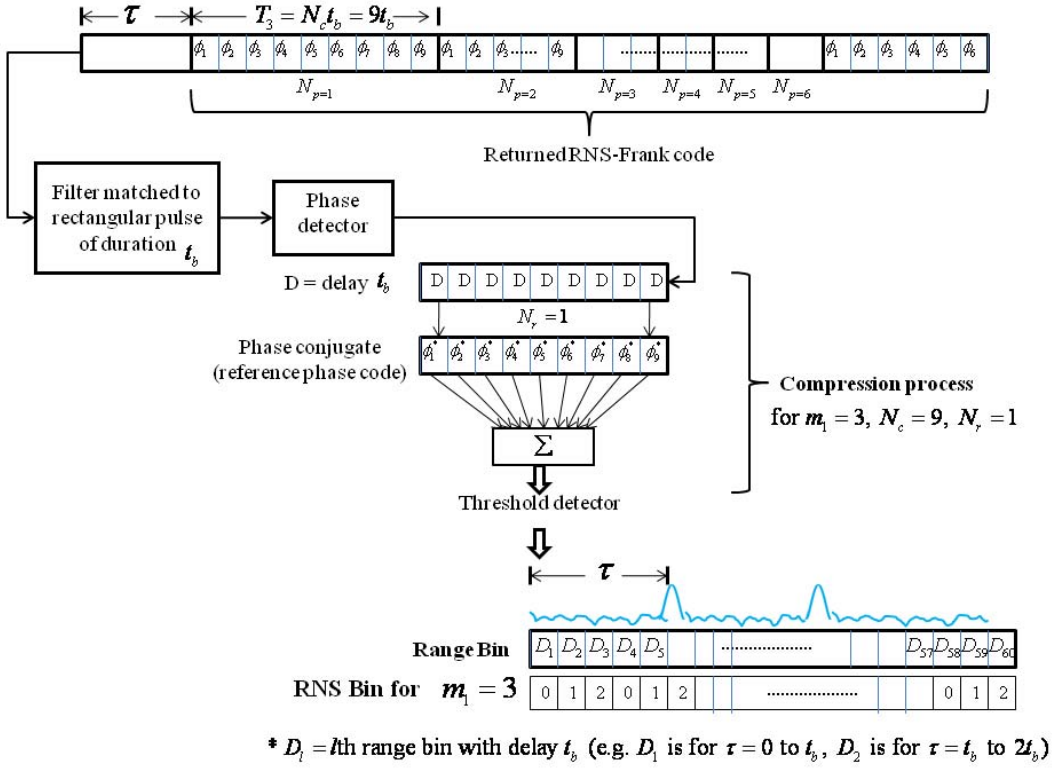

Figure 16. Illustration of compression at the receiver and the range bin for RNS $m_1 = 3,\ N_c = 9,$ and $N_r = 1.$

3. Calculating the Target Range

After the returned signal is compressed, the first sample appears in the receiver's range bin that corresponds to a duration τ. For each modular sequence, the target detection corresponds to a residue R_m. By combining the paired residue from each sequence, the target's range bin can be calculated.

Continuing the example in the previous section, we show the residues for $m_1 = 3,\ m_2 = 4,$ and $m_3 = 5$ and the corresponding target range in Table 3. Here, the signal bandwidth $B = 1$ MHz, and the subcode period $t_b = 1\ \mu$s. The unambiguous range using residue-Frank phase code is

$$R_{u,RNS} = \frac{cM_{RNS}t_b}{2}. \tag{24}$$

For this example, the maximum unambiguous range is $R_{u,RNS} = 9$ km ($M_{RNS} = 60$) and is considerably longer than that of any single code period. The range resolution is $\Delta R = ct_b / 2 = 150$ m. The target's range now has to be $R < R_{u,RNS}$ in order to be detected with no range ambiguity. The range interval for each range bin of this example is also given in the Table 3.

Table 3. Bin matrix and range intervals of $3-$channel RNS with $m_1 = 3,\ m_2 = 4,$ and $m_3 = 5.$

Bin a	$m_1 = 3$	$m_2 = 4$	$m_3 = 5$	**Range(m)**	**Bin** a	$m_1 = 3$	$m_2 = 4$	$m_3 = 5$	**Range(m)**
0	0	0	0	0–150	30	0	2	0	4500–4650
1	1	1	1	150–300	31	1	3	1	4650–4800
2	2	2	2	300–450	32	2	0	2	4800–4950
3	0	3	3	450–600	33	0	1	3	4950–5100
4	1	0	4	600–750	34	1	2	4	5100–5250
5	2	1	0	750–900	35	2	3	0	5250–5400
6	0	2	1	900–1050	36	0	0	1	5400–5550
7	1	3	2	1050–1200	37	1	1	2	5550–5700

8	2	0	3	1200–1350	38	2	2	3	5700–5850
9	0	1	4	1350–1500	39	0	3	4	5850–6000
10	1	2	0	1500–1650	40	1	0	0	6000–6150
11	2	3	1	1650–1800	41	2	1	1	6150–6300
12	0	0	2	1800–1950	42	0	2	2	6300–6450
13	1	1	3	1950–2100	43	1	3	3	6450–6600
14	2	2	4	2100–2250	44	2	0	4	6600–6750
15	0	3	0	2250–2400	45	0	1	0	6750–6900
16	1	0	1	2400–2550	46	1	2	1	6900–7050
17	2	1	2	2550–2700	47	2	3	2	7050–7200
18	0	2	3	2700–2850	48	0	0	3	7200–7350
19	1	3	4	2850–3000	49	1	1	4	7350–7500
20	2	0	0	3000–3150	50	2	2	0	7500–7650
21	0	1	1	3150–3300	51	0	3	1	7650–7800
22	1	2	2	3300–3450	52	1	0	2	7800–7950
23	2	3	3	3450–3600	53	2	1	3	7950–8100
24	0	0	4	3600–3750	54	0	2	4	8100–8250
25	1	1	0	3750–3900	55	1	3	0	8250–8400
26	2	2	1	3900–4050	56	2	0	1	8400–8550
27	0	3	2	4050–4200	57	0	1	2	8550–8700
28	1	0	3	4200–4350	58	1	2	3	8700–8850
29	2	1	4	4350–4500	59	2	3	4	8850–9000

In Figure 17, an example of the target detection process using $m_1 = 3,\ m_2 = 4,$ and $m_3 = 5$ is illustrated. The residue-Frank phase code signal is transmitted to the target and the target's return is in range bin $a = 5$ or 770 m. In the code compression step, the returned signal is compressed corresponding to each modulus in consecutive order. Shown in each graph are residues $R_{m,k}$ (stair-step waveform), the range bin index a, and

a helicopter target detection. The range bin index a goes from 0 to 59 ($M_{RNS} = 60$). Since the phase code sequence is periodic, the residues is also periodic with $R_{m,k} = R_{m,k+nm^2}$. For modulus $m_1 = 3$, the CC peak is repeated with $T_{m_1} = N_c t_b = m_1^2 t_b = 9t_b$. The threshold detector detects the correlated signal output, and the range bin residue R_3 is stored. Here, the range bin residue corresponding to the correlated output for channels $m_1 = 3$ is at $R_3 = 2$. The processes are the same for channels 2 and 3 using the moduli $m_2 = 4$ and $m_3 = 5$, respectively. The detected target range bin residues are $R_4 = 1$ and $R_5 = 0$. The residues are paired as [2 1 0], and a RNS-to-decimal algorithm is used to calculate the target's true range R. From Table 3, the paired values [2 1 0] correspond to the range bin $a = 5$, and the calculated target range is between 750 m and 900 m.

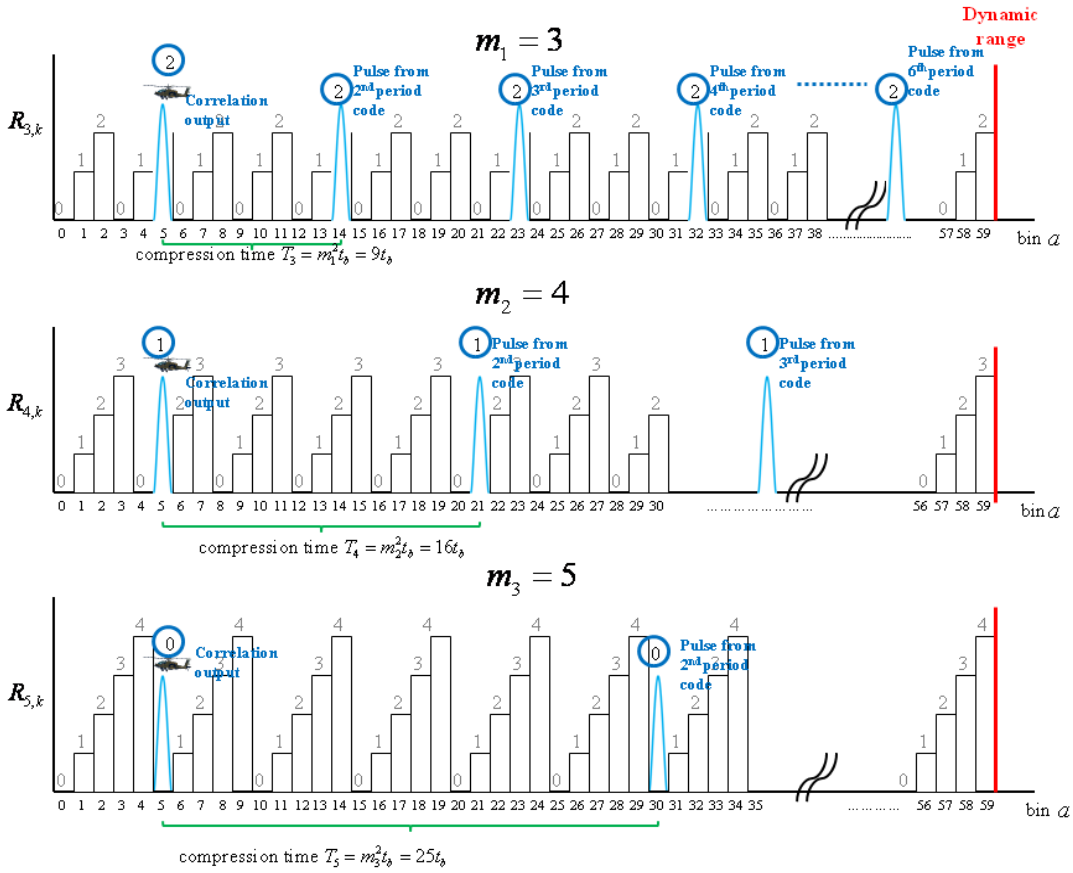

Figure 17. Example of compression output for target detection using $N = 3$ residue-Frank phase code sequences with $m_1 = 3$, $m_2 = 4$, and $m_3 = 5$.

Although the look up table in Table 3 can be used to find the target's range from the corresponding residues, for a practical implementation the table would be very large. Alternatively, the system of simultaneous congruences of the form $a \equiv R_{m_i} (\mathrm{mod}\, m_i)$ can be solved with a straightforward application of the Chinese remainder theorem (CRT). The system to be solved for this example is $a \equiv 2(\mathrm{mod}\, 3),\ a \equiv 1(\mathrm{mod}\, 4),\ a \equiv 0(\mathrm{mod}\, 5)$. This CRT algorithm only requires the target range bin residues R_{m_i}. The CRT solution of the system is

$$a = \sum_{j=1}^{N} \frac{M_{RNS}}{m_j} b_j R_{m_j} \tag{25}$$

where a is the range bin index. If we consider this number modulo m_i, we find that $a \equiv \frac{M_{RNS}}{m_i} b_i R_{m_i} \equiv R_{m_i} \bmod m_i$. The b_j values can be found with the Euclidean algorithm, which is a repeated application of the division algorithm [17]. We note that the b_j values are also hardwired into the system and depend only on the moduli and not at all on the range bin residues.

4. Resolving Multiple Target Range Ambiguities

In this section, the detection of multiple targets is considered. As illustrated in Figure 18, the residue for the two targets are periodic as $R_{m,k} = R_{m,k+nm^2}$. If there are no missed targets in the detection process, the sequence of residues within each modulus can be paired directly for the solution of the target's range. To solve for the range of each target, the residues are paired as [2 2 2] for the first target and [2 0 0] for the second target. Using the CRT or lookup table, we find the range of the first target is $150 \le R_1 \le 300$ m ($a = 2$) and the range of the second target is $3000 \le R_2 \le 3150$ m ($a = 20$).

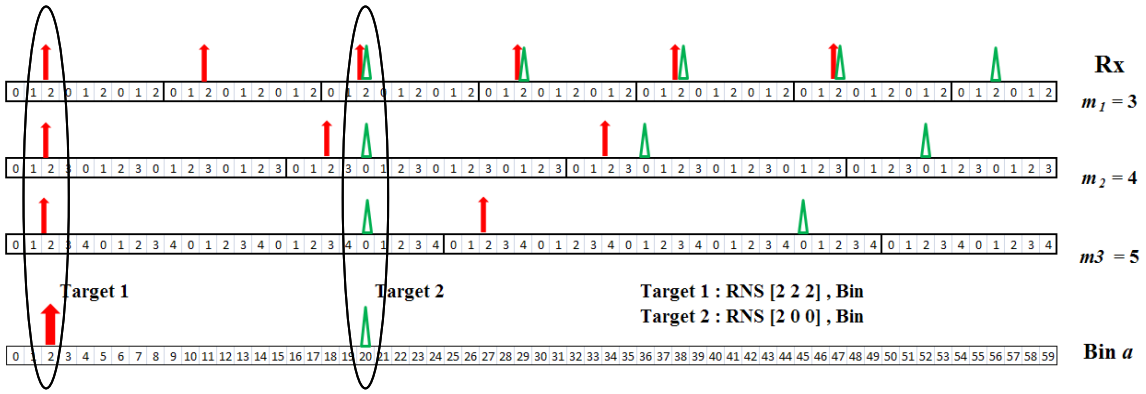

Figure 18. Resolving the range ambiguity of 2 targets using RNS for $m_1 = 3,\ m_2 = 4,$ and $m_3 = 5.$

In Figure 19, if the first set of residues for the two targets are not detected, the residue-Frank phase code waveform still allows the two target range values to be determined. Note the residues are determined but there is no information available to pair them up correctly. Additional information must be used in order to pair them correctly. For example, for m_1, we have $R_3 = \{2, 2\}$, for m_2, we have $R_4 = \{2, 0\}$, and for m_3, we have $R_5 = \{2, 0\}$. To pair them up correctly, the magnitude information associated with each subcode (from the phase detector) can be used.

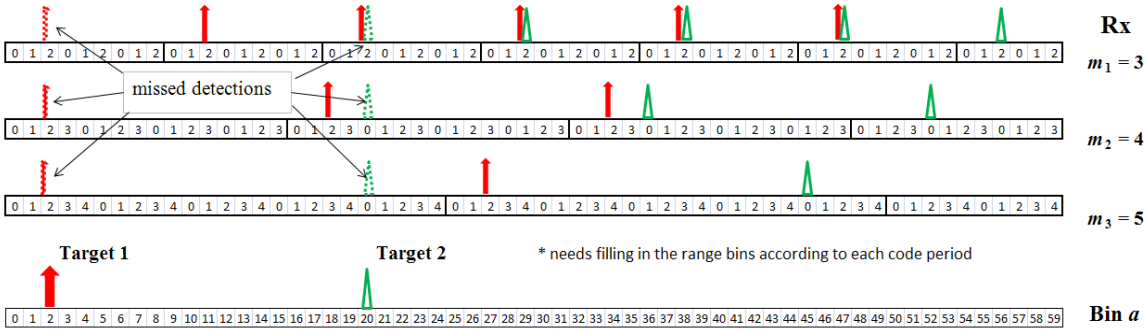

Figure 19. Missed detections of the first set of residues.

A more convenient method is to extend or fill in the residues according to their code period, which can be identified through examination of the residues throughout the unambiguous range. This result gives the same residue configuration as shown in Figure 18. Note that this method works even with the target residues overlapping.

5. Practical Considerations

a. Detection of Target in Noise Using RNS Compression

In this section, the performance of the $N = 3$ residue-Frank for $m_1 = 3,$ $m_2 = 4,$ and $m_3 = 5$ with $M_{RNS} = 60$ is examined by using MATLAB to plot the returned signals from two targets at ranges of 440 m and 5840 m. The transmitted signal has an amplitude $A = 1,$ carrier frequency $f_c = 1$ MHz, sampling frequency $f_s = 7$ MHz, $cpp = 1,$ and $t_b = 1$ μs. For a practical case, the signals are received with noise. The noise changes the returned phase sequences and affects the compression output value. Here, two different SNRs are examined. In Figure 20, the transmitted signal without noise for each channel is plotted. In Figure 21, the signal with SNR = 30 dB is plotted. The signal power is high compared to the noise power. Consequently, the noise signal does not significantly affect the phase sequences. In Figure 22, the SNR is reduced to 0 dB. The phase sequences are changed significantly.

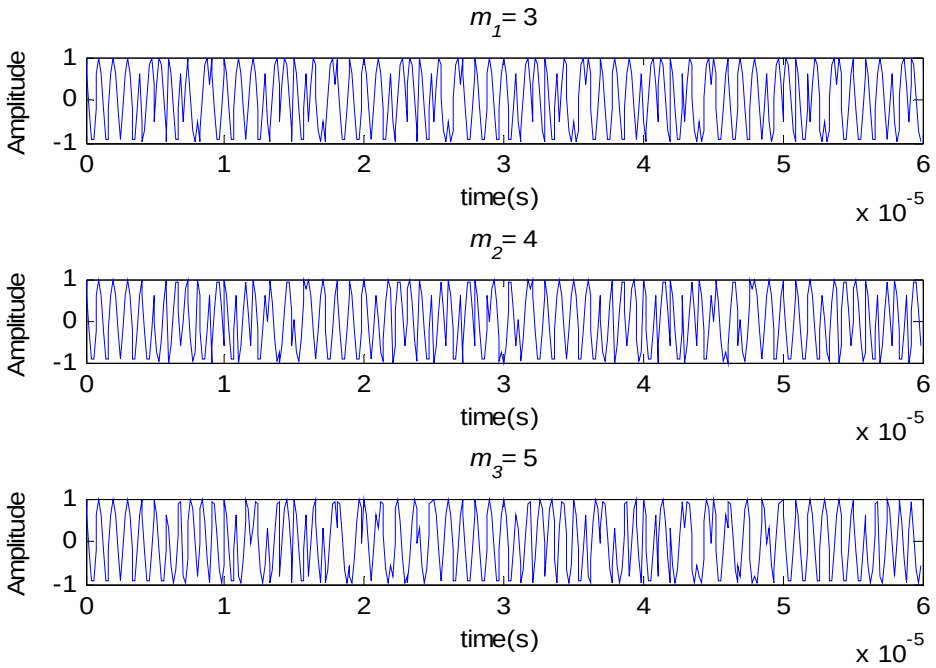

Figure 20. Residue-Frank signal without noise for $m_1 = 3,$ $m_2 = 4,$ and $m_3 = 5$ with $M_{RNS} = 60,$ $A = 1,$ $f_c = 1$ MHz, $f_s = 7$ MHz, $cpp = 1,$ and $t_b = 1$ μs.

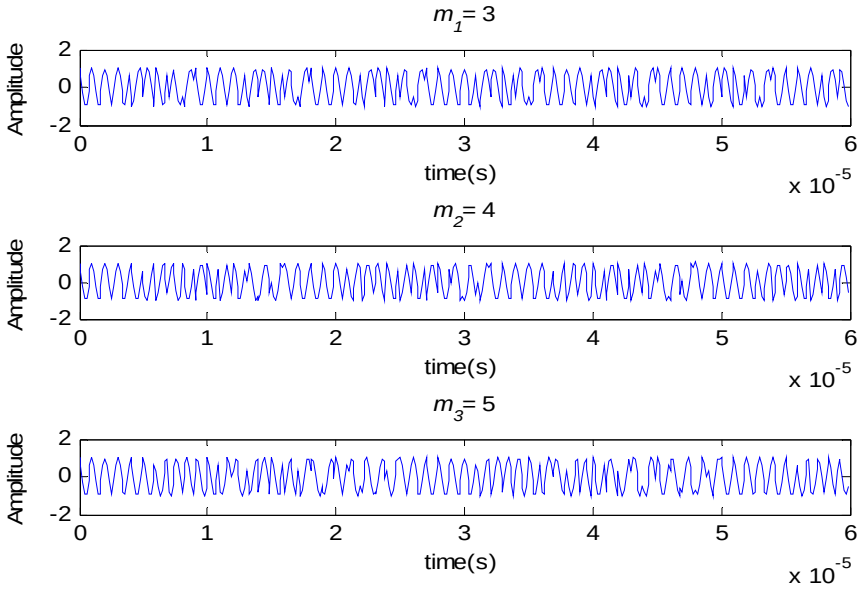

Figure 21. Residue-Frank signal with SNR = 30 dB for $m_1 = 3,\ m_2 = 4,$ and $m_3 = 5$ with $M_{RNS} = 60,\ A = 1,\ f_c = 1$ MHz, $f_s = 7$ MHz, $cpp = 1,$ and $t_b = 1\ \mu$s.

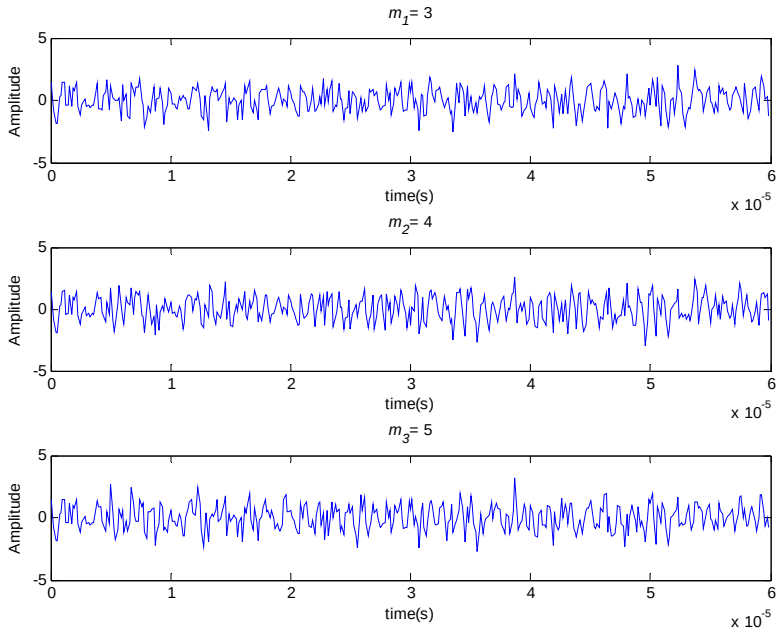

Figure 22. Residue-Frank signal with SNR = 0 dB for $m_1 = 3,\ m_2 = 4,$ and $m_3 = 5$ with $M_{RNS} = 60,\ A = 1,\ f_c = 1$ MHz, $f_s = 7$ MHz, $cpp = 1,$ and $t_b = 1\ \mu$s.

In Figures 23 and 24, the range bin profiles for each channel after threshold detection of the compression output for the two targets are shown with SNR = 30 dB and SNR = 0 dB, respectively. The first target appears at a range bin $a = 2$ with the paired residues [2 2 2] (range 300–450 m). The second target appears at range bin $a = 38$ with the paired residues [2 2 3] (range 5700–5840 m). Note that the targets straddle the range bins since the first sample received from the targets lies in the correct range bin. Also shown is the noise signal that is compressed before the signals are returned to the receiver. Shown in Figure 24, the amplitudes of compressed pulses degrade when the SNR is decreased to 0 dB. Also, the sidelobes from the compression output are higher when the noise power is increased. Another important point is that the average sidelobes from the higher modulus (e.g. $m_3 = 5$) are lower than those from the lower modulus (e.g., $m_1 = 3$ and $m_2 = 4$). This is due to the different processing gain or N_c subcodes that each sequence provides. For $m_1 = 3,\ m_2 = 4,$ and $m_3 = 5,$ the processing gains are $m_1^2 = 9,\ m_2^2 = 16,\ m_3^2 = 25,$ respectively.

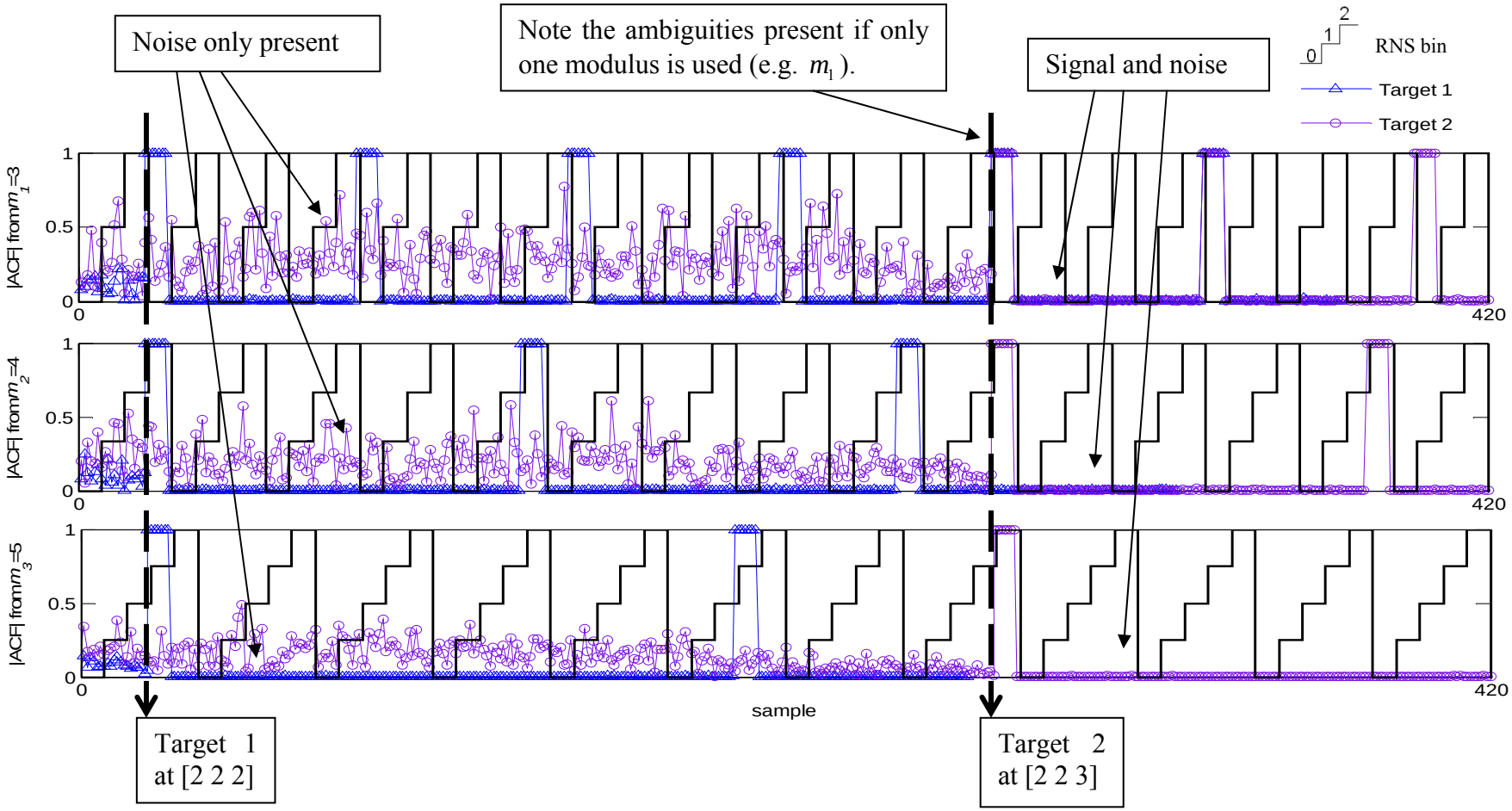

Figure 23. Target detection for SNR = 30 dB showing the range bins for $m_1 = 3$, $m_2 = 4$, and $m_3 = 5$ with the two targets at 440 m and 5840 m.

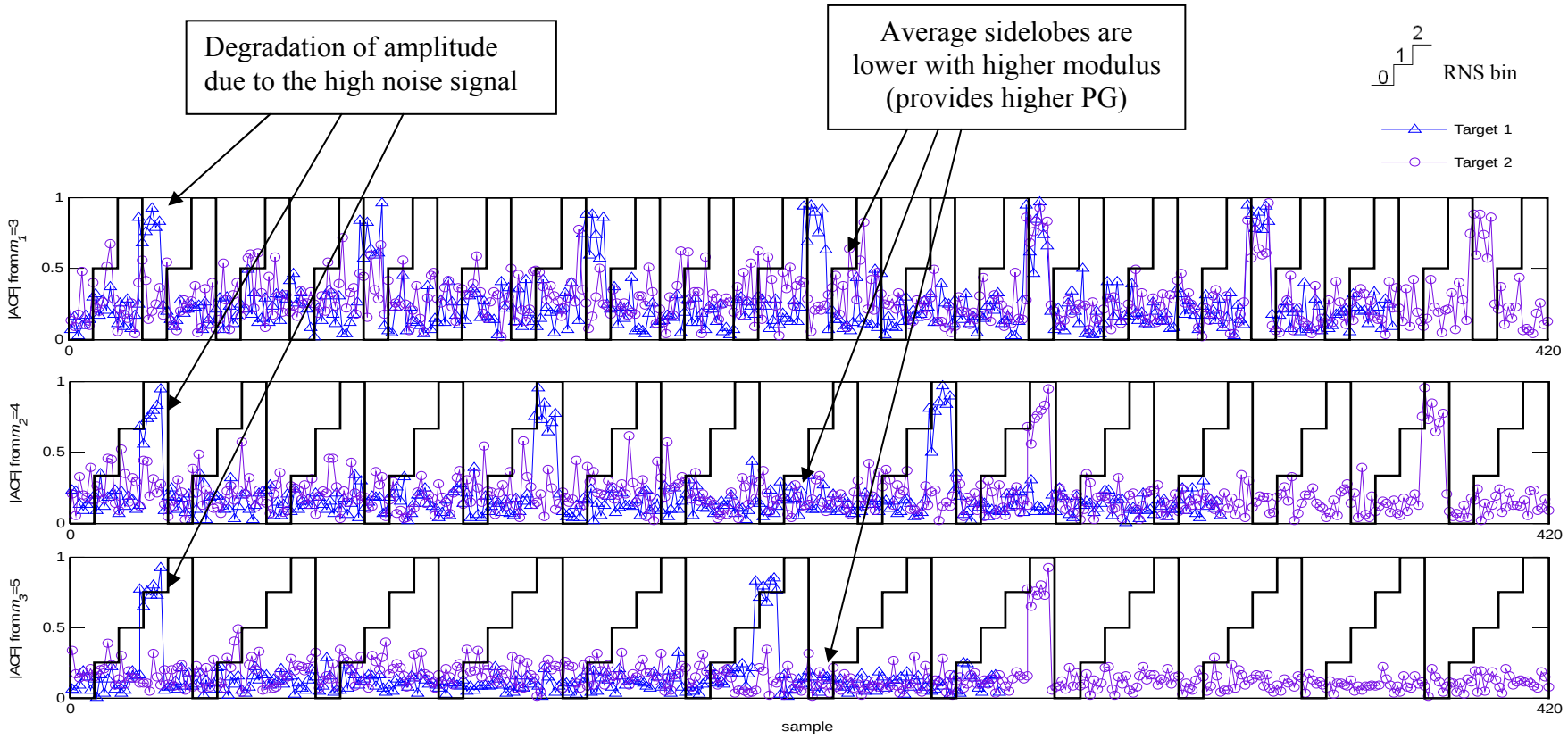

Figure 24. Target detection for SNR = 0 dB showing the range bins for $m_1 = 3$, $m_2 = 4$, and $m_3 = 5$ with two targets at 440 m and 5840 m.

One situation that may occur is that the threshold detector might read the wrong range bin because the amplitudes of the compressed pulses fluctuate due to the noise present. This results in a target range error. In Figure 25, the first target in channel $m_2 = 4$ can be seen with the compressed pulse detected by a CFAR (threshold level at 0.8) at residue $R_4 = 3$ instead of $R_4 = 2$. So the paired terms [2 3 2] (range 7050–7200 m) are computed instead of the true range at [2 2 2] (range 300–450 m). This is a large range error.

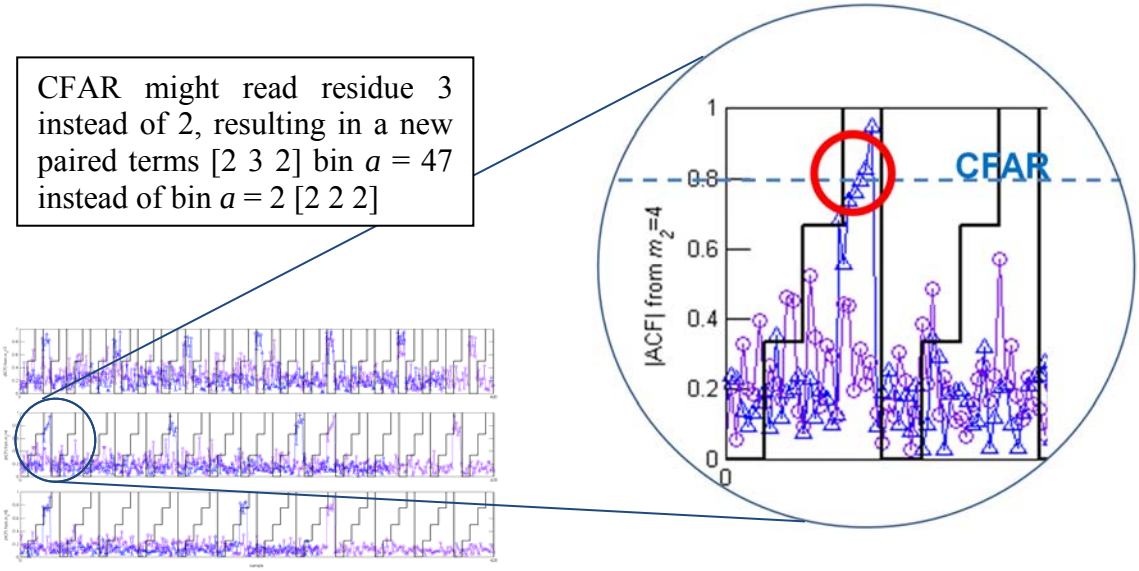

Figure 25. Illustration of detection error from the threshold detector (CFAR) using the residue-Frank for $m_1 = 3,\ m_2 = 4,$ and $m_3 = 5$.

b. Required CW Signal Power Versus Required Output SNR

In this section, the CW power required when using the residue-Frank phase code sequences to detect the target at the maximum unambiguous range is presented. Given the fixed unambiguous range $R_u = 9000$ m, the CW radar power can be changed accordingly as a function of the SNR_{Ro} at the output of compressor. The relationship between the required SNR_{Ro} and the average CW power (P_{CW}) is expressed as [1]

$$P_{CW} = \frac{R_u^4 (4\pi)^3 k_B T_0 F_R B_{Ri} L_{RT} L_{RR} (SNR_{Ro} / PG)}{G_t G_r \lambda^2 \sigma_T L_2} \tag{26}$$

where R_u is the unambiguous range, $k_B = 1.38 \times 10^{-23}$ joule/K (Boltzman's constant), T_0 is the ambient noise temperature ($T_0 = 290$ K), F_R is the receiver noise factor, B_{Ri} is the radar receiver's input bandwidth in Hz, G_t and G_r are the transmitting and receiving antenna gains, σ_T is the target's radar cross section in m^2, L_2 is the two-way atmospheric transmission factor, L_{RT} is the loss between the radar's transmitter and antenna, and L_{RR} is the loss between the radar's antenna and receiver.

In Figure 26, the CW signal power as a function of the required output signal-to-noise ratio SNR_{Ro} for $m_1 = 3$, $m_2 = 4$, and $m_3 = 5$ is plotted with $B_{Ri} = 1$ MHz, $t_b = 1$ μs, $G_t = G_r = 30$ dB, $f_c = 3$ GHz, $\lambda = 0.1$ m, $\sigma_T = 100$ m^2, $F_R = 5$ dB, $L_2 = L_{RT} = L_{RR} = 1$, and $R_u = cM_{RNS}t_b / 2 = 9000$ m (maximum detection range without ambiguity).

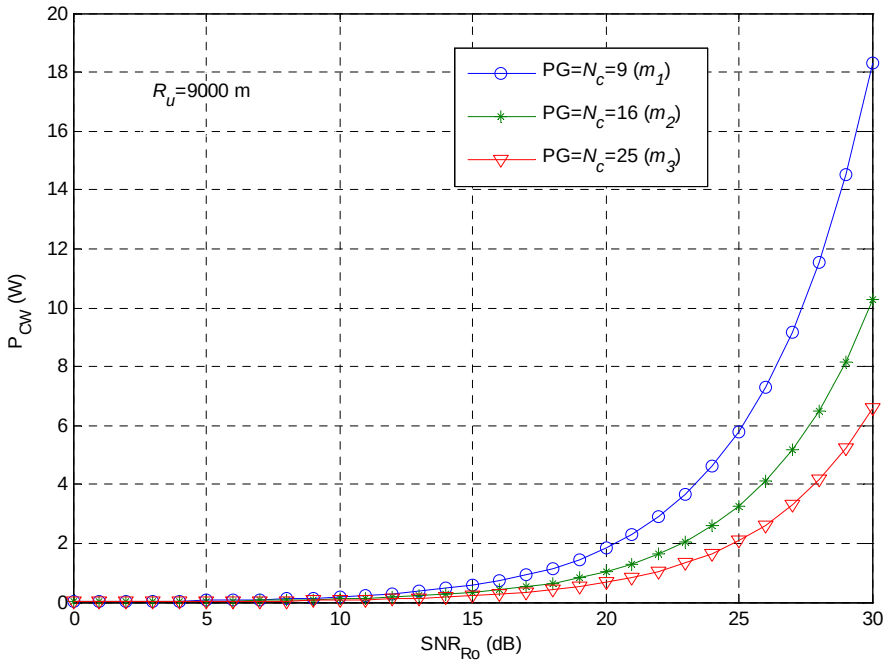

Figure 26. Average power of the CW transmitter for residue-Frank with $m_1 = 3$, $m_2 = 4$, and $m_3 = 5$.

Note the difference in the average power required in each channel due to the different PG. The channel $m_3 = 5,$ giving $PG = N_c = m_i^2 = 25,$ requires less power than the other channels, $m_1 = 3$ ($PG = 9$) and $m_2 = 4$ ($PG = 16$), to detect the targets within the same unambiguous detection range. For example, at $SNR_{Ro} = 30$ dB, the required CW power P_{CW} for $m_3 = 5, m_2 = 4,$ and $m_1 = 3$ are 7, 10.5, and 18 W, respectively. Note that this helps contribute to the LPI characteristic of the emitter.

c. Unambiguous Detection Range for a Constant Output SNR

It is important to see how superior the residue-Frank phase code is compared to a single Frank code with the unambiguous range $R_u = cT/2 = ct_b N_c/2$ and limited to only one code period. Here, the relationship between the average signal power P_{CW} and the maximum detection range $R_{\max}$ is

$$R_{\max} = \left[\frac{P_{CW} G_t G_r \lambda^2 \sigma_T L_2}{(4\pi)^3 k_B T_0 F_R B_{Ri} (SNR_{Ro}/PG) L_{RT} L_{RR}} \right]^{\frac{1}{4}}. \tag{27}$$

However, the resolvable detection range is limited by the unambiguous range. The radar, however, can detect the targets beyond R_u but there are ambiguities.

In Figure 27, the detection range $R = R_{\max}$ is plotted as a function of the required CW power with constant $SNR_{Ro} = 13$ dB, $B = 1$ MHz, $t_b = 1$ μs, $G_t = G_r = 30$ dB, $f_c = 3$ GHz, $\lambda = 0.1$ m, $\sigma_T = 100$ m^2, $T_0 = 290$ K, $F_R = 5$ dB, and $L_2 = L_{RT} = L_{RR} = 1$. Also, the performance of each Frank code using the corresponding N_c is plotted. For the Frank code (17), $M1 = 3,$ $N_c = 9$ and $M2 = 4,$ $N_c = 16,$ and $M3 = 5,$ $N_c = 25.$ Shown in the graph, the single Frank code has a limited unambiguous range, where $M1 = 3$ gives $R_u = 3\times10^8 \times10^{-6} \times 9/2 = 1350$ m, $M2 = 4$ gives $R_u = 3\times10^8 \times10^{-6} \times 16/2 = 2400$ m, and $M3 = 5$ gives $R_u = 3\times10^8 \times10^{-6} \times 25/2 = 3750$ m. These values are less than using the residue-Frank phase code, giving $R_{u_{RNS}} = cM_{RNS}t_b/2 = 9000$ m.

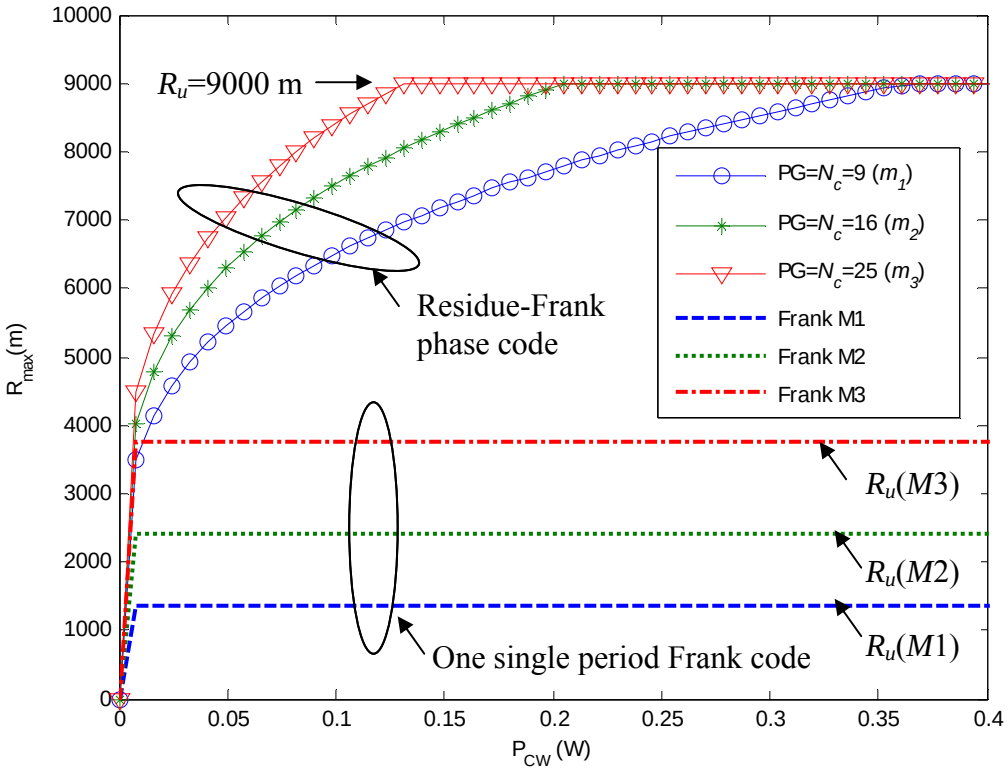

Figure 27. Comparison of the maximum unambiguous range of CW radar system for $SNR_{Ro} = 13$ dB using the residue-Frank phase code for $m_1 = 3$, $m_2 = 4$, and $m_3 = 5$ with the radar using each Frank code sequence individually with the corresponding N_c.

In conclusion, the residue-Frank phase code presented in this chapter can be used to extend the unambiguous range of the CW polyphase radar system. The issue concerned with the range bin error due to the fluctuation of the compression outputs was also introduced. In the next chapter, the relationship between the P4 code and the symmetrical number system (SNS) is presented. As will be shown in examining the PAF, the P4 has a better property in Doppler tolerance than the Frank code. This makes it more attractive when the emitter attempts to detect the moving targets.

IV. P4 POLYPHASE MODULATION AND THE SYMMETRICAL NUMBER SYSTEM

In this chapter, the P4 phase code and the SNS are introduced. Their relationship is presented.

A. P4 PHASE CODE

The P4 polyphase code is conceptually derived from a linearly frequency modulated waveform (LFMW). Such codes and compressors can be employed to obtain much larger time-bandwidth products. The significant advantages of P4 codes are low peak sidelobes and that they are more Doppler tolerant than other phase codes derived from a step approximation to an LFMW [5], [12].

In the P4 code the local oscillator frequency, which is offset in the I and Q detectors, results in a coherent double sideband detection. The phase sequence of a P4 signal is given by

$$\phi_k = \frac{\pi}{N_c}(k-1)^2 - \pi(k-1) \tag{28}$$

where k is the time index for a single phase change per subcode and ranges from 1 to N_c.

The phase values and phase values modulo 2π of a P4 code for $N_c = 64$ are shown in Figures 28 and 29, respectively. The carrier frequency is f_c = 1 kHz, the sampling frequency is f_s = 7 kHz, and the number of carrier cycles per subcode is cpp = 1. The ACF and PACF for $N_r = 1$ are shown in Figure 30. The peak-to-sidelobe level is $PSL = 20\log_{10}\sqrt{2/(N_c\pi^2)}$ or −25 dB. The PACF is a perfect code with low sidelobes. The PAF in Figure 31 shows the delay-offset and Doppler-offset sidelobes.

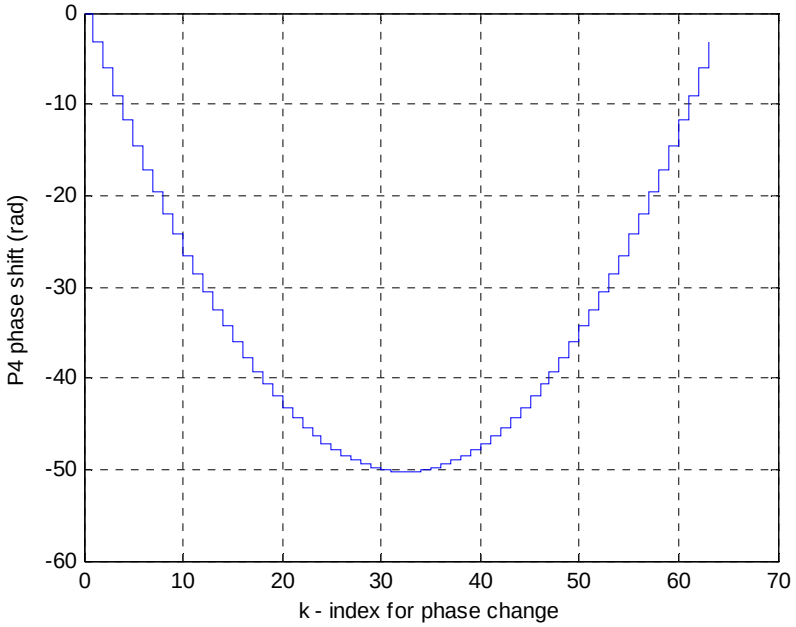

Figure 28. P4 phase sequence for $N_c = 64$ (From [1]).

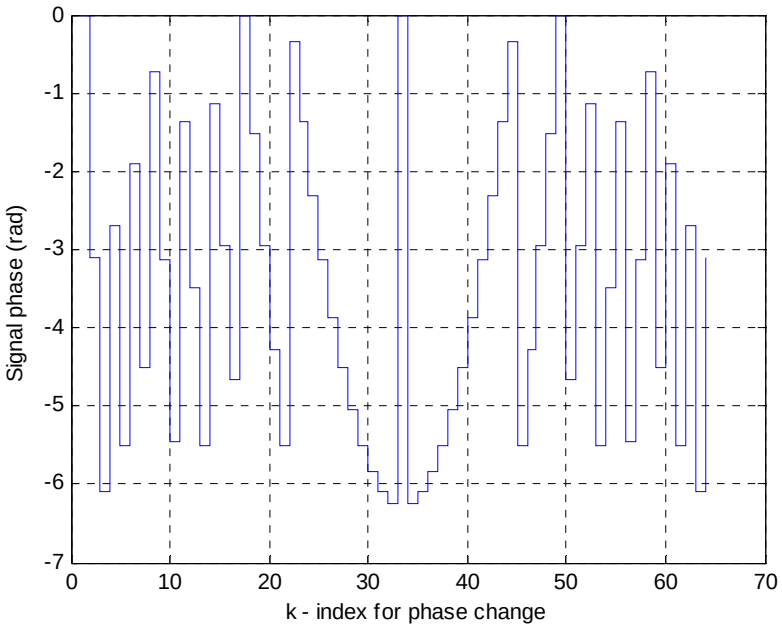

Figure 29. Signal phase (radians) modulo 2π versus k-index for phase change of the P4 code with $N_c = 64$ (From [1]).

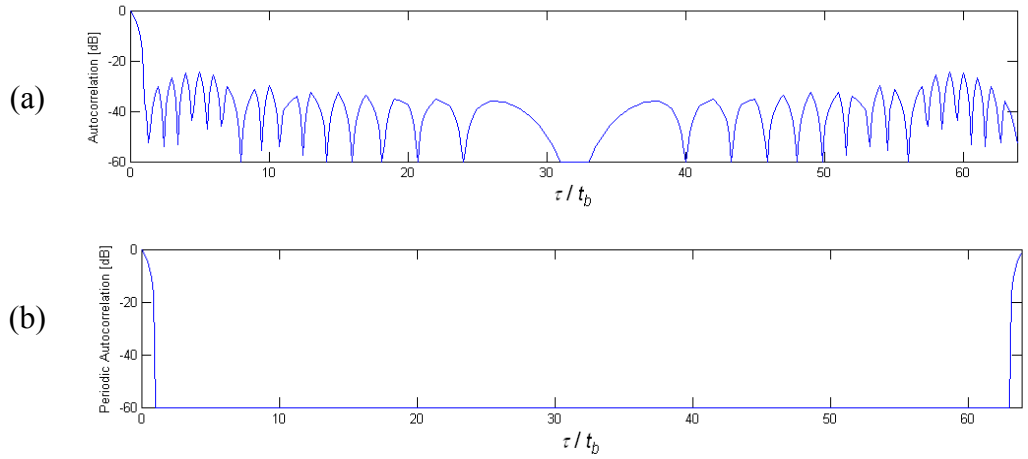

Figure 30. ACF (a) and PACF (b) for the P4 code with $N_c = 64$, $cpp = 1$, and $N_r = 1$ (From [1]).

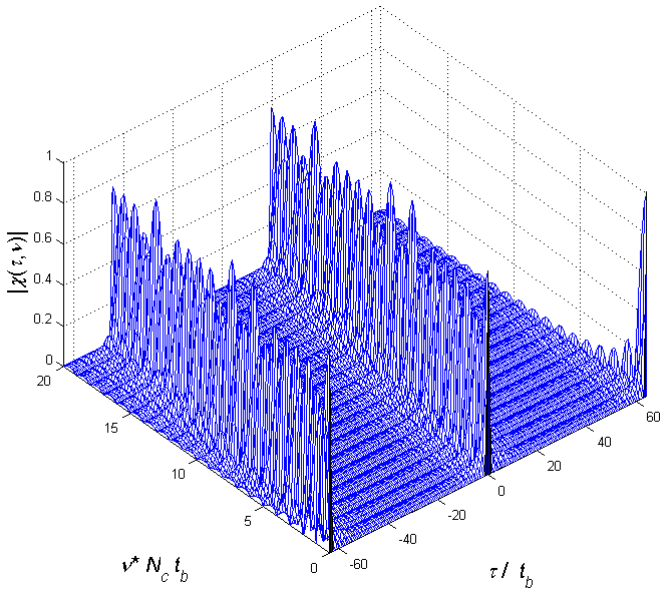

Figure 31. PAF for the P4 code modulation with $N_c = 64$, $cpp = 1$, and $N_r = 1$ (From [1]).

B. THE SYMMETRICAL NUMBER SYSTEM

The SNS is composed of N coprime moduli. The integers within each SNS modulus are derived from a symmetrically folded waveform [18]. The integer values within each SNS modulus are derived from a mid-level quantization of the symmetrical

folding waveform and, therefore, incongruent modulus m (i.e., mod 5: {0, 1, 2, 2, 1, 0, 1, 2…}). Due to the presence of ambiguities, the set of integers within each SNS modulus does not form a complete residue system by themselves. It is well known that the inclusion of additional redundant moduli can effectively detect and correct errors that may occur within a RNS representation of a number. The SNS formulation is based on a similar concept, which allows the ambiguities that arise within the SNS to be resolved by using various arrangements of the SNS moduli. The vector of integer values within a single SNS folding waveform is given as

$$S_m = \left[0,1,...,\left\lfloor \frac{m}{2} \right\rfloor,\left\lfloor \frac{m}{2} \right\rfloor,...,2,1,0,1\right], \text{when } m \text{ is odd} \tag{29}$$

and

$$S_m = \left[0,1,...,\frac{m}{2},\frac{m}{2}-1,...,2,1,0,1\right], \text{when } m \text{ is even} \tag{30}$$

where $\lfloor x \rfloor$ indicates the greatest integer less than or equal to x. An example of the SNS waveforms for $m_1 = 4$ and $m_2 = 5$ ($N = 2$) is shown in Figure 32. The period of each waveform equals the value of the modulus as

$$P_{SNS} = m. \tag{31}$$

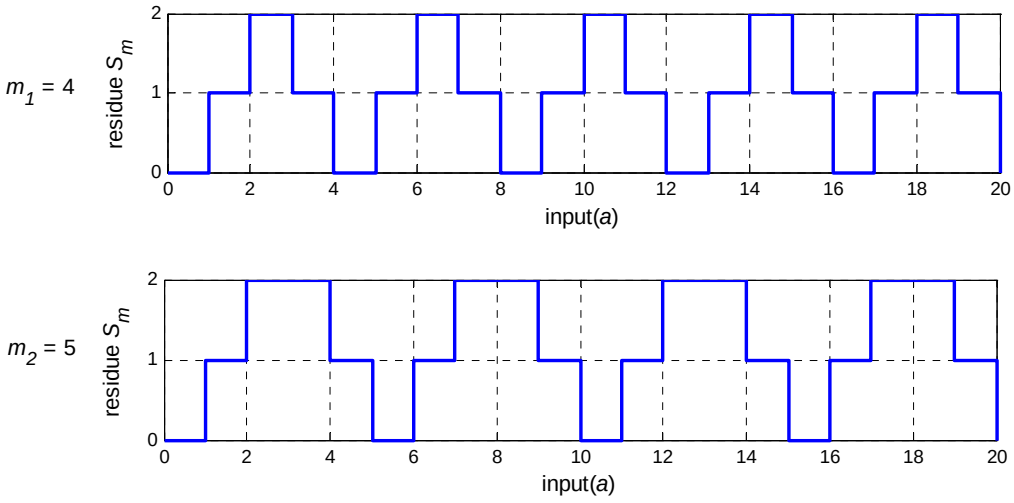

Figure 32. The SNS residues for $m_1 = 4$ and $m_2 = 5$.

The dynamic range of the SNS $\hat{M}_{SNS}$ is

$$\hat{M}_{SNS} = \min\left\{\frac{m}{2}\prod_{l=2}^{j} m_{i_l} + \prod_{l=j+1}^{N} m_{i_l}\right\} \tag{32}$$

for coprime moduli m_i, with one of the moduli even, j ranges from 1 to $N-1$, N is the number of moduli, and $m_{i2}, m_{i3}, ..., m_{iN}$ range over all permutations $\{2,3,\ldots,N\}$. The product of j from 2 to 1 is empty, and its value is 1. If all the coprime moduli in the system are odd, then

$$\hat{M}_{SNS} = \min\left\{\frac{1}{2}\prod_{l=1}^{j} m_{i_l} + \frac{1}{2}\prod_{l=j+1}^{N} m_{i_l}\right\} \tag{33}$$

where j ranges from 1 to $N-1$ and $m_{i1}, m_{i2}, m_{i3}, ..., m_{iN}$ range over all permutations $\{1,2,3,\ldots,N\}$. Note that the dynamic range for the SNS is less than the RNS ($\hat{M}_{SNS} < M_{RNS}$).

From Equation (32), for $m_1 = 4$ and $m_2 = 5$, the dynamic range is $\hat{M}_{SNS} = 7$. In Table 4, the two sequences are shown along with the input a. Starting at $a = 0$, the total number of distinct paired terms is 7, $0 \le a \le 6$. The index value $l = a + 1$ in Table 4 is shown to count the integer number of the distinct paired terms within the dynamic range. Also shaded is the region with no ambiguity.

Table 4. Finding the SNS dynamic range for $m_1 = 4$ and $m_2 = 5$.

Input(a)	0	1	2	3	4	5	6	7	8	9	10	11	12	13	14	15	16	17	18	19	20
$m_1 = 4$	0	1	2	1	0	1	2	1	0	1	2	1	0	1	2	1	0	1	2	1	0
$m_2 = 5$	0	1	2	2	1	0	1	2	2	1	0	1	2	2	1	0	1	2	2	1	0
l	1	2	3	4	5	6	7														

C. SYMMETRICAL RESIDUE-P4 PHASE CODE

The SNS symmetrical residues $S_{m,k}$ can be folded into the P4 phase sequence by associating $S_{m,k}$ with the P4 subcode phases. The phase index k starts from 1 to N_c. The symmetrical residue-P4 phase sequence is given by

$$\phi_{m,k} = \left[\frac{\pi}{m} \left(S_{m,k} - \frac{m}{2} \right)^2 \right] - \frac{\pi}{4} m \tag{34}$$

where $k = 1,2,3, \ldots, m.$ The number of subcodes within one code period is $N_c = m.$ For example, if we choose $m = 8,\ N_c = 8,$ and the SNS sequence becomes $S_{m=8,k=1,2,\ldots,8} = \{0,1,2,3,4,3,2,1\}.$

Next, the phase sequences from equations (34) and (28) are compared. First, Equation (34) is used to calculate the symmetrical residue-P4 phase code sequence using $m = 8,\ N_c = 8$ with $S_{m=8,k=1,2,\ldots,8} = \{0,1,2,3,4,3,2,1\}.$ For the P4 code in Equation (28), the parameters are $N_c = 8$ and $i = 1,2,3,\ldots.8.$ In Table 5, the phase sequences are shown for comparison.

The phase code sequences of both waveforms are identical. The ACF, PACF, and PAF of the CW waveform generated by Equation (34) with $m = N_c = 64$ are also identical to those shown in Figures 30 and 31 which were generated by Equation (28) with $N_c = 64.$

Table 5. Comparison of symmetrical residue-P4 phase code sequence ($m = 8,\ N_c = 8$) with the P4 phase code sequence ($N_c = 8$).

Phase index (k)	Symmetrical residue-P4 phase code (34)		P4 phase code (28)	
	$S_{m=8,k}$	$\phi_{m=8,k}$ (rad)	k	ϕ_k (rad)
1	0	$\phi_1=\left(\frac{\pi}{8}\left(0-\frac{8}{2}\right)^2\right)-\frac{\pi}{4}8=0$	1	$\phi_1=\frac{\pi(1-1)^2}{8}-\pi(1-1)=0$
2	1	$\phi_2=\left(\frac{\pi}{8}\left(1-\frac{8}{2}\right)^2\right)-\frac{\pi}{4}8=-2.7489$	2	$\phi_2=\frac{\pi(2-1)^2}{8}-\pi(2-1)=-2.7489$
3	2	$\phi_3=\left(\frac{\pi}{8}\left(2-\frac{8}{2}\right)^2\right)-\frac{\pi}{4}8=-4.7124$	3	$\phi_3=\frac{\pi(3-1)^2}{8}-\pi(3-1)=-4.7124$
4	3	$\phi_4=\left(\frac{\pi}{8}\left(3-\frac{8}{2}\right)^2\right)-\frac{\pi}{4}8=-5.8905$	4	$\phi_4=\frac{\pi(4-1)^2}{8}-\pi(4-1)=-5.8905$
5	4	$\phi_5=\left(\frac{\pi}{8}\left(4-\frac{8}{2}\right)^2\right)-\frac{\pi}{4}8=-6.2832$	5	$\phi_5=\frac{\pi(5-1)^2}{8}-\pi(5-1)=-6.2832$
6	3	$\phi_6=\left(\frac{\pi}{8}\left(3-\frac{8}{2}\right)^2\right)-\frac{\pi}{4}8=-5.8905$	6	$\phi_6=\frac{\pi(6-1)^2}{8}-\pi(6-1)=-5.8905$
7	2	$\phi_7=\left(\frac{\pi}{8}\left(2-\frac{8}{2}\right)^2\right)-\frac{\pi}{4}8=-4.7124$	7	$\phi_7=\frac{\pi(7-1)^2}{8}-\pi(7-1)=-4.7124$
8	1	$\phi_8=\left(\frac{\pi}{8}\left(1-\frac{8}{2}\right)^2\right)-\frac{\pi}{4}8=-2.7489$	8	$\phi_8=\frac{\pi(8-1)^2}{8}-\pi(8-1)=-2.7489$

D. RESOLVING RANGE AMBIGUITIES USING *N* SYMMETRICAL RESIDUE-P4 PHASE CODE SEQUENCES

1. Block Diagram of the Symmetrical Residue-P4 Radar System

The block diagram of a radar system using symmetrical residue-P4 phase code sequences is shown in Figure 33. This diagram is similar to the residue-Frank phase code radar system in Chapter III, except that now the symmetrical residue-P4 phase code sequences are used instead. Each phase sequence with the length equal to the dynamic

range $\hat{M}_{SNS}$ is transmitted to detect the target. In the receiver, each code sequence is compressed with its corresponding conjugate of phase code.

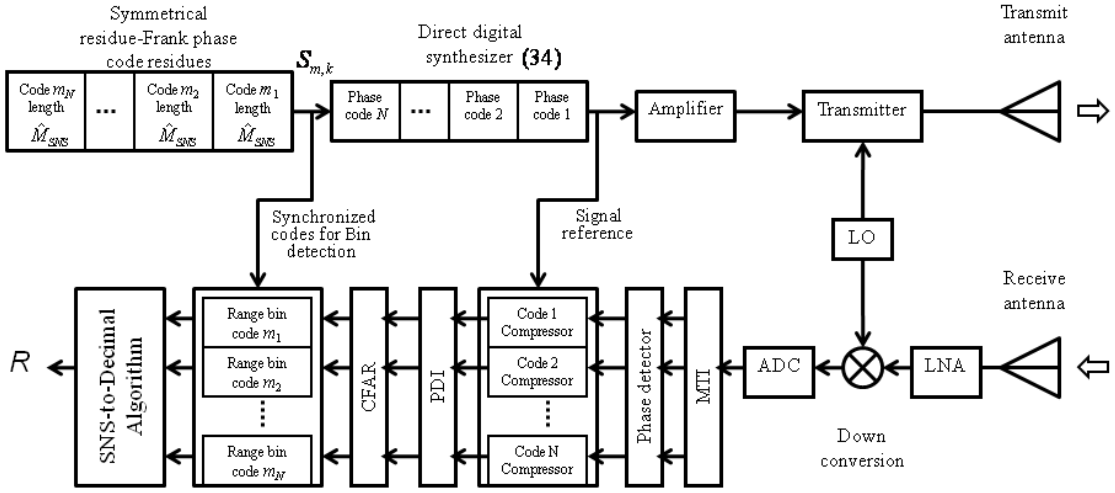

Figure 33. Block diagram for the radar using N symmetrical residue-P4 phase code sequences.

2. Transmitted and Reference Codes for Compression

In this section, the transmission of N symmetrical residue-P4 phase code sequences is explained as well as the phase code reference for compression. An example using $N = 3$ moduli with $m_1 = 7, m_2 = 8,$ and $m_3 = 9$ is illustrated. The dynamic range, using Equation (32) for these SNS moduli, is $\hat{M}_{SNS} = 37.$

Each sequence has the number of code length equal to the dynamic range with the transmitted signal as shown in Figure 34. To create the P4 code sequence, one code period requires the number of subcodes $N_c = m.$ To cover a dynamic range of subcode, the number of code periods required is

$$\hat{N}_{p,m} = \frac{\hat{M}_{SNS}}{m}. \tag{35}$$

For $m_1 = 7$ and $N_c = 7,$ Equation (35) gives $\hat{N}_{p,7} = 37/7 = 5.29,$ which last 5 subcodes $(7 \times 6 - 37 = 5)$ are not included since they are ambiguous. For modulus $m_2 = 8$ and

$m_3 = 9,$ the number of subcodes N_c for one code period are 8 and 9 respectively. Also, the maximum number of transmitted and received code periods are $\hat{N}_{p,8} = 4.63$ (the last 3 subcodes are not used) and $\hat{N}_{p,9} = 4.11$ (the last 8 subcodes are not used), respectively. In Figure 34, the code period corresponding to each modulus is denoted as $T_{m_i,p}$ where p represents the code period number.

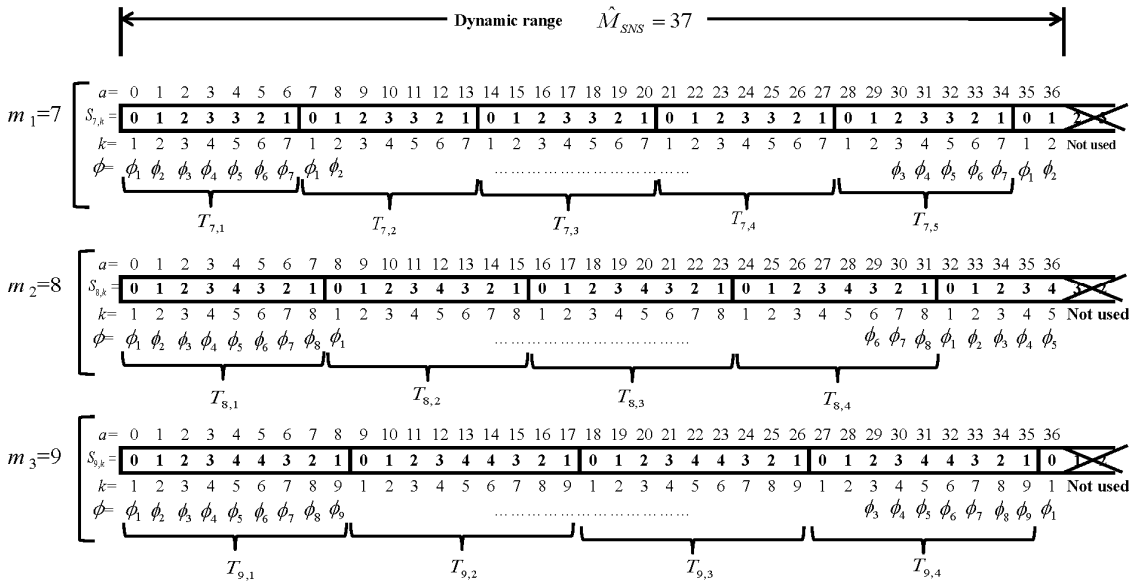

Figure 34. Illustration of transmitted signal using $N = 3$ symmetrical residue-P4 phase code sequences for $m_1 = 7, m_2 = 8,$ and $m_3 = 9.$

In Figure 35a, the symmetrical residues $S_{m,k}$ using $m_1 = 7, m_2 = 8,$ and $m_3 = 9$ ($\hat{M}_{SNS} = 37$) are shown. Since the phase sequences are periodic, $S_{m,k} = S_{m,k+nm}$ where $n \in \{0, \pm 1, \pm 2, ...\}$. The phase sequences from each channel are plotted in Figure 35b. Each symmetrical residue-P4 phase sequence has a phase code period equal to $N_c = m,$ giving $\phi_{m,k} = \phi_{m,k+nm}$. If the receiver uses one code period ($N_r = 1$), the reference code sequence for compression is the phase sequence from index $k = 1$ to $m.$

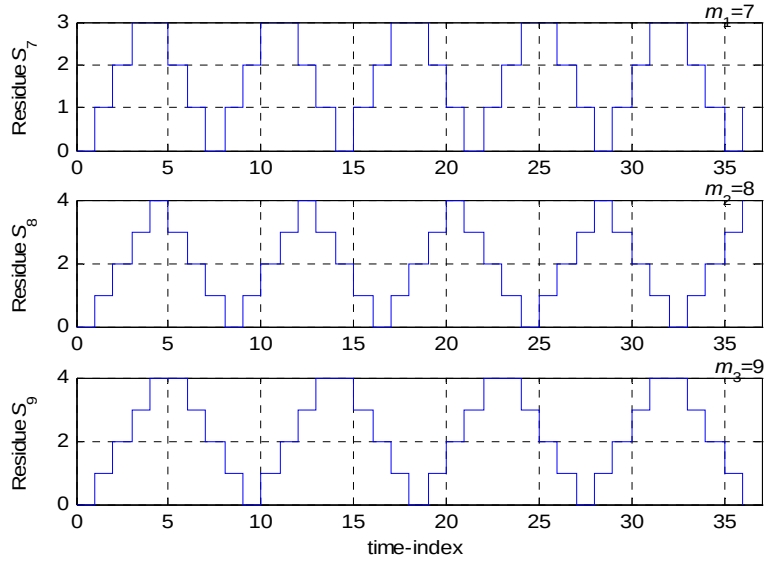

(a)

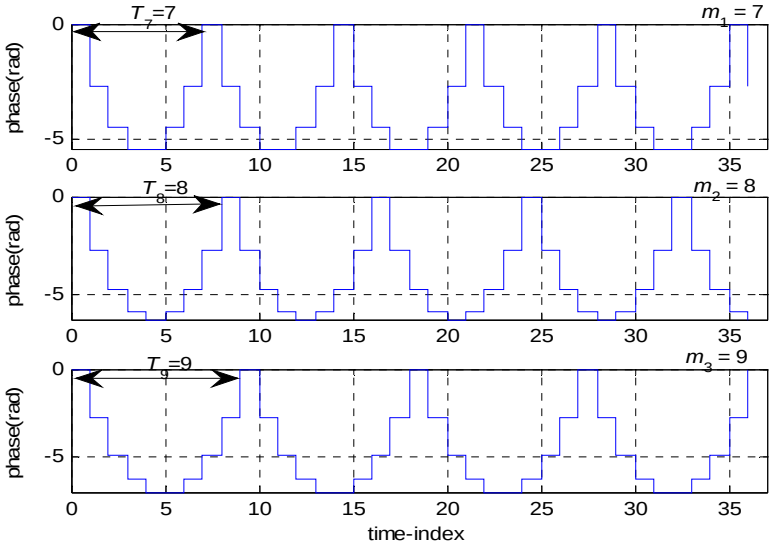

(b)

Figure 35. Plot of the symmetrical residue-P4 for $m_1 = 7$, $m_2 = 8$, and $m_3 = 9$ ($\hat{M}_{SNS} = 37$) showing (a) symmetrical residues, and (b) phase sequences from (34).

In Figure 36, the compression and range bin detection process is illustrated for $m_1 = 7$ and $N_r = 1$. The symmetrical residue-P4 phase code is returned to the radar receiver with delay τ and then processed by a filter matched to the rectangular pulse of duration t_b. Then the phase detector is used to calculate the phase of the signal and pass

it through the compressor. The output from the compression is then processed by threshold detection to see whether the amplitude reaches the desired minimum value. If the threshold detector detects the pulse, the presence of the target will be saved with the symmetrical residue value S_m. In $m_2 = 8$ and $m_3 = 9$, the process is similar, except that the phase references have to correspond to the transmitted phase code that is being received.

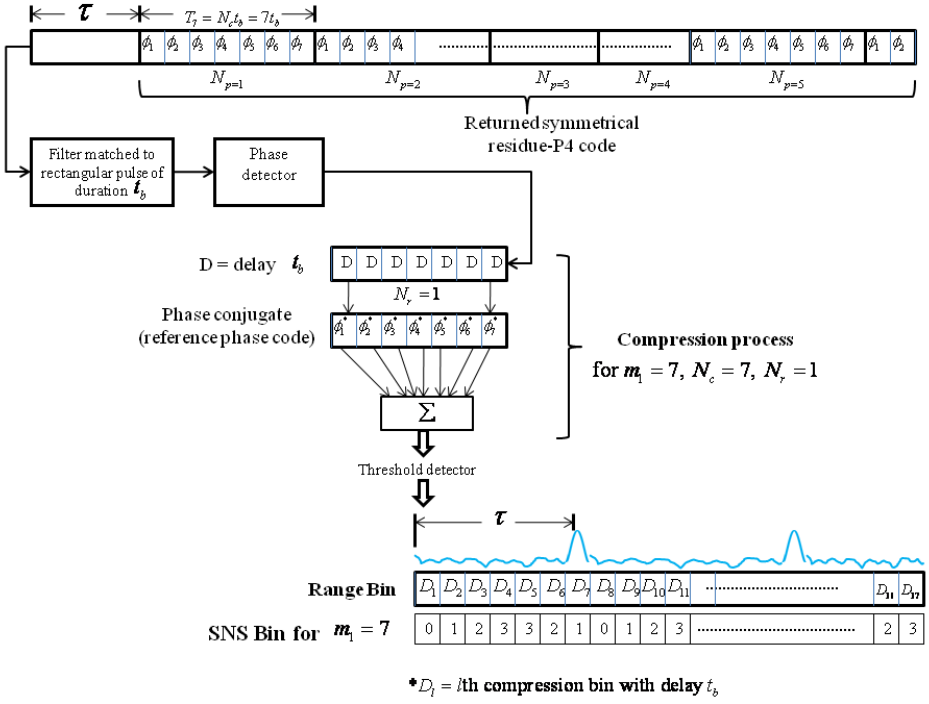

Figure 36. Illustration of compression at the receiver and the range bin for SNS $m_1 = 7,\ N_c = 7,$ and $N_r = 1$.

3. Calculating the Target Range

Using all channels, we see that the paired terms are mapped to a specific range bin input a (similar to residue-Frank code bin detection process). Continuing the example in the previous section for $m_1 = 7,\ m_2 = 8,$ and $m_3 = 9,$ we show the symmetrical residue paired values and the corresponding ranges in Table 6. The signal bandwidth $B = 1$ MHz, and the subcode period $t_b = 1\ \mu$s. The unambiguous range using symmetrical residue-P4 is

$$R_{u,SNS} = \frac{c\hat{M}_{SNS}t_b}{2}. \tag{36}$$

For this example, the maximum unambiguous range is 5550 m ($\hat{M}_{SNS} = 37$). Range resolution is 150 m ($\Delta R = ct_b / 2$).

Table 6. Bin matrix and range intervals of $3-$channel SNS for $m_1 = 7$, $m_2 = 8$, and $m_3 = 9$.

Bin a	$m_1 = 7$	$m_2 = 8$	$m_3 = 9$	Range (m)	Bin a	$m_1 = 7$	$m_2 = 8$	$m_3 = 9$	Range (m)
0	0	0	0	0 – 150	19	2	3	1	2850 – 3000
1	1	1	1	150 – 300	20	1	4	2	3000 – 3150
2	2	2	2	300 – 450	21	0	3	3	3150 – 3300
3	3	3	3	450 – 600	22	1	2	4	3300 – 3450
4	3	4	4	600 – 750	23	2	1	4	3450 – 3600
5	2	3	4	750 – 900	24	3	0	3	3600 – 3750
6	1	2	3	900 – 1050	25	3	1	2	3750 – 3900
7	0	1	2	1050 – 1200	26	2	2	1	3900 – 4050
8	1	0	1	1200 – 1350	27	1	3	0	4050 – 4200
9	2	1	0	1350 – 1500	28	0	4	1	4200 – 4350
10	3	2	1	1500 – 1650	29	1	3	2	4350 – 4500
11	3	3	2	1650 – 1800	30	2	2	3	4500 – 4650
12	2	4	3	1800 – 1950	31	3	1	4	4650 – 4800
13	1	3	4	1950 – 2100	32	3	0	4	4800 – 4950
14	0	2	4	2100 – 2250	33	2	1	3	4950 – 5100
15	1	1	3	2250 – 2400	34	1	2	2	5100 – 5250
16	2	0	2	2400 – 2550	35	0	3	1	5250 – 5400
17	3	1	1	2550 – 2700	36	1	4	0	5400 – 5550
18	3	2	0	2700 – 2850					

In Figure 37, an example of target detection for $m_1 = 7, m_2 = 8,$ and $m_3 = 9$ is illustrated. The target's return is in range bin $a = 4$ or 650 m. Shown in the graph are symmetrical residue $S_{m,k}$ (stair-step waveform), the range bin $a,$ and a helicopter target detection. The bin corresponding to the correlated output for channel $m_1 = 7$ is at $S_{m_1=7} = 3.$ Note the repeated pulse from the compression output due to the periodic phase code. The process is the same for the channel $m_2 = 8,$ and $m_3 = 9.$ The residue bins are $S_{m_2=8} = 4$ and $S_{m_3=9} = 4$ respectively. Then the three symmetrical residues are paired as [3 4 4], and the SNS-to-decimal algorithm is used to find the target's true range $R.$ From Table 6, the paired terms [3 4 4] correspond to the range bin $a = 4,$ and the calculated range is between 600 m and 750 m.

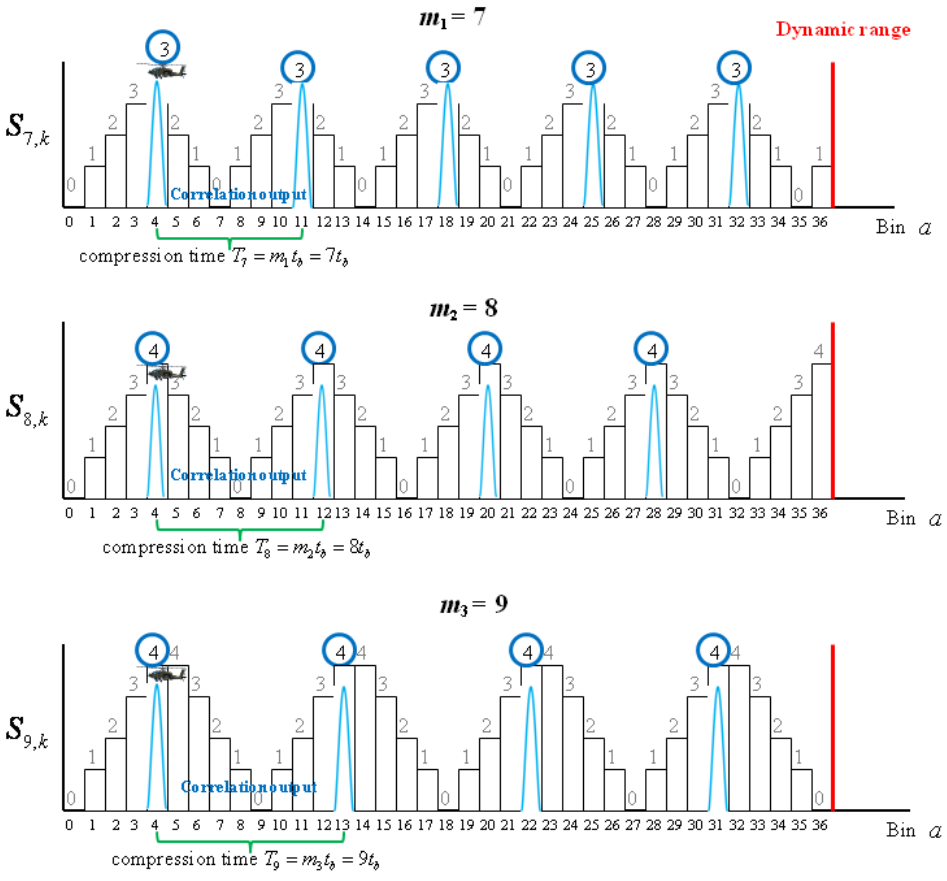

Figure 37. Illustration of target detection by using the range bin matrix for SNS-P4 code with $m_1 = 7, m_2 = 8,$ and $m_3 = 9.$

In Chapter III, we solved the system of congruences using CRT for recovering the target range bin a ($< \hat{M}_{SNS}$). Due to the definition of the SNS, $a \equiv \pm S_{m_1} (\mathrm{mod}\, m_1)$, $a \equiv \pm S_{m_2} (\mathrm{mod}\, m_2)$,…, $a \equiv \pm S_{m_N} (\mathrm{mod}\, m_N)$. For each of the congruences, either the plus or minus is correct, but we do not know which. Thus, we have $2N$ sets of N equations. For example, if $N = 2,$ we have

$$\text{i)} \quad a \equiv S_{m_1} (\mathrm{mod}\, m_1),$$
$$a \equiv S_{m_2} (\mathrm{mod}\, m_2),$$

$$\text{ii)} \quad a \equiv S_{m_1} (\mathrm{mod}\, m_1),$$
$$a \equiv -S_{m_2} (\mathrm{mod}\, m_2),$$

$$\text{iii)} \quad a \equiv -S_{m_1} (\mathrm{mod}\, m_1),$$
$$a \equiv -S_{m_2} (\mathrm{mod}\, m_2),$$

$$\text{iv)} \quad a \equiv -S_{m_1} (\mathrm{mod}\, m_1),$$
$$a \equiv S_{m_2} (\mathrm{mod}\, m_2).$$

The CRT guarantees that each of these has a unique solution modulo $m_1 m_2,$ and exactly one of these solutions lies within the dynamic range of the system. This is the value of a. In fact, it is only necessary to solve (i) and (ii) at most because the solutions to (iii) and (iv) are the negatives of the solutions to (i) and (ii), respectively.

Recall that in the standard statement of the CRT we wish to solve for a where $a \equiv S_{m_i} (\mathrm{mod}\, m_i),\ 1 \le i \le N,$ and the m_i are pairwise relatively prime. The solution is

$$a \equiv \frac{M_{RNS} b_1 a_1}{m_1} + \frac{M_{RNS} b_2 a_2}{m_2} + \ldots + \frac{M_{RNS} b_N a_N}{m_N} \tag{37}$$

where $M_{RNS} = \prod_{i=1}^{N} m_i$. Note that the values of b_i depend only on m_i and not at all on $\pm S_{m_i}$. Thus, we may assume that the constants $c_i = M_{RNS} b_i / m_i$ are known, and the SNS-

to-decimal algorithm only needs to evaluate $\pm c_1 S_{m_1} \pm c_2 S_{m_2} \pm \ldots c_N S_{m_N}$ modulo M_{RNS} and picks the one value that lies within the dynamic range $\hat{M}_{SNS}$.

4. Resolving Multiple Target Range Ambiguities

In this section, the detection of multiple targets is considered. In Figure 38, we see that the symmetrical residue for the two targets are periodic as $S_{m,k} = S_{m,k+nm}$. If there are no missed targets in the detection process, the sequence of symmetrical residues within each modulus can be paired directly for the solution of the target's range. To solve for the range of each target, the residues are paired as [2 3 4] for the first target and [2 2 1] for the second target. From the CRT or lookup table, the range of the first target is $750 \le R_1 \le 900$ m ($a = 5$), and the range of the second target is $3900 \le R_2 \le 4050$ m ($a = 26$).

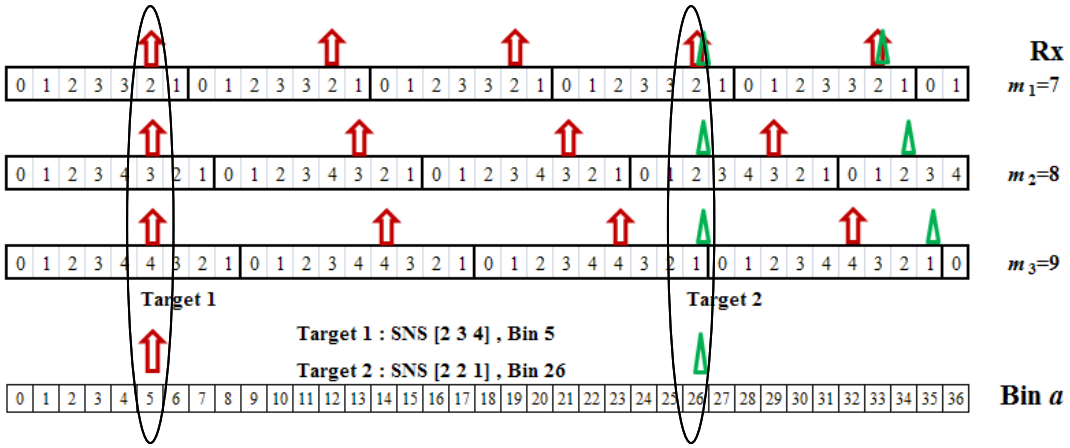

Figure 38. Resolving the range ambiguity of 2 targets using SNS for $m_1 = 7, m_2 = 8,$ and $m_3 = 9.$

In Figure 39, if the first set of symmetrical residues for the two targets are not detected, the symmetrical residue-P4 phase code still allow the two target range values to be determined. Note the symmetrical residues are determined but there is no information available to pair them up correctly. Additional information must be used. For example, for m_1, we have $S_7 = \{2, 2\}$, for m_2, we have $S_8 = \{3, 2\}$, and for m_3, we have

$S_9 = \{4, 1\}$. To pair them up correctly, the magnitude information associated with each subcode (from the phase detector) can be used.

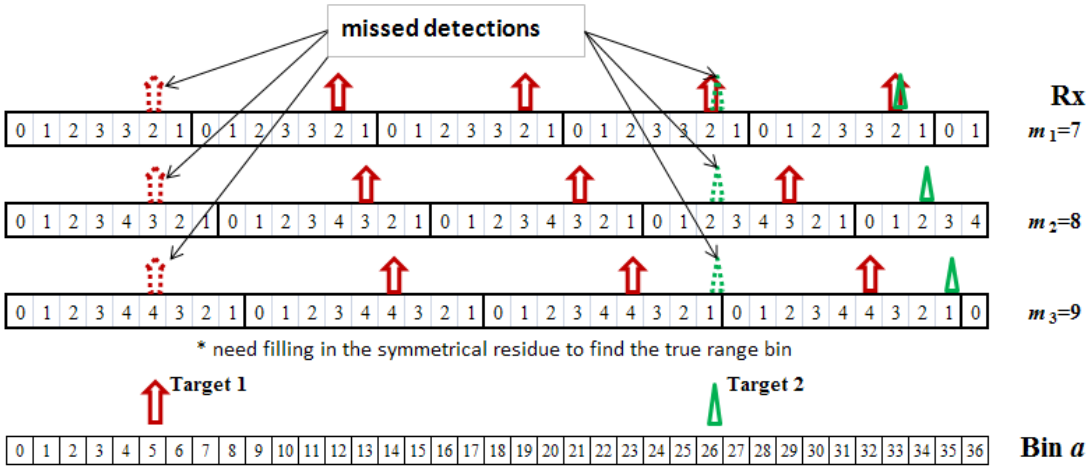

Figure 39. Missed detections of the first set of symmetrical residues.

A more convenient method is to extend or fill in the symmetrical residues according to their code periods, which can be identified through examination of the symmetrical residues throughout the unambiguous range. This result gives the same symmetrical residue configuration as shown in Figure 38. Note that this method works even with the target symmetrical residues overlapping.

5. Practical Considerations

a. Detection of Target in Noise Using SNS Compression

In this section, the performances of the $N = 3$ SNS for $m_1 = 7, m_2 = 8,$ and $m_3 = 9$ with $\hat{M}_{SNS} = 37$ are examined by using MATLAB to plot the returned signal from two targets at ranges of 890 m and 2990 m, respectively. The transmitted signal have amplitude $A = 1,$ carrier frequency $f_c = 1$ MHz, sampling frequency $f_s = 7$ MHz, $cpp = 1,$ and $t_b = 1\ \mu$s. The two different SNRs are examined. In Figure 40, the transmitted signal without noise for each channel is plotted. In Figure 41, the signal with SNR = 30 dB is plotted. For the data shown in Figure 42, the SNR is reduced to 0 dB. The phase sequences are changed significantly with the increase in noise power.

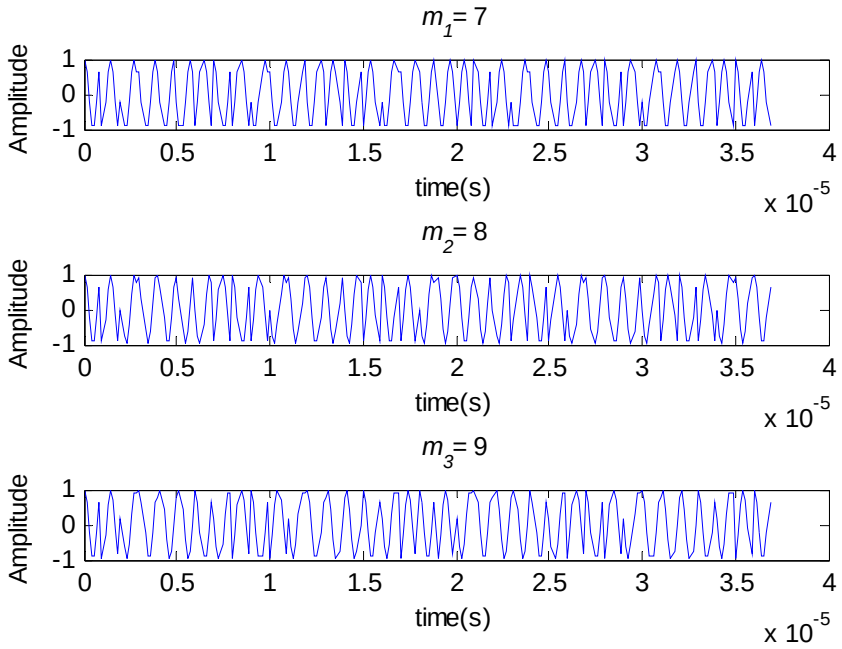

Figure 40. Symmetrical residue-P4 signal without noise for $m_1 = 7,\ m_2 = 8,$ and $m_3 = 9$ with $\hat{M}_{SNS} = 37,\ A = 1,\ f_c = 1$ MHz, $f_s = 7$ MHz, $cpp = 1,$ and $t_b = 1\ \mu$s.

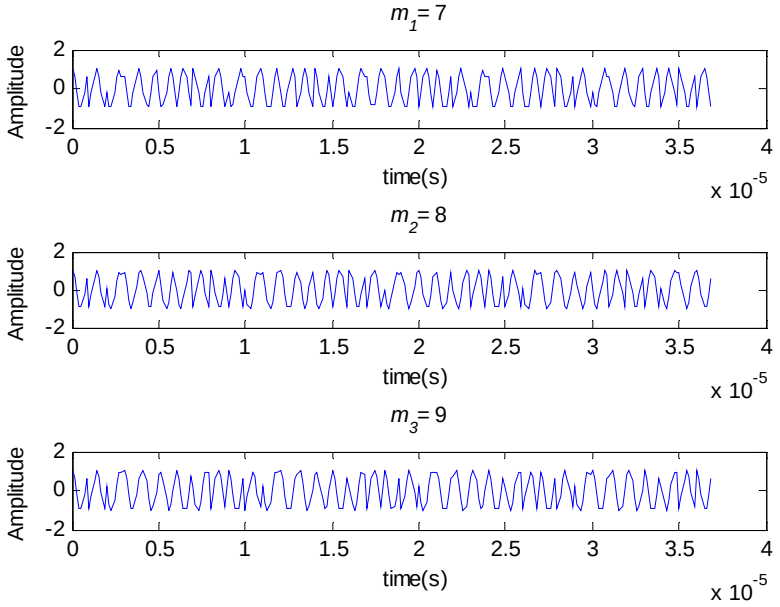

Figure 41. Symmetrical residue-P4 signal with SNR = 30 dB for $m_1 = 7,\ m_2 = 8,$ and $m_3 = 9$ with $\hat{M}_{SNS} = 37,\ A = 1,\ f_c = 1$ MHz, $f_s = 7$ MHz, $cpp = 1,$ and $t_b = 1\ \mu$s.

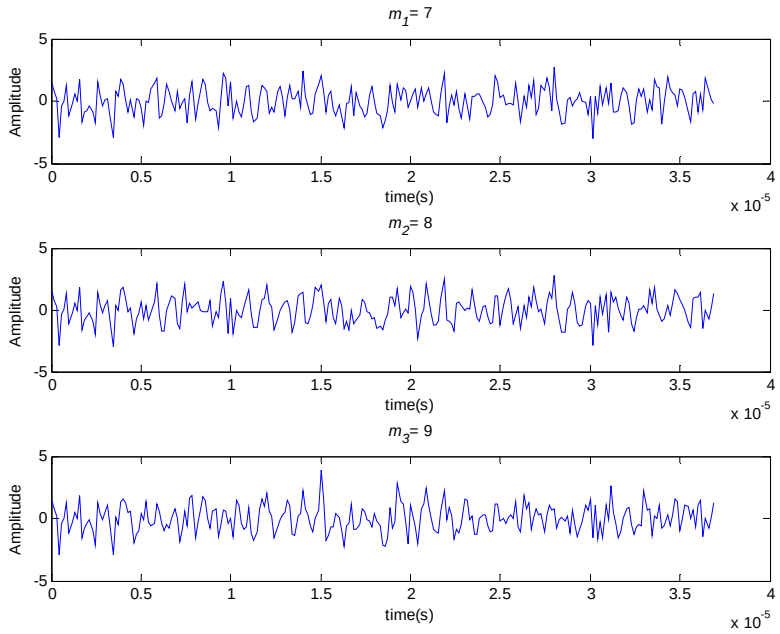

Figure 42. Symmetrical residue-P4 signal with SNR = 0 dB for $m_1 = 7$, $m_2 = 8$, and $m_3 = 9$ with $\hat{M}_{SNS} = 37$, $A = 1$, $f_c = 1$ MHz, $f_s = 7$ MHz, $cpp = 1$, and $t_b = 1$ μs.

In Figures 43 and 44, the range bin profiles for each channel are shown using SNR = 30 dB and SNR = 0 dB, respectively. The first target appears at range bin $a = 5$ with the paired symmetrical residues [2 3 4] (range 750–900 m). The second target appears at range bin $a = 19$ with the paired symmetrical residues [2 3 1] (range 2850–3000 m). Also shown is the noise signal that is compressed before the returned signals from the targets arrive at the receiver. In Figure 44, the amplitudes of compressed pulses degrade when the SNR is decreased to 0 dB. The effect from the noise signal degrades the ability to detect the targets similar to that discussed in the residue-Frank phase code radars. The average sidelobes from the higher modulus (e.g. $m_3 = 9$) are lower than those from the lower modulus (e.g., $m_1 = 7$ and $m_2 = 8$) due to the different processing gain. For $m_1 = 7, m_2 = 8,$ and $m_3 = 9,$ the processing gains are $N_{c1} = 7$, $N_{c2} = 8,$ and $N_{c3} = 9,$ respectively.

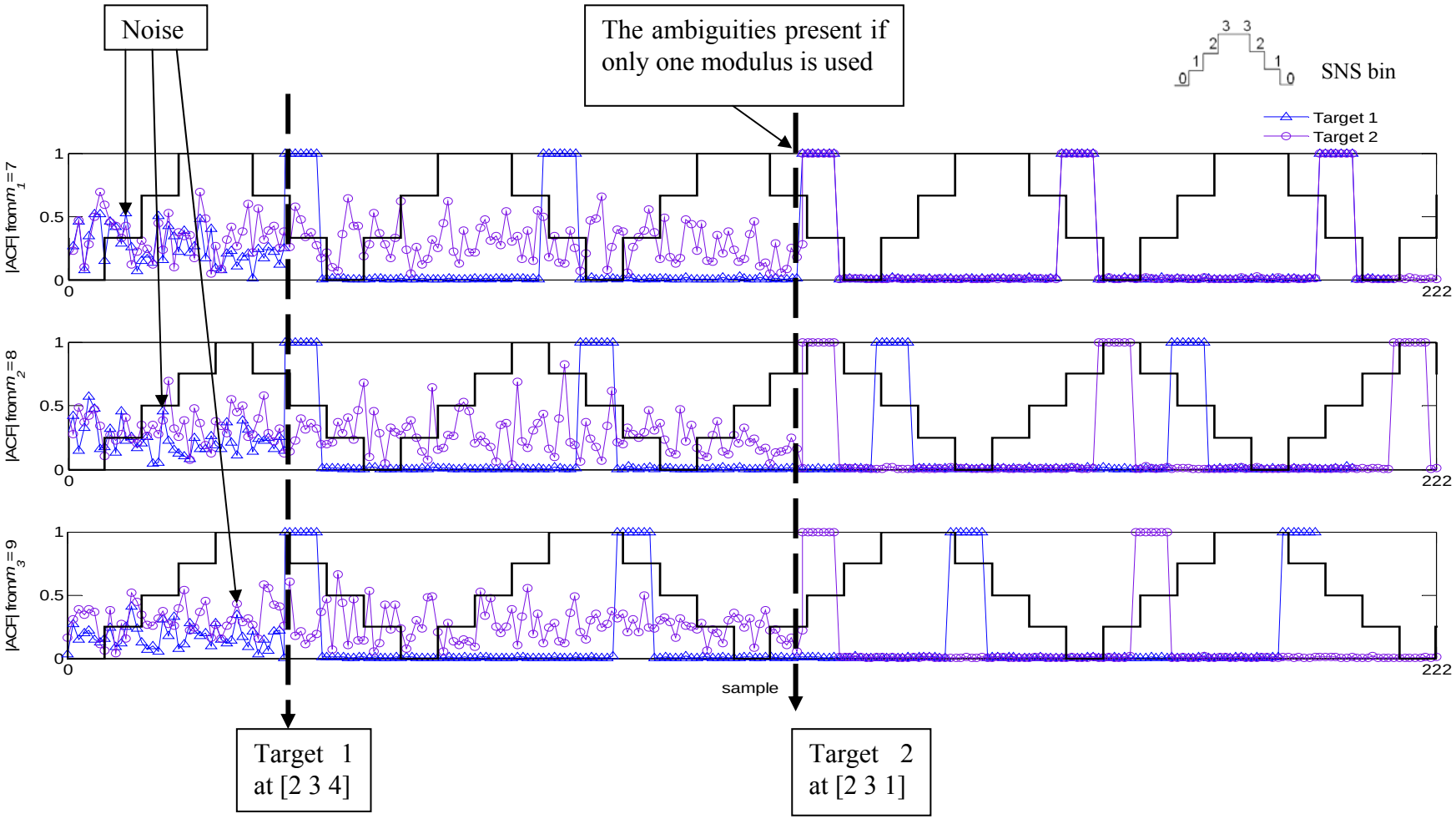

Figure 43. Target detection for SNR = 30 dB showing the range bins for $m_1 = 7$, $m_2 = 8$, and $m_3 = 9$ with two targets at 890 m and 2990 m.

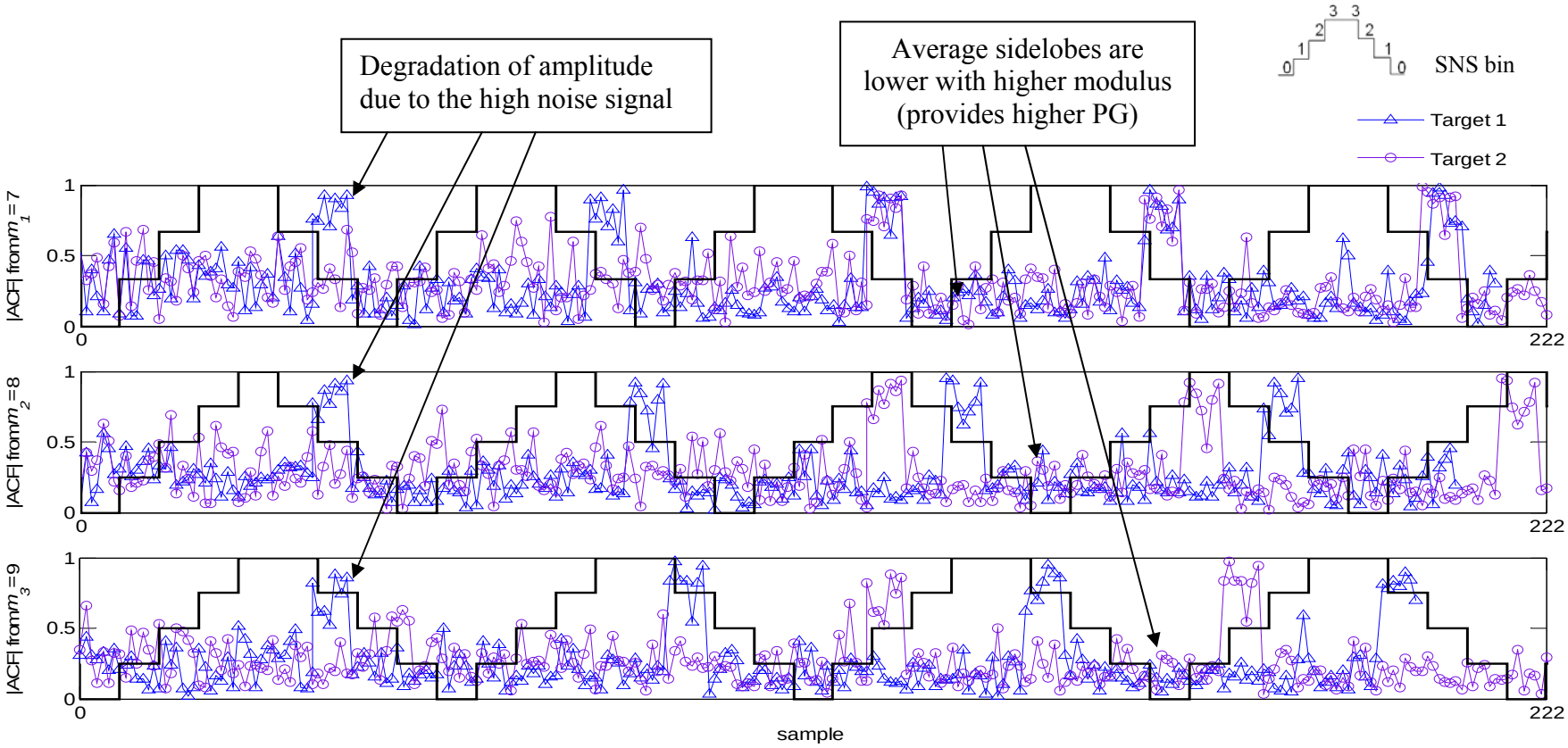

Figure 44. Target detection for SNR = 0 dB showing the range bins for $m_1 = 7$, $m_2 = 8$, and $m_3 = 9$ with two targets at 890 m and 2990 m.

Like the RNS phase code, a situation in where the threshold detector might read the wrong residue bin can occur because the amplitudes of the compressed pulses fluctuate due to the noise. This results in the target range error. In Figure 45, the first target in channel $m_2 = 8$ is seen with the compressed pulse detected by CFAR (threshold level at 0.85) at symmetrical residue $S_8 = 2$ instead of $S_8 = 3$. So, the paired terms are now [2 2 4] (no range match) instead of the true range at [2 3 4] (range 750–900 m). This results in target range error.

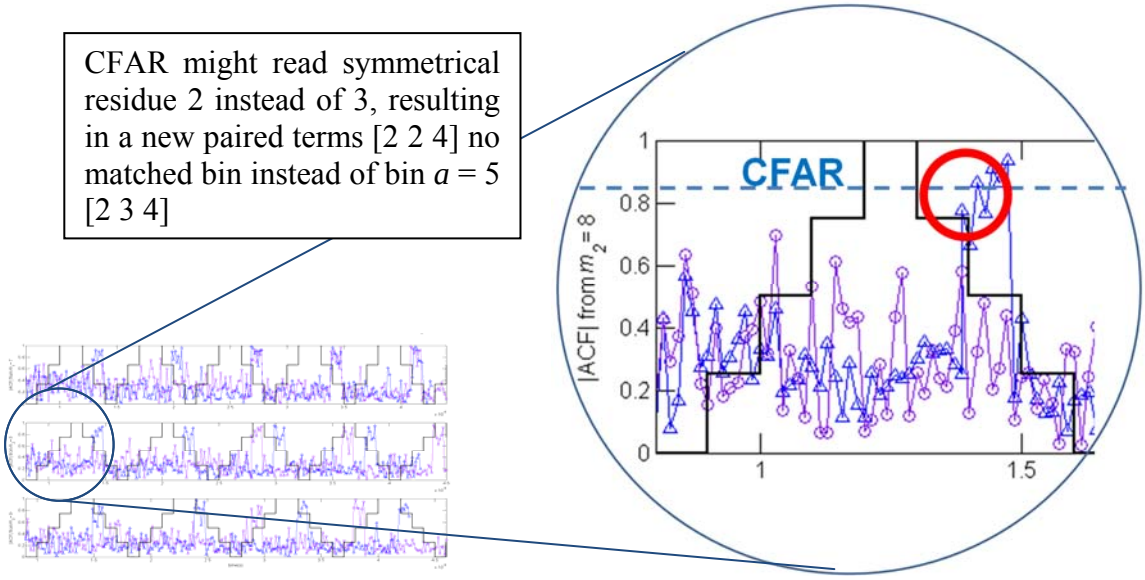

Figure 45. Illustration of detection error from the threshold detector (CFAR) using the symmetrical residue-P4 for $m_1 = 7,\ m_2 = 8,$ and $m_3 = 9$.

b. Required CW Signal Power Versus Required Output SNR

In this section, the CW power required when using the symmetrical residue-P4 phase code sequences to detect the target at the fixed unambiguous range $R_u = 5550$ m is presented. The relationship between the required SNR_{Ro} and the average CW power P_{CW} is given by Equation (26).

In Figure 46, the CW signal power as a function of the required output SNR_{Ro} for $m_1 = 7,\ m_2 = 8,$ and $m_3 = 9$ is plotted with $B_{Ri} = 1$ MHz, $t_b = 1\ \mu$s,

$G_t = G_r = 30$ dB, $f_c = 3$ GHz, $\lambda = 0.1$ m, $\sigma_T = 100$ m^2, $F_R = 5$ dB, $L_2 = L_{RT} = L_{RR} = 1$, and $R_u = c\hat{M}_{SNS} t_b / 2 = 5550$ m (maximum detection range without ambiguity).

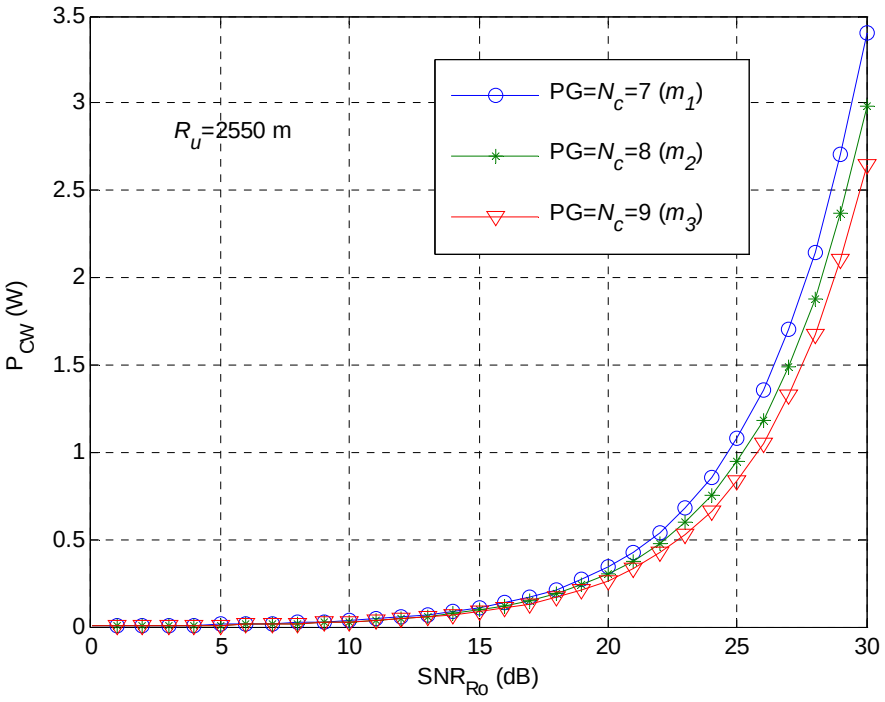

Figure 46. Average power of the CW transmitter for symmetrical residue-P4 with $m_1 = 7$, $m_2 = 8$, and $m_3 = 9$.

Note that the difference of the average power used in each channel is due to the PG. The channel $m_3 = 9$, giving $PG = N_c = m_i = 9$, requires less power than the other channels, $m_1 = 7$ ($PG = 7$) and $m_2 = 8$ ($PG = 8$).

c. Unambiguous Detection Range for a Constant Output SNR

For a single P4 code, the unambiguous range is limited to only one code period ($R_u = cT / 2 = ct_b N_c / 2$). In this section, we compare the maximum unambiguous range using the symmetrical residue-P4 phase code sequences with the corresponding single P4 code sequences. The relationship between the average signal power P_{CW} and the maximum detection range $R_{\max}$ is given by Equation (27).

In Figure 47, the detection range is plotted as a function of the required CW power using $N = 3$ SNS for $m_1 = 7$, $m_2 = 8$, and $m_3 = 9$ with $SNR_{Ro} = 13$ dB, $B = 1$ MHz, $t_b = 1\ \mu$s, $G_t = G_r = 30$ dB, $f_c = 3$ GHz, $\lambda = 0.1$ m, $\sigma_T = 100$ m^2, $T_0 = 290$ K, $F_R = 5$ dB, and $L_2 = L_{RT} = L_{RR} = 1$. For comparison, the performance of each P4 code using the corresponding N_c is plotted. For the P4 code from Equation (28), $N_{c1} = 7$ and $N_{c2} = 8$, and $N_{c3} = 9$. The single P4 code has a limited unambiguous range, $N_{c1} = 7$ gives $R_u = 3\times10^8 \times10^{-6} \times 7/2 = 1050$ m, $N_{c2} = 8$ gives $R_u = 3\times10^8 \times10^{-6} \times 8/2 = 1200$ m, and $N_{c3} = 9$ gives $R_u = 3\times10^8 \times10^{-6} \times 9/2 = 1350$ m. These values are less than using the $N = 3$ symmetrical residue-P4 phase code sequences, giving $R_{u_{RNS}} = cM_{SNS}t_b/2 = 5550$ m.

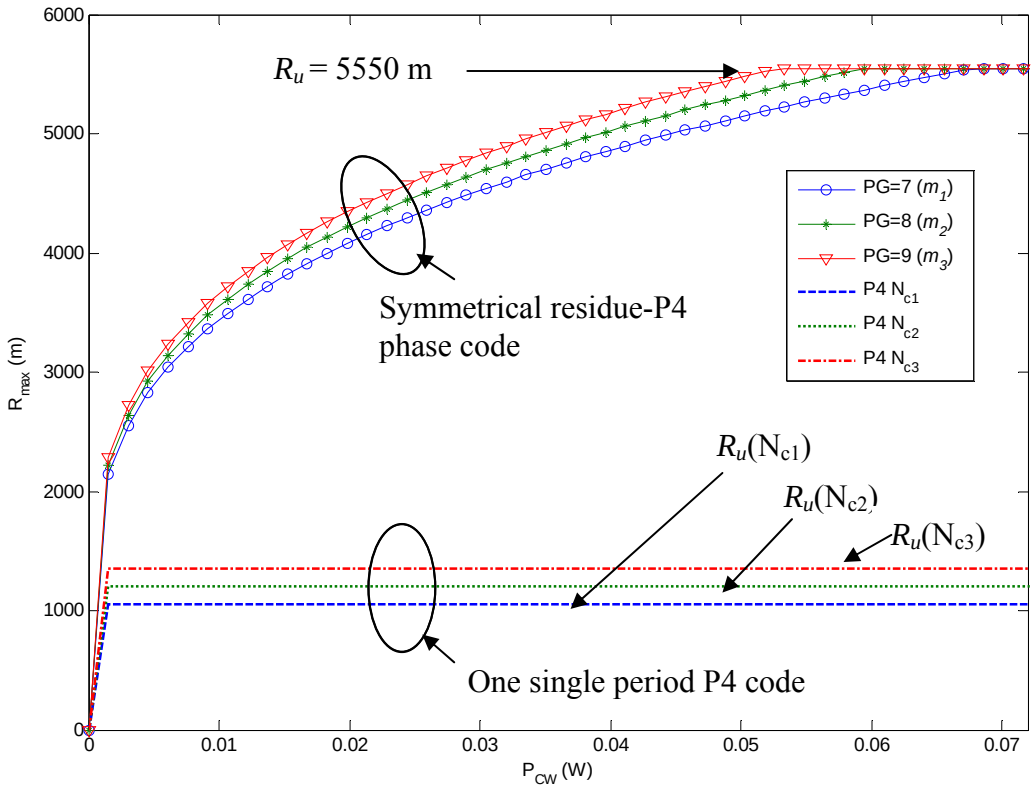

Figure 47. Comparison of the maximum unambiguous range of a CW radar system for $SNR_{Ro} = 13$ dB using symmetrical residue-P4 phase code for $m_1 = 7$, $m_2 = 8$, and $m_3 = 9$ with the radar using each P4 code individually with the corresponding N_c.

In conclusion, the symmetrical-P4 phase code sequence presented in this chapter can be used to extend the unambiguous range of the CW polyphase radar systems. The issue concerned with the range bin error due to the fluctuation of the compression outputs was considered. In the next chapter, the relationship between the P4 code and the robust symmetrical number system (RSNS) is presented to examine the integer Gray code properties and how they can prevent an error in the detected symmetrical residues.

V. P4 POLYPHASE MODULATION AND THE ROBUST SYMMETRICAL NUMBER SYSTEM

As discussed in Chapters III and IV, using the RNS and the SNS may give a large error in the target's range when the threshold detector detects the wrong residue due to the presence of noise which can change the phase of the received signal. In this chapter, the RSNS is presented, and it is shown that the range errors in the robust symmetrical residue-P4 phase code sequence can be bounded to a small value due to the Gray code property of the RSNS [20]. The P4 phase expression is presented and examples are given to illustrate the target detection process with this new waveform.

A. P4 PHASE CODE

The details of the P4 phase code are discussed in Chapter IV. The P4 phase code is derived from a linearly frequency modulated waveform (LFMW). To calculate the phase sequence, Equation (28) is used. Recall the characteristics of the P4 code sequence is its superior PAF sidelobe structure and its Doppler tolerance properties.

B. THE ROBUST SYMMETRICAL NUMBER SYSTEM

The RSNS is a modular system consisting of $N \geq 2$ integer sequences with each sequence associated with a coprime modulus m_i. Due to the presence of ambiguities, the set of integers within each RSNS sequence do not form a *complete residue system*. A set of integers $y_0, y_1, \ldots, y_{m-1} (\mathrm{mod}\, m)$ form a complete residue system if $y_g \equiv g (\mathrm{mod}\, m)$ for $g = 0,1,\ldots,m-1$ [21]. The ambiguities within each modulus sequence are resolved by the use of additional moduli and considering the vector of paired integers from all *N* sequences. The RSNS is based on the sequence

$$\left\{RS'_{m,h}\right\} = [0,1,2,\ldots,m-1,m,m-1,\ldots,2,1] \tag{38}$$

for an integer h such that $0 \leq h < 2m$. To form the *N*-sequence RSNS, each term in (38) is repeated N times in succession. The integers within one folding period of a sequence are then

$$\left\{RS_{m,h}\right\} = [0,0\cdots,0,1,1,\cdots,1,\cdots,m-1,\cdots,m-1, \\ m,m,\cdots m,m-1,\cdots,m-1,\cdots,1,\cdots,1]. \tag{39}$$

This results in a periodic sequence with a period of [20]

$$P_m = 2Nm. \tag{40}$$

That is, each RSNS sequence contains m_i integers with the folding period of each sequence equal to $2Nm_i$. The construction of the N sequences ensures that any two successive RSNS vectors (paired integers from the N sequences) differ by only one integer, resulting in an *integer Gray code* property.

Each sequence corresponding to m_i is right (or left) shifted by $s_i = i-1$ places. The chosen shift values $\{s_1, s_2, \ldots, s_N\}$ must also form a complete residue system modulo N. Further, if each sequence is extended periodically with period $2Nm$ as $RS_{m,h+n2Nm} = RS_{m,h}$ where $n \in \{0, \pm 1, \pm 2, ...\}$, then $RS_{m,h}$ is called a symmetrical residue of $(h + n2Nm)$ modulo $2Nm$.

The calculation of $\hat{M}_{RSNS}$ and its location in the sequence are a function of N and the choices for m_i and s_i. A closed-form solution for computing $\hat{M}_{RSNS}$ for $N = 2$ moduli is reported in [22], and summarized as follows:

For $m_1 \geq 3$ and $m_2 = m_1 + 1$

$$\hat{M}_{RSNS} = 3(m_1 + m_2) - 6 = 6m_1 - 3. \tag{41}$$

For $5 \leq m_1 < m_2$ and $m_2 \leq m_1 + 2$

$$\hat{M}_{RSNS} = 4m_1 + 2m_2 - 5. \tag{42}$$

For $5 \leq m_1 < m_2$ and $m_2 \geq m_1 + 3$

$$\hat{M}_{RSNS} = 4m_1 + 2m_2 - 2. \tag{43}$$

A closed-form solution for $N = 3$ moduli of the form $2^z - 1, 2^z, 2^z + 1$ is

$$\hat{M}_{RSNS} = \frac{3}{2}m_1^2 + \frac{15}{2}m_1 + 7 \tag{44}$$

where z is any integer and $m_1 \geq 3$ [23]. An efficient algorithm for computing $\hat{M}_{RSNS}$ and its position for any general set of moduli is reported in [24]–[25].

The shift values s_i for each sequence do not affect the RSNS dynamic range but do make a difference in the location of the beginning position h of the dynamic range and the ending position $h + \hat{M}_{RSNS} - 1$. After choosing the beginning h, it is useful to know the symmetrical residues at this point (e.g., to align the symmetrical residues for each sequence). Since each folding period consists of $2Nm_i$ integers, the symmetrical residues are determined by first subtracting off an integer number of $2Nm_i$ integers as

$$n_i = h - \left\lfloor \frac{h}{2Nm_i} \right\rfloor 2Nm_i \ . \tag{45}$$

This value is then used to find the symmetrical residue $RS_{m_i,h}$ as [20]

$$RS_{m,h} = \begin{cases} \left\lfloor \dfrac{n_i - s_i}{N} \right\rfloor & s_i \leq n_i \leq Nm_i + s_i + 1 \\ \left\lfloor \dfrac{2Nm_i + N - n_i + s_i - 1}{N} \right\rfloor & Nm_i + s_i + 2 \leq n_i \leq 2Nm_i + s_i - 1. \end{cases} \tag{46}$$

Let X_h be the vector of N paired integers from each sequence at h where h is the position of the vector X_h within the RSNS. In Table 7, h and X_h for an N = 3 RSNS system with $m_i = [3\ 4\ 5]^T$ and right shift $s_i = [0,1,2]^T$ are shown. For this example, the RSNS dynamic range $\hat{M}_{RSNS} = 43,$ and the position begins at $h = 61$ [20]. The vector $X_{61} = [2\ 4\ 1]^T$. The set of integers that lie within the dynamic range $\hat{M}_{RSNS} = 43$ contain no ambiguities. Also note in Table 7 the integer Gray code property where any code transition results in just one integer changing value by ± 1. Also shown is the bin index a which runs from 0 to 42 (total 43) that will be used to refer to the range bin detection.

Table 7. The RSNS folding waveforms for $m_1 = 3$ $(s_1 = 0)$, $m_2 = 4$ $(s_2 = 1)$, and $m_3 = 5$ $(s_3 = 2)$ (After [20]).

h	61	62	63	64	65	66	67	68	.....	96	97	98	99	100	101	102	103
$m_1 = 3$	2	2	3	3	3	2	2	2		2	2	2	3	3	3	2	2
$m_2 = 4$	4	4	4	3	3	3	2	2		1	0	0	0	1	1	1	2
$m_3 = 5$	1	0	0	0	1	1	1	2		1	1	2	2	2	3	3	3
a	0	1	2	3	4	5	6	7	.....	35	36	37	38	39	40	41	42

C. ROBUST SYMMETRICAL RESIDUE-P4 PHASE CODE

Similar to the SNS phase code, the RSNS folding waveform can be related to the P4 code sequence. The RSNS symmetrical residues $RS_{m,k'}$ can be folded into the P4 phase sequence by associating $RS_{m,k'}$ with the P4 subcode phases. The phase index k' starts from 1 to $N_{c_{RSNS}}$, where $N_{c_{RSNS}}$ is the number of RSNS subcodes within one code period. The robust symmetrical residue-P4 phase sequence is given by

$$\phi_{m,k'} = \left[\frac{\pi}{2m}\left(RS_{m,k'} - m\right)^2\right] - \frac{\pi}{2}m \tag{47}$$

and

$$N_{c_{RSNS}} = 2mN \tag{48}$$

where N is the number of channels. For example, if we choose $m = 4$, $N = 2$, and $N_{c_{RSNS}} = 16$. The robust symmetrical residue-P4 phase code sequence is $RS_{m=4,k'} = \{0,0,1,1,2,2,3,3,4,4,3,3,2,2,1,1\}$. Note that the folding sequence is similar to SNS with $m = 8$, $S_{m=8,k} = \{0,1,2,3,4,3,2,1\}$ except that the robust symmetrical residue-P4 phase is repeated N times; there are N phase values for each robust symmetrical-P4 phase for every P4 phase value. That is, both $k' = 1$ and $k' = 2$ of the RSNS corresponds to $k = 1$

for the P4 phase. Consequently, the number of subcodes N_c for the P4 code is related to the number of RSNS subcodes $N_{c_{RSNS}}$ as

$$N_c = \frac{N_{c_{RSNS}}}{N}. \tag{49}$$

Also, the PG for the robust symmetrical residue-P4 waveform is

$$PG_{RSNS} = N_c = \frac{N_{c_{RSNS}}}{N} = 2m. \tag{50}$$

1. Example of Phase Sequence Calculation

In this section, the phase code sequences from equations (47) and (28) are compared. Equation (47) is used to calculate the phase sequence for $m = 4,\ N = 2,$ and $N_{c_{RSNS}} = 16.$ Using the RSNS, we find that the robust symmetrical residues are $RS_{m=4,k'} = \{0,\ 0,\ 1,\ 1,\ 2,\ 2,\ 3,\ 3,\ 4,\ 4,\ 3,\ 3,\ 2,\ 2,\ 1,\ 1\}$ where $k' = 1, 2, ..., 16.$ In order to compare to the P4 phase sequence in Equation (28) with $N_c = N_{c_{RSNS}} / N = 16/2 = 8,\ k =$ 1,2,3,…,8, the two phase sequences are shown in Table 8.

Table 8. Comparison of the robust symmetrical residue-P4 phase code sequence ($m = 4,\ N = 2,\ N_{c_{RSNS}} = 16$) with the P4 phase code ($N_c = 8$).

Phase index	Robust symmetrical reside-P4 phase code (47)		P4 phase code (28)	
(k')	$RS_{m=4,k'}$	$\phi_{m=4,k'}$ (rad)	k	ϕ_k (rad)
1	0	$\phi_1 = \left(\frac{\pi}{2\cdot 4}(0-4)^2\right) - \frac{\pi}{2}4 = 0$	1	$\phi_1 = \frac{\pi(1-1)^2}{8} - \pi(1-1) = 0$
2	0	$\phi_2 = \left(\frac{\pi}{2\cdot 4}(0-4)^2\right) - \frac{\pi}{2}4 = 0$		
3	1	$\phi_3 = \left(\frac{\pi}{2\cdot 4}(1-4)^2\right) - \frac{\pi}{2}4 = -2.7489$	2	$\phi_2 = \frac{\pi(2-1)^2}{8} - \pi(2-1) = -2.7489$
4	1	$\phi_4 = \left(\frac{\pi}{2\cdot 4}(1-4)^2\right) - \frac{\pi}{2}4 = -2.7489$		

5	2	$\phi_5=\left(\frac{\pi}{2\cdot 4}(2-4)^2\right)-\frac{\pi}{2}4=-4.7124$	3	$\phi_3=\frac{\pi(3-1)^2}{8}-\pi(3-1)=-4.7124$
6	2	$\phi_6=\left(\frac{\pi}{2\cdot 4}(2-4)^2\right)-\frac{\pi}{2}4=-4.7124$		
7	3	$\phi_7=\left(\frac{\pi}{2\cdot 4}(3-4)^2\right)-\frac{\pi}{2}4=-5.8905$	4	$\phi_4=\frac{\pi(4-1)^2}{8}-\pi(4-1)=-5.8905$
8	3	$\phi_8=\left(\frac{\pi}{2\cdot 4}(3-4)^2\right)-\frac{\pi}{2}4=-5.8905$		
9	4	$\phi_9=\left(\frac{\pi}{2\cdot 4}(4-4)^2\right)-\frac{\pi}{2}4=-6.2832$	5	$\phi_5=\frac{\pi(5-1)^2}{8}-\pi(5-1)=-6.2832$
10	4	$\phi_{10}=\left(\frac{\pi}{2\cdot 4}(4-4)^2\right)-\frac{\pi}{2}4=-6.2832$		
11	3	$\phi_{11}=\left(\frac{\pi}{2\cdot 4}(3-4)^2\right)-\frac{\pi}{2}4=-5.8905$	6	$\phi_6=\frac{\pi(6-1)^2}{8}-\pi(6-1)=-5.8905$
12	3	$\phi_{12}=\left(\frac{\pi}{2\cdot 4}(3-4)^2\right)-\frac{\pi}{2}4=-5.8905$		
13	2	$\phi_{13}=\left(\frac{\pi}{2\cdot 4}(2-4)^2\right)-\frac{\pi}{2}4=-4.7124$	7	$\phi_7=\frac{\pi(7-1)^2}{8}-\pi(7-1)=-4.7124$
14	2	$\phi_{14}=\left(\frac{\pi}{2\cdot 4}(2-4)^2\right)-\frac{\pi}{2}4=-4.7124$		
15	1	$\phi_{15}=\left(\frac{\pi}{2\cdot 4}(1-4)^2\right)-\frac{\pi}{2}4=-2.7489$	8	$\phi_8=\frac{\pi(8-1)^2}{8}-\pi(8-1)=-2.7489$
16	1	$\phi_{16}=\left(\frac{\pi}{2\cdot 4}(1-4)^2\right)-\frac{\pi}{2}4=-2.7489$		

2. ACF, PACF, and PAF

In this section, we examine the ACF, PACF, and PAF of the signal. To compare the robust symmetrical reside-P4 phase code sequence with the P4 phase code sequence, the ACF, PACF, and PAF are examined for each waveform. In Figure 48, the robust symmetrical residues using $m_i = 16,\ N = 2,$ and $N_{c_{RSNS}} = 64$ are shown. In Figure 49, the robust symmetrical residue-P4 phase code sequence residues are shown (using Equation (47)) with $f_c = 1$ kHz, $f_s = 7$ kHz, and $cpp = 2.$ Note that cpp represents the number of

carrier cycles per phase change, and the cpp value for the P4 is N times that of the robust symmetrical residue-P4 phase code. For the P4, the subcode period is

$$t_b = \frac{cpp}{f_c}. \tag{51}$$

For the robust symmetrical residue-P4, the subcode period is

$$t_b' = \frac{cpp}{Nf_c}. \tag{52}$$

From (51) and (52), we have

$$t_b = Nt_b'. \tag{53}$$

Using Equation (48), we see that the phase sequence from the robust symmetrical residue-P4 for $m_i = 16,\ N = 2,$ and $N_{c_{RSNS}} = 64$ is actually the same as the P4 phase code sequence using $N_c = 32.$

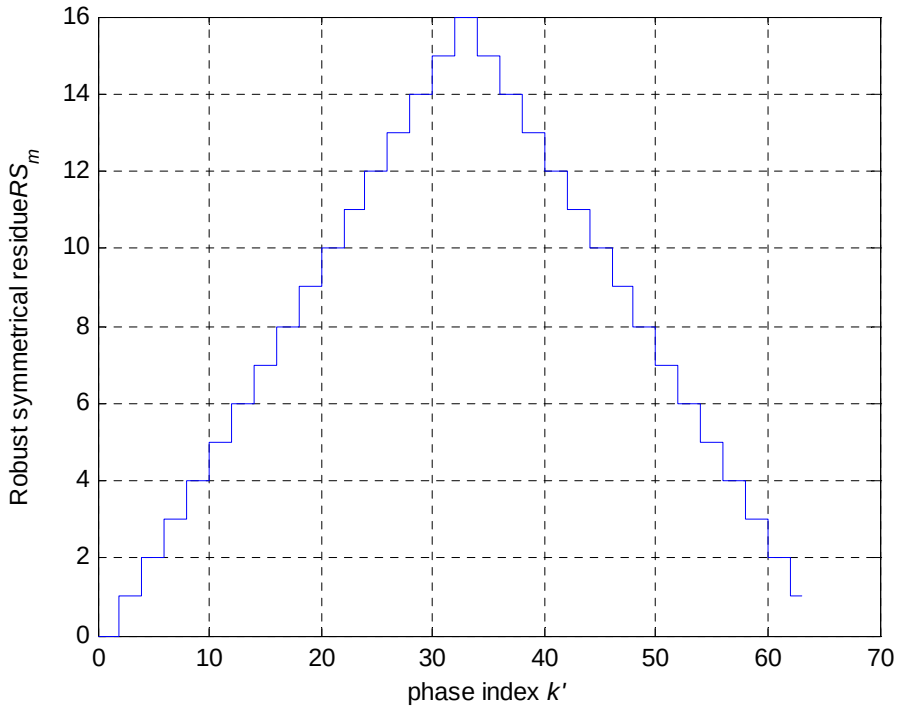

Figure 48. RSNS residues $RS_{m,k}$ for modulus $m = 16,\ N = 2,$ and $N_{c_{RSNS}} = 64.$

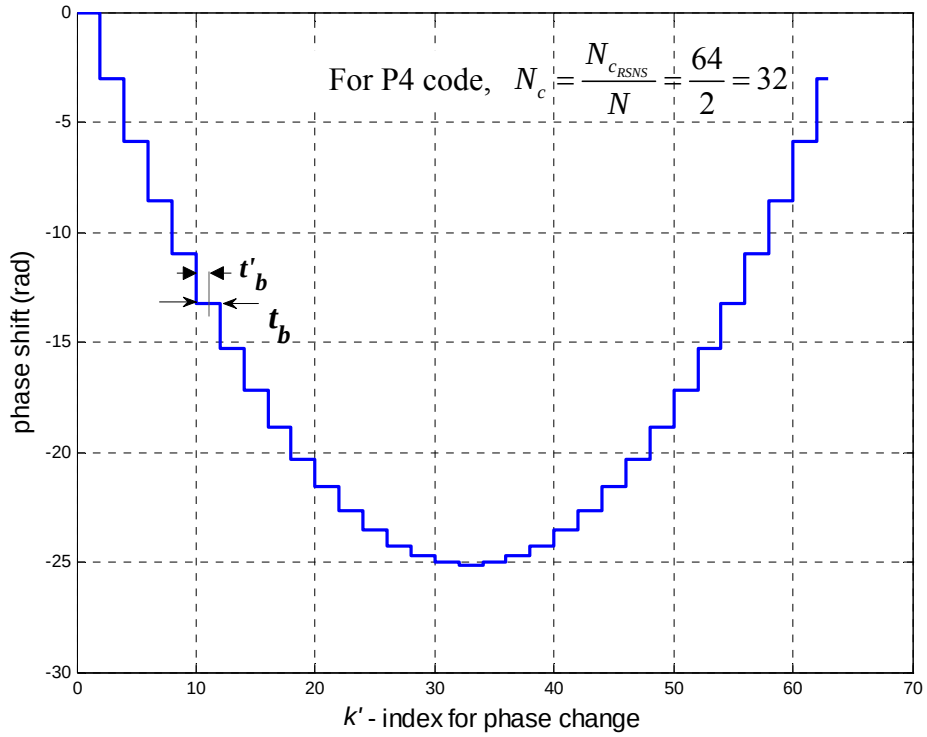

Figure 49. The robust symmetrical residue-P4 phase code sequence using $m = 16$, $N = 2$, $N_{c_{RSNS}} = 64$ is shown with the relationship with the P4 code using $N_c = 32$.

The power spectral density (PSD) of the signal is shown in Figure 50. The signal bandwidth B is reduced by the factor of N. With $cpp = 2$, the bandwidth of the robust symmetrical-P4 signal is $B = f_c / cpp = 1/t_b = 500$ Hz (instead of $B = 1$ kHz when $cpp = 1$). In Figure 51, the ACF and PACF are plotted. The signal's characteristics are the same as the P4 phase code sequence using $N_c = 32$, $t_b = 2$ ms. In the ACF plot, the output gives PSL = $20\log_{10}\left(\sqrt{2/(N_c\pi^2)}\right)$ = –22 dB. Note that the width of the mainlobe in the ACF plot is $2t'_b$ and is proportional to the number of moduli N. That is, the higher the number of moduli N, the broader the mainlobe. In Figure 52, the PAF is plotted. The PAF from the robust symmetrical residues using $m_i = 16$, $N = 2$, and $N_{c_{RSNS}} = 64$ in Figure 52a is compared to the PAF from the P4 code sequence using $N_c = 32$ in Figure 52b. Both PAFs are the same.

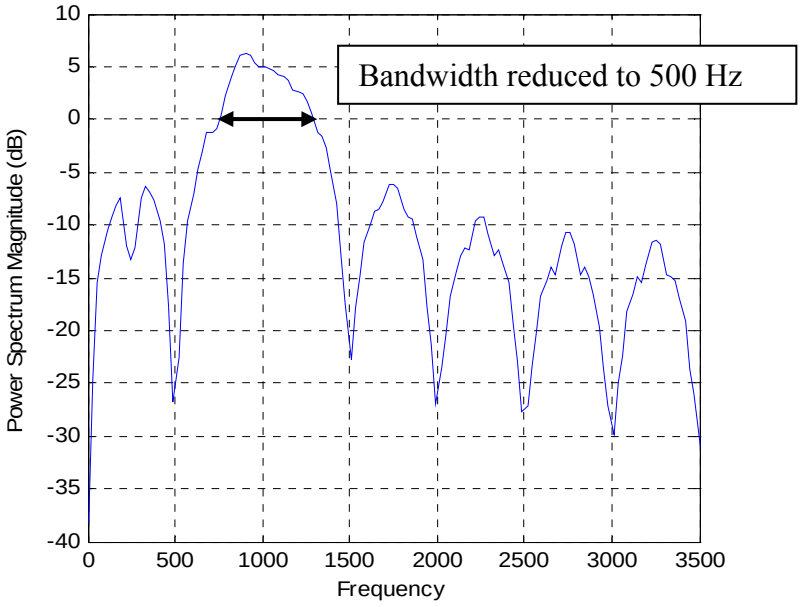

Figure 50. Power spectral density of the robust symmetrical residue-P4 signal using $m = 16,\ N = 2,$ and $N_{c_{RSNS}} = 64$ with $f_c = 1$ kHz, $f_s = 7$ kHz, and $cpp = 2.$

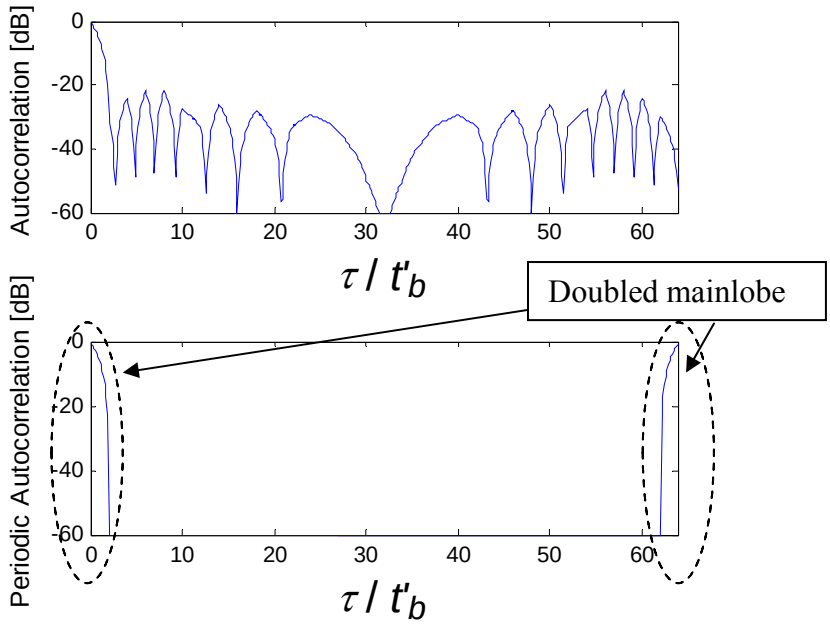

Figure 51. The ACF and PACF of RSNS phase-coded signal ($m = 16,\ N = 2,\ N_{c_{RSNS}} = 64$) at the receiver with $N_r = 1,$ $f_c = 1$ kHz, $f_s = 7$ kHz, and $cpp = 2.$

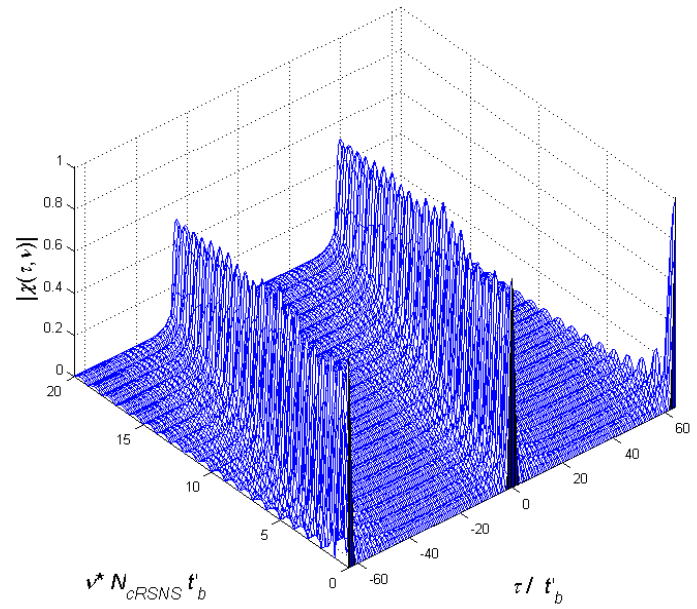

(a)

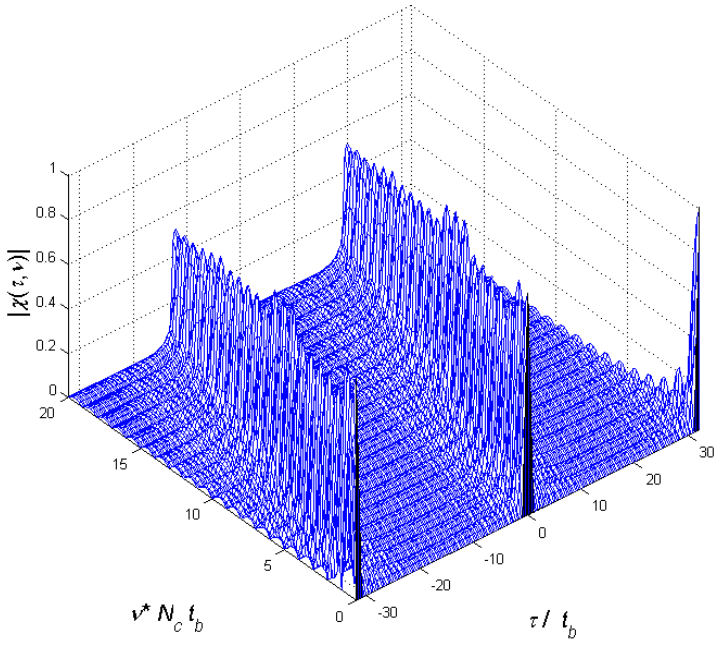

(b)

Figure 52. The PAF of the signal for (a) the robust symmetrical residue-P4 phase code sequence using $m = 16,\ N = 2,\ N_{c_{RSNS}} = 64$, and $t_b' = 1$ ms, and (b) the P4 code using $N_c = 32$, and $t_b = 2$ ms.

D. RESOLVING RANGE AMBIGUITIES USING N ROBUST SYMMETRICAL RESIDUE-P4 PHASE CODE SEQUENCES

1. Block Diagram of the Robust Symmetrical Residue-P4 Radar System

To extend the unambiguous detection range, $N \geq 2$ coprime RSNS sequences are used. The block diagram of the radar using $N-$channel RSNS phase coding is shown in Figure 53. This diagram is similar to the residue-Frank phase code radar system except that now the RSNS moduli are used instead. Each phase sequence with the length equal to the dynamic range $\hat{M}_{RSNS}$ is transmitted to detect the target. In the receiver, each code sequence is compressed with its corresponding reference phase code.

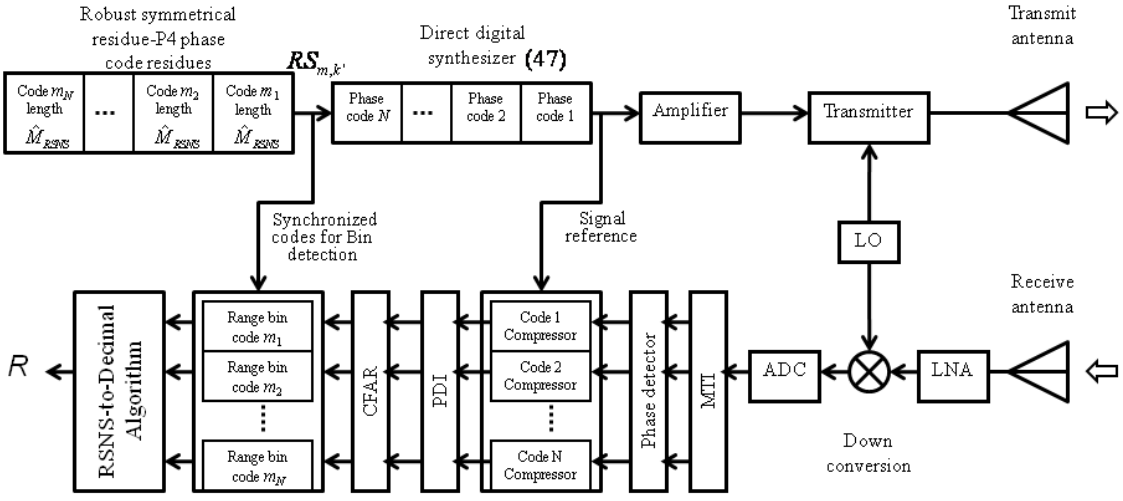

Figure 53. Block diagram for the radar using N robust symmetrical residue-P4 phase code sequences.

2. Transmitted and Reference Codes for Compression

In this section, the transmission of a set of N robust symmetrical residue-P4 phase coded sequences is explained. Also, the use of the phase code sequences as the reference sequence for code compression is discussed. An example using $N = 3$ RSNS moduli with $m_1 = 3,\ m_2 = 4,$ and $m_3 = 5$ is illustrated. The dynamic range for these RSNS moduli from Equation (44) is $\hat{M}_{RSNS} = 43.$ The starting position h and ending position

$h + \hat{M}_{RSNS} - 1$ are 61 and 103, respectively [20]. The robust symmetrical residues within the RSNS moduli are paired as shown in Table 7.

The transmitted signal is shown in Figure 54. Each sequence has a length equal to the dynamic range. For $m_1 = 3,$ there are four robust symmetrical residues within the sequence, $RS_3 = 0,\ 1,\ 2,$ and 3. To create the P4 code sequence, one code period needs the number of subscodes $N_{c_{RSNS}} = 2Nm_1 = 2 \times 3 \times 3 = 18.$ For $m_2 = 4,$ the robust symmetrical residues are 0, 1, 2, 3, and 4. The required number of subcodes is $2 \times 3 \times 4 = 24.$ For $m_3 = 5,$ the robust symmetrical residues are 0, 1, 2, 3, 4, and 5. The number of subcodes is $2 \times 3 \times 5 = 30.$ As shown in the Figure 54, the beginning of each sequence is not necessarily the beginning of the phase code sequence $k' = 1$ (e.g., the beginning phase sequences for $m_1 = 3,\ m_2 = 4,$ and $m_3 = 5$ are $k' = 8,\ k' = 13,$ and $k' = 30,$ respectively. The reference code sequences in the compressors can be chosen to be either starting at the beginning of the sending signal waveforms or the starting of phase sequence at $k' = 1.$ The importance is that the reference code has to have a length equal to the code period T_m for each channel in order to correctly calculate the code compression output. In this example, we choose to use the reference signals starting from the beginning of the transmitted signal (ϕ_8 to ϕ_7 for $m_1 = 3,$ ϕ_{13} to ϕ_{12} for $m_2 = 4,$ and ϕ_{30} to ϕ_{29} for $m_3 = 5$). The number of sequence periods is calculated as

$$\hat{N}_{p,m} = \frac{\hat{M}_{RSNS}}{N_{c_{RSNS}}} = \frac{\hat{M}_{RSNS}}{2mN}. \tag{54}$$

Sending 43 subcodes, the modulus $m_1 = 3$ needs $\hat{N}_{p,3} = 43/18 = 2.4$. For modulus $m_2 = 4$ and $m_3 = 5,$ the number of subcodes $N_{c_{RSNS}}$ are 24 and 30, respectively. Also, the number of transmitted code periods are $\hat{N}_{p,4} = 1.8$ and $\hat{N}_{p,5} = 1.4,$ respectively. Here, only channel $m_1 = 3$ is sending more than one complete code period. So we can expect to see two compressed pulses from channel $m_1 = 3$ if all subcodes return back to the receiver (there will be only one pulse in the other two channels).

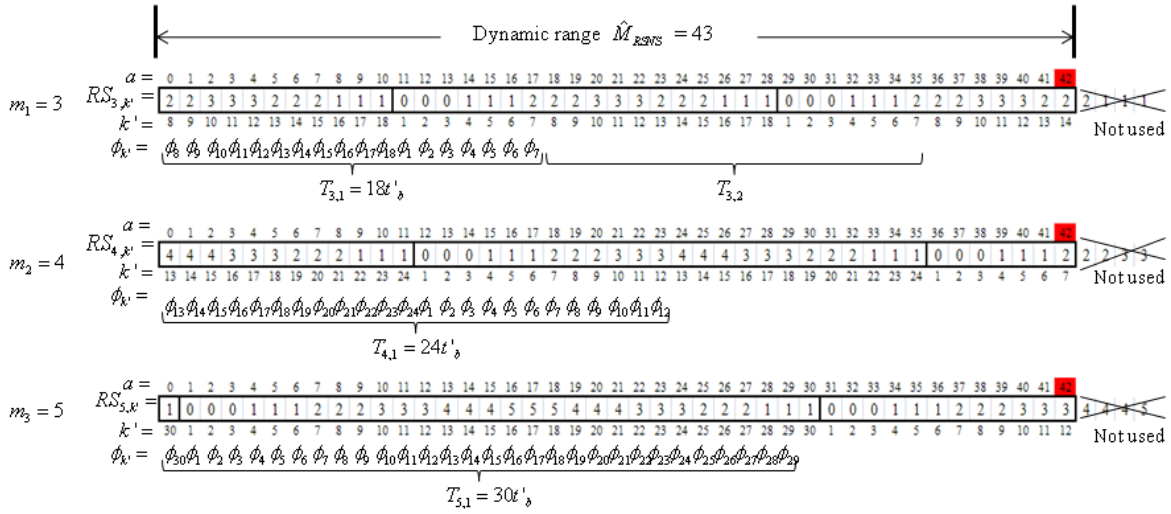

Figure 54. Illustration of transmitted signal using $N = 3$ robust symmetrical residue-P4 phase code sequences for $m_1 = 3,\ m_2 = 4,$ and $m_3 = 5.$

In Figure 55a, the RSNS folding waveforms for $m_1 = 3,\ m_2 = 4,$ and $m_3 = 5$ with $\hat{M}_{RSNS} = 43$ are plotted. Also, the phase sequences from each channel are plotted in Figure 55b. Since $RS_{m,h+n2Nm} = RS_{m,h}$ where $n \in \{0, \pm 1, \pm 2, \ldots\}$, the phase sequences are periodic as $\phi_{m,k'+n2Nm} = \phi_{m,k'}$.

In Figure 56, the compression and range bin detection process is illustrated for RSNS $m_1 = 3,$ and $N_r = 1.$ The returned phase coded signal is first processed by a filter matched to the rectangular pulse of duration $t'_b.$ The phase detector is used to calculate the phase of each sample and then pass it through the compressor. The output from the compression is then processed by the threshold detection to see whether the amplitude reaches the desired minimum value. If the threshold detector detects the pulse, the presence of the target will be saved with the robust symmetrical residue value $RS_m.$ In $m_2 = 4$ and $m_3 = 5,$ the process is similar, except that the phase references have to match with the transmitted phase code that is being received.

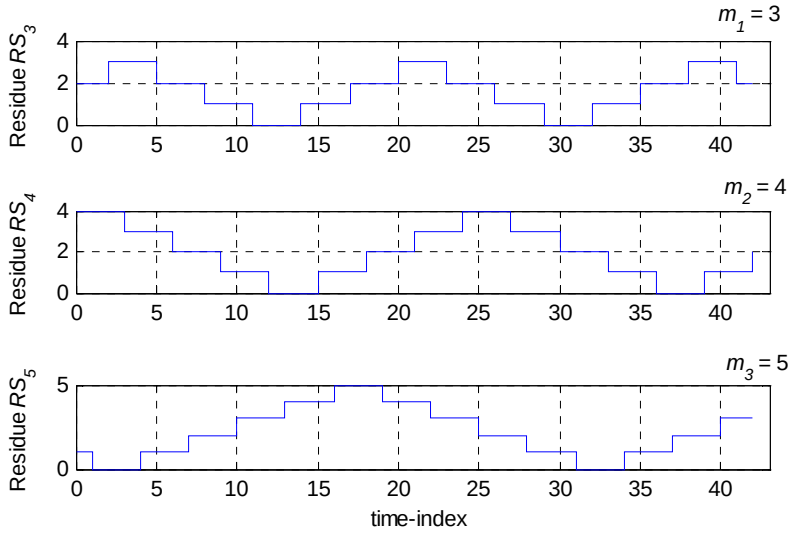

(a)

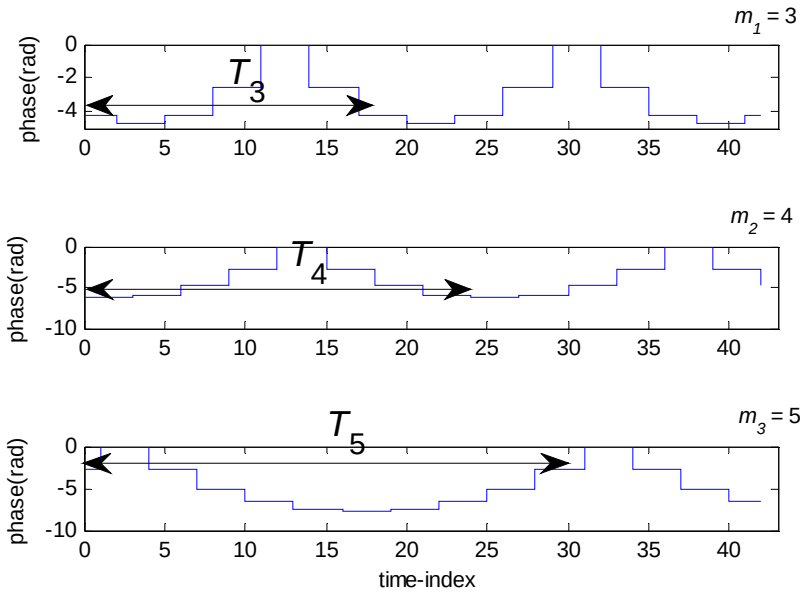

(b)

Figure 55. Plot of the RSNS using $m_1 = 3,\ m_2 = 4,$ and $m_3 = 5$ with $\hat{M}_{RSNS} = 43$ for (a) folding waveforms, and (b) their phase sequences.

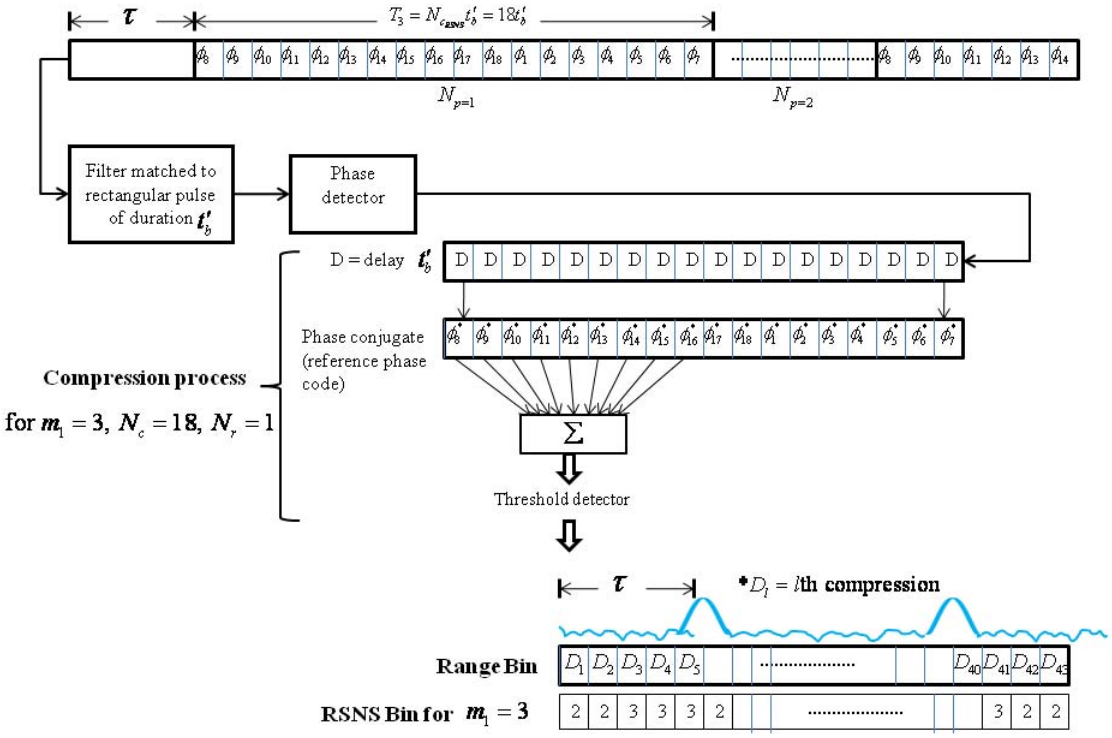

Figure 56. Illustration of compression at the receiver and the range bin for RSNS $m_1 = 3,\ N_c = 18,$ and $N_r = 1$.

3. Calculating the Target Range

Using all sequences, we map the paired terms to a specific range bin a (similar to the residue-Frank code bin process in Chapter III). Continuing the example in the previous section for $m_1 = 3,\ m_2 = 4,$ and $m_3 = 5,$ we show the robust symmetrical residue paired values and the corresponding ranges in Table 9. The signal bandwidth is $B = 1$ MHz, and the subcode period is $t_b' = t_b / N = 0.33\ \mu$s. The new expression formula for calculating the unambiguous range using RSNS is

$$R_{u,RSNS} = \frac{c\hat{M}_{RSNS} t_b'}{2}. \tag{55}$$

For this example, the maximum unambiguous range is $R_{u,RSNS} = 2150$ m. The range resolution is 50 m ($\Delta R = ct_b' / 2$).

Table 9. Bin matrix and range intervals of $3-$channel RSNS for $m_1 = 3,\ m_2 = 4,$ and $m_3 = 5.$

Bin a	$m_1 = 3$	$m_2 = 4$	$m_3 = 5$	Range (m)	Bin a	$m_1 = 3$	$m_2 = 4$	$m_3 = 5$	Range (m)
0	2	4	1	0 – 50	23	2	3	3	1150 – 1200
1	2	4	0	50 – 100	24	2	4	3	1200 – 1250
2	3	4	0	100 – 150	25	2	4	2	1250 – 1300
3	3	3	0	150 – 200	26	1	4	2	1300 – 1350
4	3	3	1	200 – 250	27	1	3	2	1350 – 1400
5	2	3	1	250 – 300	28	1	3	1	1400 – 1450
6	2	2	1	300 – 350	29	0	3	1	1450 – 1500
7	2	2	2	350 – 400	30	0	2	1	1500 – 1550
8	1	2	2	400 – 450	31	0	2	0	1550 – 1600
9	1	1	2	450 – 500	32	1	2	0	1600 – 1650
10	1	1	3	500 – 550	33	1	1	0	1650 – 1700
11	0	1	3	550 – 600	34	1	1	1	1700 – 1750
12	0	0	3	600 – 650	35	2	1	1	1750 – 1800
13	0	0	4	650 – 700	36	2	0	1	1800 – 1850
14	1	0	4	700 – 750	37	2	0	2	1850 – 1900
15	1	1	4	750 – 800	38	3	0	2	1900 – 1950
16	1	1	5	800 – 850	39	3	1	2	1950 – 2000
17	2	1	5	850 – 900	40	3	1	3	2000 – 2050
18	2	2	5	900 – 950	41	2	1	3	2050 – 2100
19	2	2	4	950 – 1000	42	2	2	3	2100 – 2150
20	3	2	4	1000 –1050					
21	3	3	4	1050 –1100					
22	3	3	3	1100 – 1150					

In Figure 57, an example of target detection for $m_1 = 3$, $m_2 = 4$, and $m_3 = 5$ is illustrated. The return signal is in the range bin $a = 5$ or 270 m. First, the phase code signal of the modulus $m_1 = 3$ (top) is compressed. Recall that the RSNS has a width of the compression output that covers $N = 3$ code sequences at robust symmetrical residues $RS_3 =$ 3, 2, and 2. So the threshold detection has to decide to take one bin, e.g., at the peak of the compressed pulse, giving the robust symmetrical residue $RS_3 = 2$. The process is the same for the channels $m_2 = 4$ and $m_3 = 5$. The robust symmetrical residues are $RS_4 = 3$ and $RS_5 = 1$, respectively. The three robust symmetrical residues are paired as [2 3 1] and must be converted to the decimal RSNS bin number. In Table 9, the corresponding range is between 250 m and 300 m (bin $a = 5$).

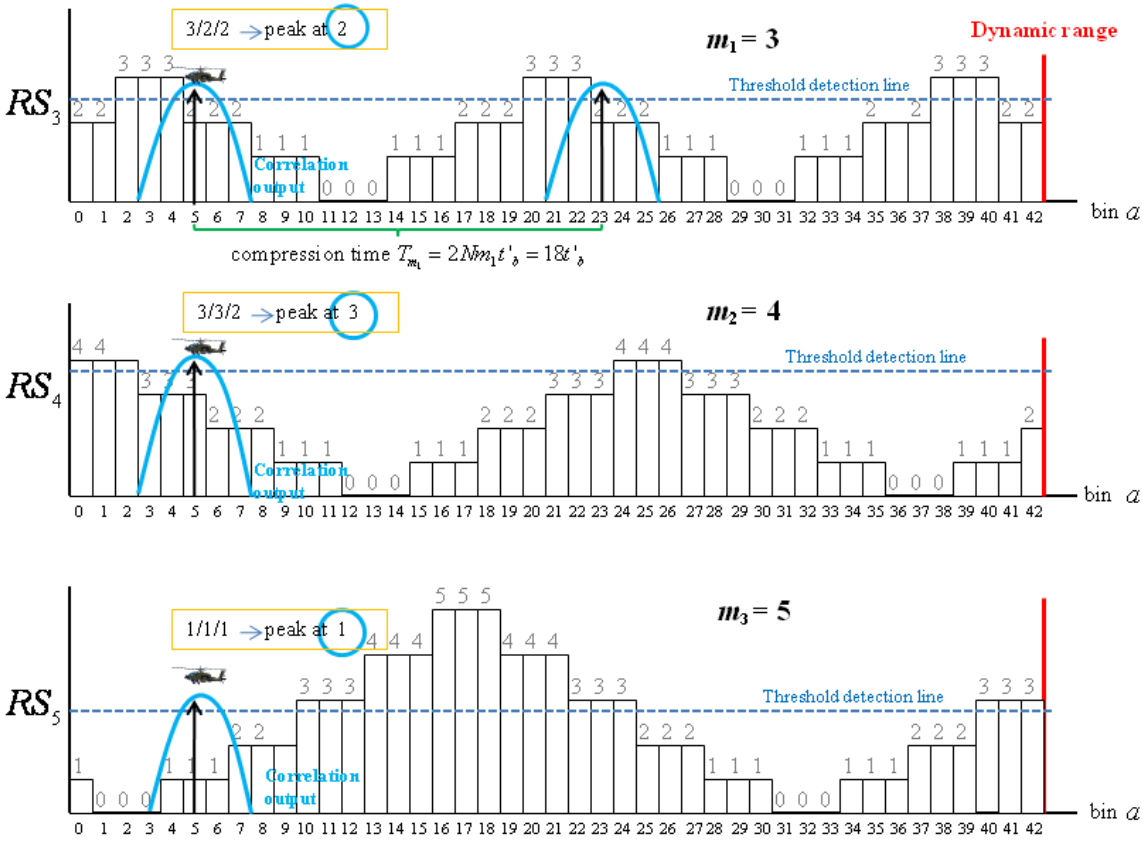

Figure 57. Illustration of target detection by using the range bin matrix for RSNS-P4 code with $m_1 = 3$, $m_2 = 4$, and $m_3 = 5$.

4. Resolving Multiple Target Range Ambiguities

In Figure 58 for $m_1 = 3,$ the compressed pulses are repeated as the returned code runs through the reference code in the compressor. The two target returns overlap one another at range bins $a = 19,\ 20,$ and 21 and are ambiguous. Next we resolve the range ambiguity by using 3 channels. If the threshold detector is set to measure at the peak of the compression output, the robust symmetrical residues from the first target are paired as [3 4 0], giving a range bin $a = 2$ (range 50–100 m). Similarly, the robust symmetrical residue paired terms from the second target are [3 2 4], giving a range bin $a = 20$ (range 1,000–1,050 m). The two targets have different paired terms, so the range ambiguity can be resolved.

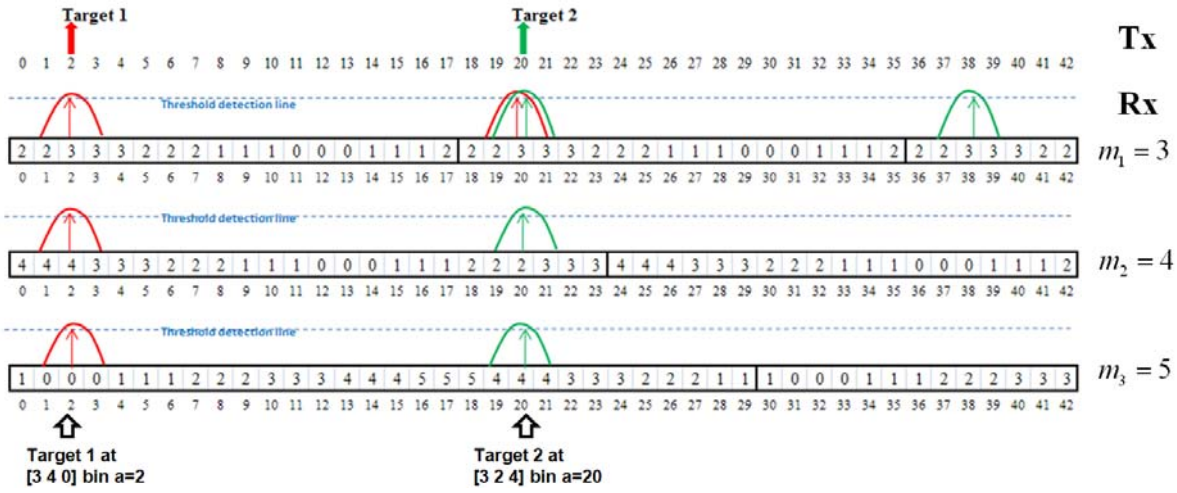

Figure 58. Resolving the range ambiguity of 2 targets using RSNS for $m_1 = 3,\ m_2 = 4,$ and $m_3 = 5.$

As mentioned in Chapters III and IV, we can resolve the targets even if the first set of the residues are not detected. Imagine we use a higher set of RSNS moduli and the dynamic range is higher with the result that the code period repeats. To find the true range of the targets that are missed, the magnitude information or the filling in the range bin according to the code periodicity can be used.

5. Practical Considerations

a. Detection of Target in Noise Using RSNS Compression

In this section, the performances of the $N = 3$ RSNS for $m_1 = 3,\ m_2 = 4,$ and $m_3 = 5$ with $\hat{M}_{RSNS} = 43$ are examined by using MATLAB to plot the returned signal from two targets at ranges of 140 m and 1040 m. The transmitted signal has amplitude $A = 1,$ carrier frequency $f_c = 1$ MHz, sampling frequency $f_s = 9$ MHz, $cpp = 1,\ t_b = 1\ \mu$s, and $t_b' = 0.33\ \mu$s. In Figure 59, the transmitted signal without noise for each channel is plotted. In Figure 60, the signal with SNR = 30 dB is plotted. The signal power is high compare to the noise power. As a result, the noise signal does not significantly affect the phase sequences. In Figure 61, the SNR is reduced to 0 dB. The phase sequences are changed significantly.

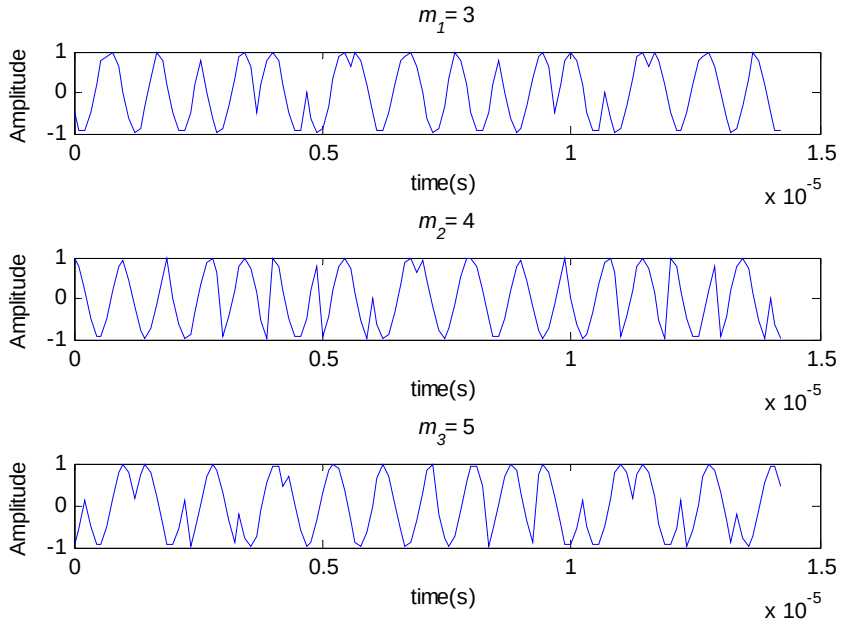

Figure 59. Robust symmetrical residue-P4 signal without noise for $m_1 = 3,\ m_2 = 4,$ and $m_3 = 5$ with $\hat{M}_{RSNS} = 43,\ A = 1,\ f_c = 1$ MHz, $f_s = 9$ MHz, $cpp = 1,$ and $t_b' = 0.33\ \mu$s.

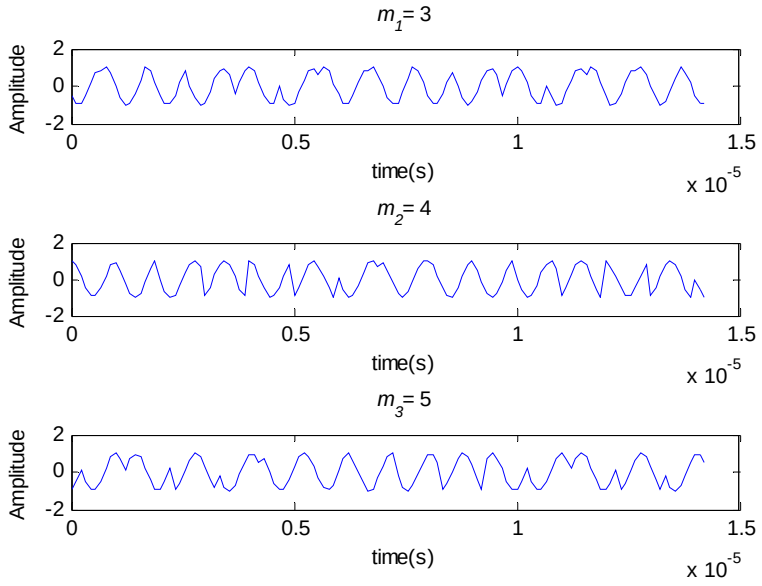

Figure 60. Robust symmetrical residue-P4 signal with SNR = 30 dB for $m_1 = 3,\ m_2 = 4,$ and $m_3 = 5$ with $\hat{M}_{RSNS} = 43,\ A = 1,\ f_c = 1$ MHz, $f_s = 9$ MHz, $cpp = 1,$ and $t_b' = 0.33\ \mu$s.

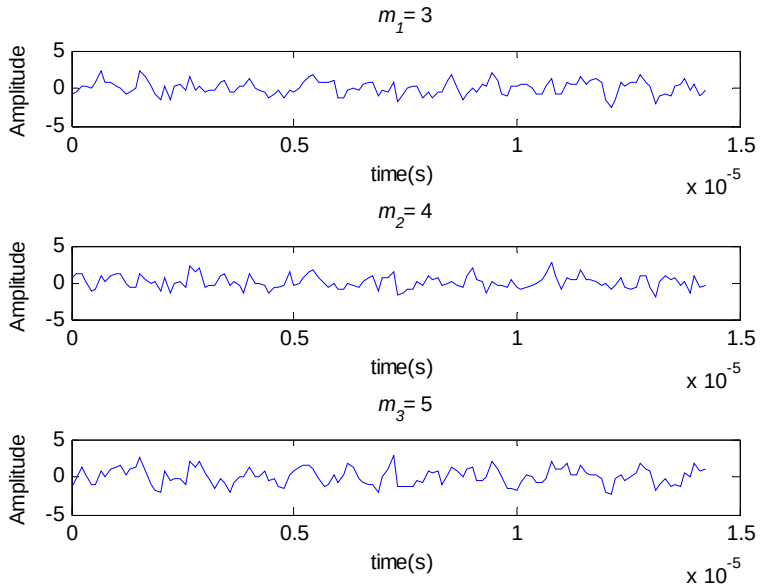

Figure 61. Robust symmetrical residue-P4 signal with SNR = 0 dB for $m_1 = 3,\ m_2 = 4,$ and $m_3 = 5$ with $\hat{M}_{RSNS} = 43,\ A = 1,\ f_c = 1$ MHz, $f_s = 9$ MHz, $cpp = 1,$ and $t_b' = 0.33\ \mu$s.

In Figures 62 and 63, the range bin profiles from two targets are shown using SNR = 30 dB and SNR = 0 dB, respectively. The first target appears at range bin $a = 2$ with the paired robust symmetrical residues [3 4 0] (range 100–150 m). The second target appears at range bin $a = 20$, giving paired terms [3 2 4] (range 1000–1050 m). As shown in Figure 63, the amplitudes of the compressed pulses degrade when the SNR is decreased to 0 dB. Also, the sidelobes from the compression output are higher when the noise power is increased. Another important point is that the average sidelobes from the higher modulus (e.g. $m_3 = 5$) are lower than those from the lower modulus (e.g. $m_1 = 3$ and $m_2 = 4$) due to the different processing gains. For $m_1 = 3,\ m_2 = 4,$ and $m_3 = 5,$ the processing gains are $N_{c1} = 2m_1 = 6,\ N_{c2} = 2m_2 = 8,$ and $N_{c3} = 2m_3 = 10,$ respectively.

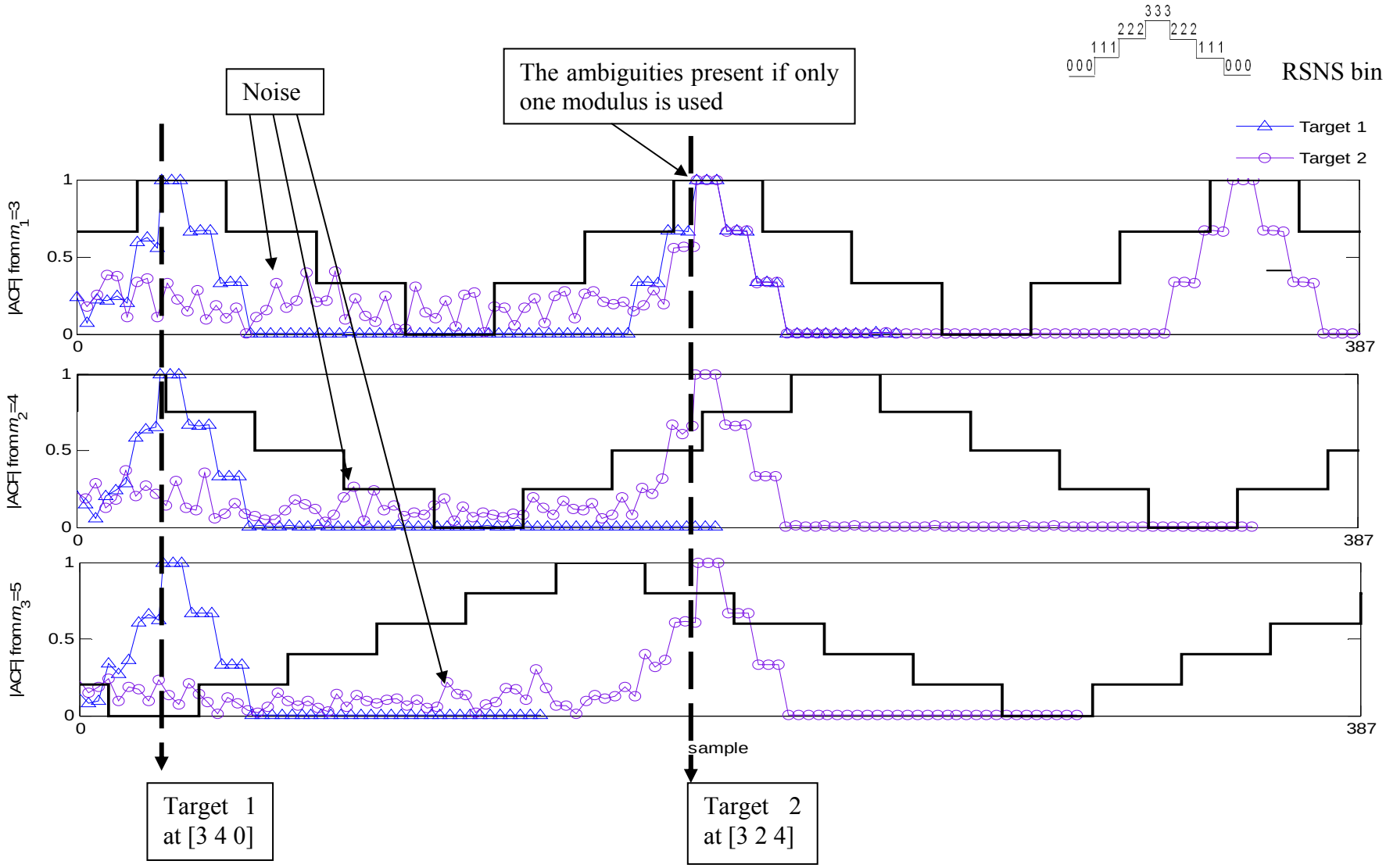

Figure 62. Target detection for SNR = 30 dB showing the range bins for $m_1 = 3$, $m_2 = 4$, and $m_3 = 5$ with two targets at 140 m and 1040 m.

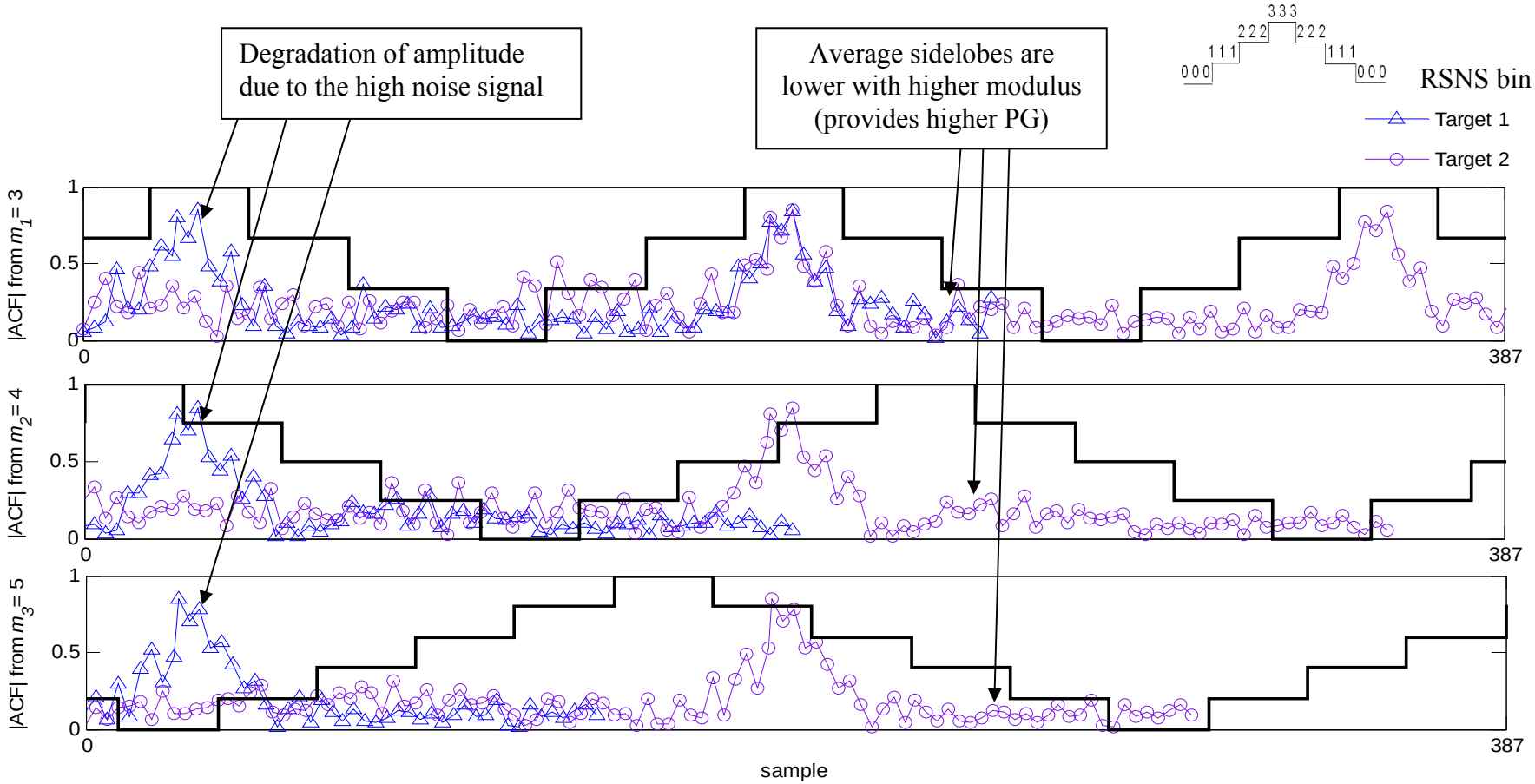

Figure 63. Target detection for SNR = 0 dB showing the range bins for $m_1 = 3$, $m_2 = 4$, and $m_3 = 5$ with two targets at 140 m and 1040 m.

Using N robust symmetrical residue-P4 phase code sequences allows control of the range coding error. The threshold detector might read the wrong robust symmetrical residue bin because the amplitudes of the compressed pulses are fluctuating. However, the paired terms from the robust symmetrical residues will change only one position (the Gray code property). In Figure 64, the compressed pulse from the first target in $m_2 = 4$ is detected by CFAR (threshold level at 0.85) at the robust symmetrical residue $RS_4 = 3$ instead of $RS_4 = 4$. The paired terms are now [3 3 0] (range 150–200 m) instead of the true range at [3 4 0] (range 100–150 m). The maximum range error is only one range bin or 50 m.

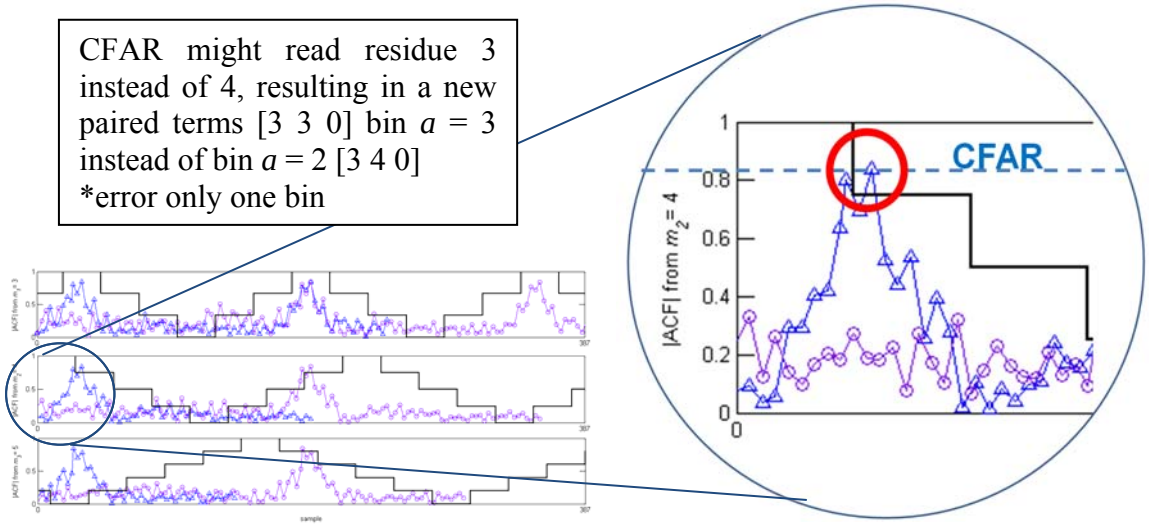

Figure 64. Illustration of detection error from the threshold detector (CFAR) using the robust symmetrical residue-P4 for $m_1 = 3,\ m_2 = 4,$ and $m_3 = 5$.

b. Plot of Required Signal Power Versus Required SNR Output

In this section, the power required when using the robust symmetrical residue-P4 phase code sequence to detect the target at the maximum unambiguous range is presented (given the fixed unambiguous range $R_u = 2150$ m). The relationship between the required SNR_{Ro} and the average CW power P_{CW} is given by Equation (26).

In Figure 65, the CW signal power as a function of the required SNR_{Ro} for $m_1 = 3,\ m_2 = 4,$ and $m_3 = 5$ is plotted with $B_{Ri} = 1$ MHz, $t_b = 1\ \mu$s, $t_b' = 0.333\ \mu$s,

$G_t = G_r = 30$ dB, $f_c = 3$ GHz, $\lambda = 0.1$ m, $\sigma_T = 100$ m^2, $F_R = 5$ dB, and $L_2 = L_{RT} = L_{RR} = 1$, and $R_{\max} = R_u = c\hat{M}_{RSNS}t_b'/2 = 2150$ m (maximum detection range without ambiguity).

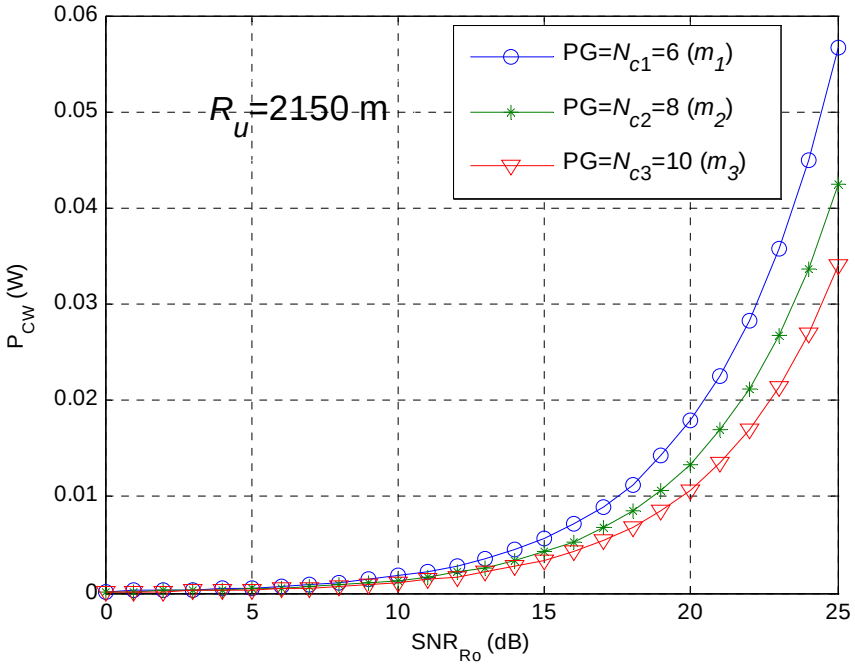

Figure 65. Average power of the CW transmitter for robust symmetrical residue-P4 with $m_1 = 3$, $m_2 = 4$, and $m_3 = 5$.

Note that the difference of the average power used in each channel is due to the PG. The channel $m_3 = 5$, giving $PG = 2m = 10$, requires less power than the other channels, $m_1 = 3$ ($PG = 6$) and $m_2 = 4$ ($PG = 8$).

c. Unambiguous Detection Range for a Constant Output SNR

For a single P4 code, the unambiguous range is limited to only one code period duration $R_u = cT/2 = ct_bN_c/2$. In this section, we compare the maximum unambiguous range using the robust symmetrical residue-P4 phase code sequence with the corresponding single P4 code sequences. The relationship between the average signal power P_{CW} and the maximum detection range $R_{\max}$ is given by Equation (27).

In Figure 66, the detection range is plotted as a function of the required CW power using $N=3$ RSNS for $m_1=3, m_2=4,$ and $m_3=5$ with a constant $SNR_{Ro}=13$ dB, $B=1$ MHz, $t_b=1\ \mu$s, $t_b'=0.333\ \mu$s, $G_t=G_r=30$ dB, $f_c=3$ GHz, $\lambda=0.1$ m, $\sigma_T=100$ m^2, $T_0=290$ K, $F_R=5$ dB, and $L_2=L_{RT}=L_{RR}=1$. Also, the performance of each P4 code using the corresponding N_c is plotted. For the P4 code from Equation (28), $N_{c1}=N_{c,RSNS}/N=18/3=6, N_{c2}=8,$ and $N_{c3}=10$. The single P4 codes have a limited unambiguous range; $N_{c1}=6$ gives $R_u=3\times10^8\times10^{-6}\times6/2=900$ m, $N_{c2}=8$ gives $R_u=3\times10^8\times10^{-6}\times8/2=1200$ m, and $N_{c3}=10$ gives $R_u=3\times10^8\times10^{-6}\times10/2=$ 1500 m. These values are less than achieved using the $N=3$ robust symmetrical residue-P4 phase code sequences, $R_{u_{RSNS}}=c\hat{M}_{RSNS}t_b'/2=2150$ m.

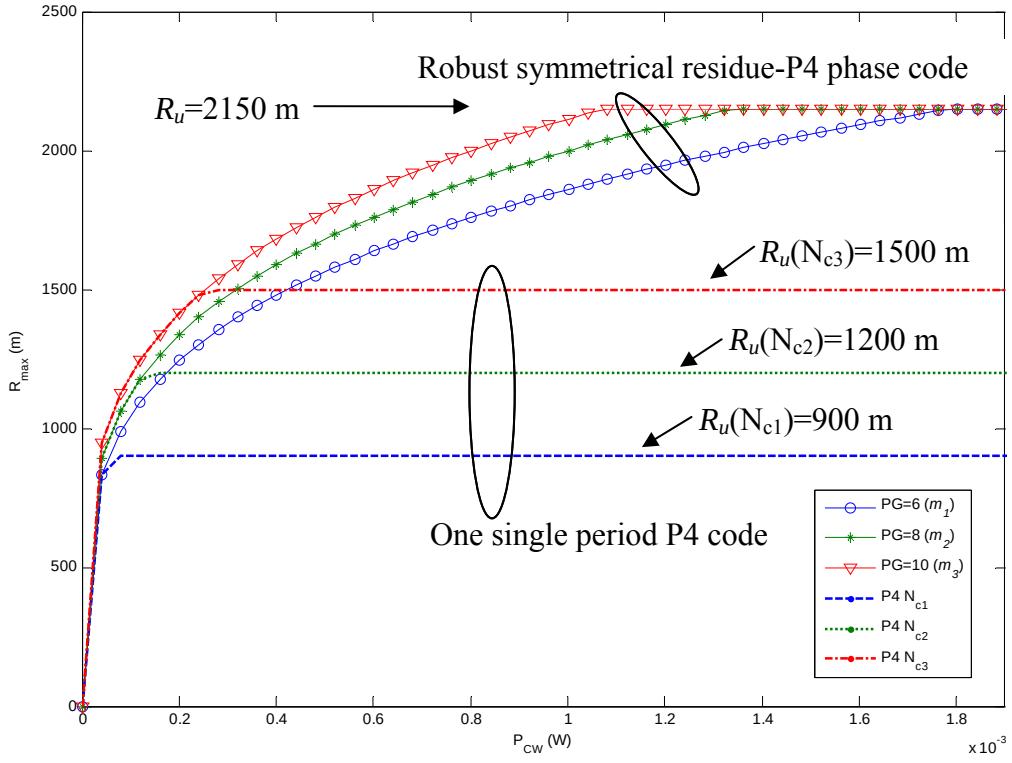

Figure 66. Comparison of the maximum unambiguous range of CW radar system for $SNR_{Ro}=13$ dB using robust symmetrical residue-P4 code for $m_1=3,$ $m_2=4,$ and $m_3=5$ with the radar using each P4 code individually for the corresponding $N_c=N_{c_{RSNS}}/N$.

In conclusion, the robust symmetrical-P4 phase code sequence presented in this chapter can be used to extend the unambiguous range of CW polyphase radar systems. The issue concerned with the range bin error due to the fluctuation of the compression outputs is also resolved. The integer Gray code properties can prevent an error in the detected robust symmetrical residues. In the next chapter, the concluding results from using the number theoretic transforms from Chapters III to V to extend the unambiguous range in CW polyphase radar systems are discussed.

THIS PAGE INTENTIONALLY LEFT BLANK

VI. CONCLUDING RESULTS AND RECOMMENDATIONS

A. EQUATION SUMMARY

The summary of equations used to compute the signal and range detection parameters for each modular phase code (residue-Frank phase code, symmetrical residue-P4 phase code, and robust symmetrical residue-P4 phase code) that results in extending the unambiguous range are shown in the Table 10. The equations are used for any of the coprime system moduli.

Table 10. Summary of equations for each modular phase code.

Parameters	RNS-Frank	SNS-P4	RSNS-P4
Phase sequence $(\phi_k, \phi_{k'})$	$\phi_{m,k} = \frac{2\pi}{m}\left\lfloor \frac{k-1}{m} \right\rfloor R_{m,k}$	$\phi_{m,k} = \left[\frac{\pi}{m}\left(S_{m,k} - \frac{m}{2}\right)^2\right] - \frac{\pi}{4}m$	$\phi_{m,k'} = \left[\frac{\pi}{2m}\left(RS_{m,k'} - m\right)^2\right] - \frac{\pi}{2}m$
Subcode period (t_b, t_b')	$t_b = cpp / f_c$	$t_b = cpp / f_c$	$t_b' = t_b / N = cpp / Nf_c$
Signal bandwidth (B)	$1/t_b$	$1/t_b$	$1/t_b = 1/(Nt_b')$
The number of subcodes $(N_c, N_{c_{RSNS}})$	m^2	m	$2mN$
Processing gain (PG)	m^2	m	$2m$
Code period (T)	$m^2 t_b$	mt_b	$2mNt_b'$

Using a set of moduli, we can extend the maximum detection ranges beyond those of individual moduli. The equations for calculating the dynamic range, the number of code periods within the dynamic range, the range resolution, and the unambiguous range are shown in Table 11.

Table 11. Summary of equations for $N-$channel modular number system.

Parameters	**RNS-Frank**	**SNS -P4**	**RSNS -P4**
Dynamic range $(M_{RNS},\ \hat{M}_{SNS}, \hat{M}_{RSNS})$	$\prod_{i=1}^{N} m_i$	$\min\left\{\frac{m}{2}\prod_{l=2}^{j} m_{i_l} + \prod_{l=j+1}^{N} m_{i_l}\right\}$ (even) $\min\left\{\frac{1}{2}\prod_{l=1}^{j} m_{i_l} + \frac{1}{2}\prod_{l=j+1}^{N} m_{i_l}\right\}$ (odd)	$\frac{3}{2}m_1^2 + \frac{15}{2}m_1 + 7$ for $N=3$ moduli of the form $2^z-1, 2^z, 2^z+1$
The number of code periods $(\hat{N}_{p,m})$	$\frac{M_{RNS}}{m^2}$	$\frac{\hat{M}_{SNS}}{m}$	$\frac{\hat{M}_{RSNS}}{2Nm}$
Range resolution (ΔR)	$\frac{ct_b}{2}$	$\frac{ct_b}{2}$	$\frac{ct_b'}{2}$
Unambiguous range (R_u)	$\frac{c\hat{M}t_b}{2}$	$\frac{c\hat{M}_{SNS}t_b}{2}$	$\frac{c\hat{M}_{RSNS}t_b'}{2}$

In the SNS and RSNS, the dynamic range is not necessarily greater with an increasing value of the moduli values. For example, the dynamic range of a 3-channel SNS system with moduli [7, 13, 16] is $\hat{M}_{SNS} = 69.$ On the other hand, the dynamic range of a 3-channel RSNS system with moduli [7, 13, 19] is only $\hat{M}_{RSNS} = 55.$ That is, m_1 and m_2 are equal, but the last RSNS modulus is $m_3 = 19,$ which is larger than the last SNS modulus $m_3 = 16.$ However, the dynamic range of the RSNS is less than the SNS.

B. COMPARISON OF 3-CHANNEL MODULAR NUMBER SYSTEMS WITH THE SAME DYNAMIC RANGE

In Table 12, a comparison of each modular number system having the same dynamic range (60), the same subcode period (1 μs), the same unambiguous range (9000 m), and the same range resolution is shown. Note the bandwidth for the RSNS-P4 system is smaller since it is contains N phase values that are equal.

Table 12. Comparison of each modular phase code in which each has the same dynamic range = 60, and $t_b,\ t_b' = 1\ \mu$s .

Parameters	**RNS-Frank**	**SNS-P4**	**RSNS-P4**
Set: Dynamic range	60	60	60
Set: Subcode period (μs)	1	1	1
Bandwidth (MHz)	1	1	0.33
Unambiguous range (m)	9,000	9,000	9,000
Range resolution (m)	150	150	150
Moduli	[3, 4, 5]	[7, 13, 29]	[3, 5, 7]
Numbers of phase values	[3, 4, 5]	[4, 7, 15]	[4, 6, 8]
code period (μs)	[9, 16, 25]	[7, 13, 29]	[18, 30, 42]
Number of code periods	[6.67, 3.75, 2.4]	[8.6, 4.6, 2.1]	[3.3, 2, 1.4]

The RNS compared to the SNS is more efficient in covering R_u since fewer code periods are required in the compression. The phase values from the phase detector are also less for the same R_u. Comparison with the RSNS shows that it is the most efficient of all schemes due to the fewer number of phase values used, the smallest number of code periods required in the compression and its Gray code properties that limit the range error to one range bin. In terms of complexity, the size of the compressor is longest for the

RSNS since the dynamic range incorporates the fewest code period (assuming $N_r = 1$). The SNS requires the fewest code periods in the compressor.

C. COMPARISON OF 3-CHANNEL MODULAR NUMBER SYSTEMS WITH THE SAME MODULI

In Table 13, each number theoretic transform that has the same set of moduli [3 4 5] with the subcode period equal to 1 μs is shown.

Table 13. Comparison of each modular number system in which each has the same moduli [3 4 5], and $t_b,\ t_b' = 1\mu s$

Parameters	**RNS-Frank**	**SNS-P4**	**RSNS-P4**
Set: Moduli	[3 4 5]	[3 4 5]	[3 4 5]
Dynamic range (units)	60	11	43
Set: Subcode period (μs)	1	1	1
Bandwidth (MHz)	1	1	0.33
Unambiguous range (m)	9,000	1,650	6,450
Range resolution (m)	150	150	150
Number of phase values	[3, 4, 5]	[2, 3, 3]	[4, 5, 6]
Number of code periods	[6.67, 3.75, 2.4]	[3.7, 2.8, 2.2]	[2.4, 1.8, 1.4]

In the RNS phase code, the extended unambiguous range is maximized due to its maximum dynamic range. In the SNS phase code, the number of phase values is lowest due to the construction of the SNS integers within the modulus. However, it gives the shortest unambiguous range since its dynamic range is the smallest. The RSNS gives the next largest unambiguous range of the three schemes. The Gray code properties make it an attractive choice.

D. RANGE DETECTION ERROR CONTROL

As shown, only the robust symmetrical residue-P4 phase code sequence could prevent a range error due to the noise changing the phase of the return signal. This is due to the Gray code property that the RSNS has. For the other modular phase codes (residue-Frank and symmetrical residue-P4), the range error is large when the target straddles two range bins. The higher set of moduli might help control the range error due to its higher processing gain. However, increasing the modular number would increase the number of phase steps, resulting in increasing receiver's complexity and a longer code period, resulting in higher compression loss and required dwell time on targets.

E. RECOMMENDATIONS FOR FUTURE WORK

The modular phase codes used in this thesis were shown to be able to extend the unambiguous range in CW polyphase modulation radar systems. The applications of these modular phase codes in different types of radar systems would be interesting to study. Also, the performance of each moduli set with the different trade-offs should be further considered. The Doppler tolerant property that the P4 code has could also be investigated for the symmetrical residue-P4 and the robust symmetrical residue-P4 phase code sequences. Finally, the hardware implementation has to be examined and a simulation that includes hardware imperfections and errors must be conducted.

THIS PAGE INTENTIONALLY LEFT BLANK

APPENDIX – LIST OF VARIABLES

There are many variables used throughout this thesis. All of the important variables are listed here to provide unambiguous meanings.

Table 14. List of variables.

Variable	Meaning
a	Range bin index
c	Speed of light (m)
cpp	Number of carrier cycles within a subcode
f_c	Carrier frequency
f_s	Sampling frequency (Hz)
h	Integer position in RSNS
k	Phase index
k_B	Boltzman's constant (joule/K)
m	Coprime modulus
m_i	Coprime moduli
t_b	Subcode period (s)
B	Bandwidth (Hz)
B_{Ri}	Receiver's input bandwidth (Hz)
F_R	Receiver noise factor
G_r	Gain of receiving antenna
G_t	Gain of transmitting antenna
L_{RR}	Loss between the radar's antenna and receiver
L_{RT}	Loss between the radar's transmitter and antenna
L_2	Two-way atmospheric transmission loss
M	Frank frequency step
M_{RNS}	Dynamic range of the RNS
$\hat{M}_{SNS}$	Dynamic range of the SNS
$\hat{M}_{RSNS}$	Dynamic range of the RSNS
N	Number of coprime modular sequences
N_c	Number of subcodes within a code period
N_{cRSNS}	Number of subcodes within a code period (RSNS)
N_p	Number of code periods returned from target

Variable	Meaning
$\hat{N}_{p,m}$	Number of code periods used for modulus m
N_r	Number of receiver reference codes
PG	Processing gain
PSL	Peak-to-sidelobe level
P_{RNS}	Period of a single RNS sequence
P_{SNS}	Period of a single SNS sequence
P_{RSNS}	Period of a single RSNS sequence
R	Range to target (m)
R_u	Unambiguous range (m)
$R_{u,RNS}$	Unambiguous range of RNS (m)
$R_{u,SNS}$	Unambiguous range of SNS (m)
$R_{u,RSNS}$	Unambiguous range of RSNS (m)
$R_{m,k}$	RNS residue kth for modulus m
$RS_{m,k}$	RSNS symmetrical residue kth for modulus m
$S_{m,k}$	SNS symmetrical residue kth for modulus m
SNR_{Ri}	Input signal-to-noise ratio
SNR_{Ro}	Output signal-to-noise ratio
T	Code period (s)
T_{m_i}	Code period for coprime modulus m_i
V	Target velocity (m/s)
τ	Roundtrip time delay (s)
τ_{PW}	Pulse width
λ	Signal wavelength (m)
ν	Doppler frequency (Hz)
ΔR	Range resolution (m)
σ_T	Target's radar cross section (m^2)
$\phi_{m,k}$	Phase code for modulus m with index k

LIST OF REFERENCES

[1] P. E. Pace, *Detection and Classifying Low Probability of Intercept Radar* (2nd ed.). Artech House, Norwood, Massachusetts, 2009.

[2] V. F. Kroupa, *Direct Digital Frequency Synthesizers*. New York, IEEE Reprint Press Book, 1998.

[3] R. H. Barker, "Group synchronizing of binary digital systems," in *Communications Theory*, Butterworth, London, pp. 273–287, 1953.

[4] Frank, R. L., "Polyphase codes with good nonperiodic correlation properties," *IEEE Transactions on Information Theory*, vol. IT-9, pp. 43–45, 1963.

[5] L. B. Lewis, "Linear frequency modulation derived poly pulse compression codes," *IEEE Transactions on Aerospace and Electronic systems*, vol. AES-18, no. 5, pp. 637–641, 1982.

[6] T. J. Pizzillo and H. B. Wallace, *A Technique for Calibrating the Phase Detector of Wideband Radars Using a Phase Modulation and Demodulation Scheme*. Army Research Laboratory, ARL-TR-1567, May 1998.

[7] P. E. Pace, R. E. Leino, and D. Styer, "Use of the symmetrical number system in resolving single-frequency undersampling aliases," *IEEE Transactions on Signal Processing*, vol. 45, no. 5, pp. 1153–1160, May 1997.

[8] B. Getz and N. Levanon, "Weight effects on the periodic ambiguity function," *IEEE Transactions on Aerospace and Electronic Systems*, vol. 31, no. 1, pp. 182–193, January 1995

[9] N. Levanon, "CW alternatives to the coherent pulse train-signals and processors," *IEEE Transactions on Aerospace and Electronic Systems,* vol. 28, no. 2, pp. 387–395, April 1992.

[10] N. Levanon, *Radar signals*, John Wiley & Sons, New Jersey, 2004.

[11] N. Levanon and A. Freedman, "Periodic ambiguity function of CW signals with perfect periodic autocorrelation," *IEEE Transactions on Aerospace and Electronic Systems*, vol. 28, no. 2, pp. 387–395, April 1992.

[12] B. L. Lewis and F. F. Kretschmer, Jr., "A new class of polyphase pulse compression codes and techniques," *IEEE Transactions on Aerospace and Electronic Systems*, vol. AES-17, no. 3, pp. 364–372, May 1981.

[13] N. S. Szabo and R. J. Tanaka, *Residue Arithmetic and Its Applications to Computer Technology*, McGraw Hill Inc., New York, 1967.

[14] M. A. Soderstrand, W. K. Jenkins, G.A. Jullien and F.J. Taylor, Eds., *Modern Applications of Residue Number System Arithmetic to Digital Signal Processing*, New York, NY: IEEE Press, 1986.

[15] W. K. Jenkins, "Techniques for residue-to-analog conversion for residue-encoded digital filters," *IEEE Transaction on Circuits and Systems*, vol. CAS-25, pp. 555–562, 1978.

[16] K. M. Ibrahim and S. N. Saloum, "An efficient residue to binary converter design," *IEEE Transaction on Circuits and Systems*, vol. 35, pp. 1156–1162, 1988.

[17] P. E. Pace, *Advanced Techniques for Digital Receivers*, Artech House, Norwood, Massachusetts, 2000.

[18] P. E. Pace, P. A. Rammamoorthy, and D. Styer, "A preprocessing architecture for resolution enhancement in high-speed analog-to-digital converters," *IEEE Transactions on Circuits and Systems*, vol. 41, no. 6, pp. 373–379, June 1994.

[19] P. E. Pace, R. E. Leino, D. Styer, "Use of the symmetrical number system in resolving single-frequency undersampling aliases," *IEEE Transactions on Signal Processing*, vol. 45, no. 5, pp. 1153–1160, May 1997.

[20] P. E. Pace, D. Styer, and I. A. Akin, "A folding ADC preprocessing architecture employing a robust symmetrical number system with gray-code properties," *IEEE Transactions on Circuits and Systems*, vol. 47, no. 5, pp. 462–467, May 2000.

[21] M. R. Arvizo, J. Calusdian, K. B. Hollinger, P. E. Pace, "Robust symmetrical number system preprocessing for minimizing encoding errors in photonic analog-to-digital converters," *SPIE Digital Library*, vol. 50(80), August 2011.

[22] D. Styer and P. E. Pace, "Two-channel RSNS dynamic range," *IEEE Transactions on Circuits and Systems*, vol. 49, no. 3, pp. 395–397, March 2002.

[23] B. L. Luke and P. E. Pace, "N-sequence RSNS redundancy analysis," *ISIT 2006*, Seattle, USA, pp. 2744–2748, July 9–14, 2006.

[24] B. L. Luke and P. E. Pace, "N-sequence RSNS ambiguity analysis," *IEEE Transactions on Information Theory*, vol. 53, no. 5, pp. 1759–1766, May 2007.

[25] B. L. Luke and P. E. Pace, “Computation of the robust symmetrical number system dynamic range,” *IEEE Information Theory Workshop*, ITW, Dublin 2010.

THIS PAGE INTENTIONALLY LEFT BLANK

INITIAL DISTRIBUTION LIST

1. Defense Technical Information Center
   Ft. Belvoir, Virginia

2. Dudley Knox Library
   Naval Postgraduate School
   Monterey, California

3. Dr. Clark Robertson
   Chairman, Department of Electrical & Computer Engineering
   Naval Postgraduate School
   Monterey, California

4. Dr. Dan C. Boger
   Chairman, Department of Information Sciences
   Naval Postgraduate School
   Monterey, California

5. Professor Phillip E. Pace
   Department of Electrical & Computer Engineering
   Naval Postgraduate School
   Monterey, California

6. Professor David C. Jenn
   Department of Electrical & Computer Engineering
   Naval Postgraduate School
   Monterey, California

7. LT Nattaphum Paepolshiri
   Naval Communications & Information Technology Department
   Royal Thai Navy
   Bangkok, Thailand

8. Professor Nadav Levanon
   Department of Electrical Engineering – Systems
   Tel Aviv University
   Ramat Aviv, Israel